NWT Open File 2018-02

# Geology of the Mactung tungsten skarn and area – Review and 2016 field observations

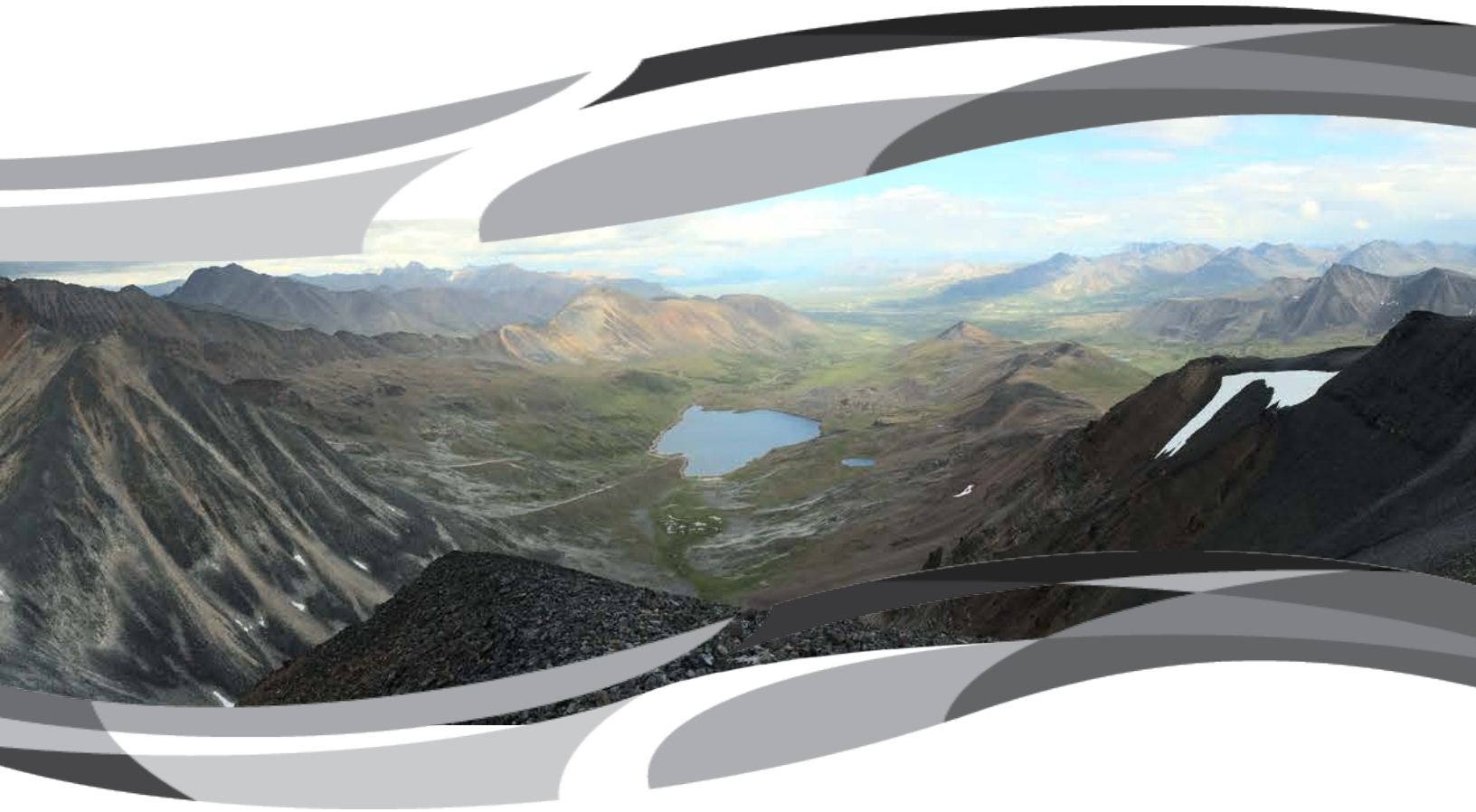

B.J. Fischer, E. Martel, and H. Falck

NORTHWEST TERRITORIES
GEOLOGICAL SURVEY

Government of
Northwest Territories

*Cover Image*
*Looking east at Cirque Lake from the top of Mount Allan below which the tungsten mineralization is found.*

If you would like this information in another official language, call us.
English

---

Si vous voulez ces informations dans une autre langue officielle, contactez-nous.
French

---

Kīspin ki nitawihtīn ē nīhīyawihk ōma ācimōwin, tipwāsinān.
Cree

---

Tłı̨chǫ yatı k'ę̀ę̀. Dı wegodı newǫ dè, gots'o gonede.
Tłı̨chǫ

---

Ɂerıhtł'ís Dëne Sųłıné yatı t'a huts'elkër xa beyáyatı theɂą ɂat'e, nuwe ts'ën yółtı.
Chipewyan

---

Edı gondı dehgáh got'ı̨e zhatıé k'ę́ę́ edatł'éh enahddhę nıde naxets'ę́ edahłí.
South Slavey

---

K'áhshó got'ı̨ne xədə k'é hederı ɂedı̨htl'é yerınıwę nídé dúle.
North Slavey

---

Jii gwandak izhii ginjìk vat'atr'ijąhch'uu zhit yinohthan jì', diits'àt ginohkhìi.
Gwich'in

---

Uvanittuaq ilitchurisukupku Inuvialuktun, ququaqluta.
Inuvialuktun

---

ᑌᖅᑯᐊ ᑎᑎᖅᑲᐃᑦ ᐱᓕᒍᐃᖅᑎᑦ ᐃᓄᖅᑎᑐᓕᖅᓯᒪᓂᑎᖅ, ᐅᕐᕈᑎᐅᓂᓄᑦ ᐅᖃᖅᑕᓕᕆᓂᖅᑐᑎᑦ.
Inuktitut

---

Hapkua titiqqat pijumagupkit Inuinnaqtun, uvaptinnut hivajarlutit.
Inuinnaqtun

---

Aboriginal Languages Secretariat: 867-767-9346 ext. 71037
Francophone Affairs Secretariat: 867-767-9343

Government of Northwest Territories
Gouvernement des Territoires du Nord-Ouest

Blank Page

# NWT Open File 2018-02

# Geology of the Mactung tungsten skarn and area – Review and 2016 field observations

**B.J. Fischer, E. Martel, and H. Falck**

*Distributed by:*
*Northwest Territories Geological Survey*
*Department of Industry, Tourism and Investment*
*Government of Northwest Territories*
*P.O. Box 1320, 4601-B 52nd Avenue Yellowknife,*
*Northwest Territories Canada*
*X1A 2L9*
*867-767-9211*
*www.nwtgeoscience.ca*

*Corresponding Author:*
*B.J. Fischer*
*Northwest Territories Geological Survey*
*Email: Beth_Fischer@gov.nt.ca*

*Recommended Citation:*
Fischer, B.J., Martel, E., and Falck, H., 2018. Geology of the Mactung tungsten skarn and area – Review and 2016 field observations; Northwest Territories Geological Survey, NWT Open File 2018-02, 84 pages and appendices.

# Executive Summary

The Mactung tungsten (-copper-gold) skarn deposit, discovered on the border between Northwest Territories and Yukon in 1962 and explored to a pre-feasibility stage, contains a significant drill-defined resource of tungsten oxide (an indicated mineral resource of 33.0 Mt grading 0.88% $WO_3$, including a probable mineral reserve of 8.5 Mt grading 1.18% $WO_3$, and additional inferred resources of 11.9 Mt grading 0.78% $WO_3$; Narisco 2009). The Northwest Territories Geological Survey (NTGS) conducted a short field program and geological review of the deposit in 2016. The results, as well as the results of previous and concurrent work by company, government, and academic geologists, are summarized in this report and a companion map (Martel *et al.* 2018). In addition, NTGS commissioned a resource modelling study, a draft of which is presented in Appendix A. The latter study shows the sensitivity of resource estimates to the selection of cut-off grade, providing a model estimate of 17 Mt total mineral resources (note that this is not a "Mineral Resource" for National Instrument 43-101 purposes) grading 0.969% $WO_3$ and 0.078% Cu for a cut-off grade of 0.5% *versus* 10 Mt grading 1.21% $WO_3$ and 0.117% Cu for a higher cut-off of 0.8%. Both gold and bismuth are anomalous in at least some parts of the orebody (Gebru 2017); few samples have been assayed for these metals.

The Mactung deposit is located within the foreland fold-and-thrust belt of the Cordilleran orogen, within a succession that includes late Neoproterozoic to Early Devonian, terrigenous and carbonate strata deposited on the eastern slope of the Selwyn Basin, and Middle to Late Devonian, terrigenous clastic strata of a successor basin. This succession was deformed primarily by thrusting and folding in the Mesozoic, and was cut by the Tungsten suite of post-compressional plutons in the Late Cretaceous. Regional metamorphism associated with deformation produced biotite in the mudrocks and converted carbonate rocks to marbles, generating micaceous foliation in the former and cleavage in the latter.

Two intrusions at Mactung, the Cirque Lake stock north of the orebody and the Rockslide Mountain stock south of it, comprise various phases of biotite granitoid dated at 97.1 to 97.6 Ma (± 0.2 to 0.4 Ma; Gebru 2017), except for a phase of the Cirque Lake stock dated at ± 0.2 Ma (Selby *et al*. 2003). The stocks crystallized from a strongly reduced, I-type magma derived from partial melting of meta-igneous crust, although a late, leucogranitic phase incorporated supracrustal material (Gebru 2017). Crystallization of the Cirque Lake stock took place over a range of depths from at least 22 km to 8 km. The intrusions caused thermal metamorphism and metasomatic alteration in the country rocks. The thermal metamorphism converted terrigenous mudstones to hornfels, calcareous mudstones to calc-silicate rocks, and marbles to re-crystallized marbles. The metasomatic alteration did not affect the intrusions themselves, but in the country rocks, led to the development of various types of scheelite-bearing and scheelite-poor skarns in the limestone, marble, and calc-silicate hornfels, and bleaching and invasion of quartz ± calc-silicate veins in the terrigenous hornfels. Two ore zones, referred to as the Lower and Upper ore zones, developed. In the Lower ore zone, the intensity of metasomatic alteration increases across a series of intergradational zones, from bleached limestone on the eastern periphery of the

deposit, through scheelite-poor marble skarn to scheelite-bearing pyroxene skarn and finally to scheelite-rich pyrrhotite skarn in the core of the Lower ore zone (Atkinson and Baker 1986; Harris 1980). Tungsten is hosted mainly in scheelite, copper in chalcopyrite, and gold mainly in native bismuth. Skarn mineralization was co-eval with crystallization of the oldest phases of the two stocks (97.2 ± 0.2 Ma by Re-Os of molybdenite in quartz veins, by Gebru (2017), and 97.1 ± 4.1 Ma by U-Pb of titanite in skarn, by Selby *et al.* (2003)).

Skarn formation and mineralization were co-eval with crystallization of the oldest phases of the Cirque Lake and Rockslide Mountain stocks. The source pluton is agreed to lie beneath the orebody. One suggestion is that the source is a buried pluton that has not yet been discovered (Atkinson and Baker 1986); a more recent suggestion is that the Cirque Lake pluton extends south under the ore zones (Gebru 2017).

Both the Lower and Upper ore zones dip gently to the south, concordant with bedding. Folds on the property are mostly open, although two tight folds are recognized (one on Fold Mountain and an underground one affecting the Sekwi Formation). Plunges are shallow to the west or west-northwest in the west part of the map area, shallow to the east in the east part of the map area, and perhaps shallow to the northeast on Fold Mountain. A north-verging thrust fault passes north of the deposit, truncated by the Cirque Lake stock. A few north-trending steep faults cross the map area, one of them displacing part of the Rockslide Mountain stock but apparently truncated by the Cirque Lake stock (Abbott 2013), which if true implies that the fault pre-dates one pluton and post-dates the other. A number of northeast- and northwest-trending faults on the north face of Mount Allan show metre-scale displacements.

The skarn mineralization is hosted by originally carbonate rocks of the Early Cambrian Sekwi Formation in the Lower ore zone, and Cambro-Ordovician Rabbitkettle Formation in the Upper ore zone. The Sekwi Formation host was a limestone debrite of varying thickness that probably originated by slope failure of semi-lithified nodular lime muds. The Rabbitkettle Formation host consists of three stacked layers collectively forming the Upper ore zone. The lowermost layer coincides with member D, the basal member of the formation, which is a phosphatic, quartz-sandy limestone conglomerate to calcareous sandstone interstratified with thin-bedded silty limestone, and the skarned, calc-silicate equivalents of those rocks. Member D probably originated through prolonged bottom-current winnowing, repeated sediment gravity flows possibly caused by seismic events, and episodic fluvial input on a carbonate shelf where phosphogenesis was a significant contributor to sediment formation. The middle and upper layers of the Upper ore zone are in member EF of the Rabbitkettle Formation. Member EF consists of interbedded limestone and mudstone, and the hornfelsed and skarned equivalents of those rocks. The middle and upper layers of the Upper ore zone coincide with thick intervals of calc-silicate rock; protoliths were mainly limestone and minor mudstone. These thick intervals are separated by layers of unmineralized rock; protoliths were mainly mudstone. Member EF was deposited on a deep slope subject to minor gravity-flow events.

Other stratigraphic units recognized on the property include the late Proterozoic to Cambrian meta-siltstone of the Narchilla Formation below the ore horizons. Outside of the

ore zone, the Sekwi Formation varies in thickness and lithology across the map area. It consists dominantly of nodular and thin-bedded limestone and silty limestone, slump breccias, and chaotic debrites, but includes platy, non-calcareous mudstone; all of these rocks were deposited on a slope or basin floor. Between the two ore-hosting formations, the middle Cambrian Hess River Formation is mainly a mudstone, meta-mudstone, or hornfels. Above the ore horizons the following units are recognized: resistant dolostone, talc-tremolite schist, and calc-silicate rock of member G at the top of the Rabbitkettle Formation; a lower red-brown mudstone member and an upper, black, graptolitic shale member of the Ordovician to Silurian Duo Lake Formation; bioturbated mudstone of the late Silurian Steel Formation; mudstone and graptolitic silty limestone of the late Silurian to Middle Devonian Sapper Formation; and various terrigenous clastic rocks of the Devonian Portrait Lake Formation (Niddery Lake and Macmillan Pass members).

Two samples taken in 2016 of rusty weathering mudrock, from the Rabbitkettle and Hess River formations, contained low metal values. Geochemical analyses of samples of member D confirmed the presence of phosphate minerals. Processing for conodonts of a sample from the top of member D of the Rabbitkettle Formation is pending.

The current study has generated the following thoughts:

- Mineralized skarns at Mactung are best developed in the sediment gravity-flow deposits of the Sekwi Formation and member D of the Rabbitkettle Formation. An understanding of the paleogeographic and tectonic setting of Mactung during Sekwi and Rabbitkettle time, and especially those aspects that led to deposition of the conglomerates, should therefore be pursued by detailed mapping and stratigraphic studies.
- Member D, in particular, is complex and poorly understood. The processes leading to the generation of the phosphatic clasts as well as the processes that mixed them with lime mudstone clasts, re-brecciated the breccia, and transported clasts to the final site of deposition should be investigated, to predict sites where additional skarn-susceptible conglomerates may lie.
- It is of interest to establish the source of the mineralizing fluids at Mactung, whether it is a buried pluton yet to be discovered, or a deep extension of the Cirque Lake pluton, as suggested by Gebru (2017). Elucidation of the location and geometry of the source pluton will have important implications for predicting the locations of additional mineral resources.
- If the structures that controlled emplacement of the source pluton are Devonian or Neoproterozoic faults that were re-activated during pluton emplacement, then similarly re-activated structures are prospective. The conduits traversed by mineralizing fluids should be identified, to seek other skarn-susceptible units along them.
- A structural/stratigraphic study should determine if post-mineralization faults have significantly affected the distribution of ore, if the geometry of the Z-fold in the Lower ore zone as depicted on mine sections is accurate, and how the geometry of the Z-fold changes to the west.
- Additional work should test the gold potential at Mactung and evaluate the potential of Member D as a phosphate resource.

# Résumé

*Fischer, B.J., Martel, E., et and Falck, H., 2018. Géologie du gisement de skarn minéralisé en Tungstène de Mactung – compte rendu et observations sur le terrain en 2016; Commission Géologique des Territoires du Nord-Ouest, Dossier public des TNO. 2018-02, 84 pages et annexes.*

Le gisement de skarn tungsténique (avec cuivre et or) de Mactung, découvert à la frontière entre les Territoires-du-Nord-Ouest et le Yukon en 1962 et exploré jusqu'à une étape de préfaisabilité, contient une ressource considérable définie par le forage d'oxyde de tungstène (une ressource minérale indiquée de 33,0 Mt de minerai titrant 0,88 % de $WO_3$, y compris une réserve minérale probable de 8,5 Mt de minerai titrant 1,18 % de $WO_3$ et des ressources supplémentaires inférées de 11,9 Mt de minerai titrant 0,78 % de $WO_3$; Narisco 2009). Des géologues de la Commission Géologique des Territoires du Nord-Ouest (CGTNO) ont exécuté un court programme en 2016 consistant d'une étude géologique du gisement. Ces résultats et les résultats des travaux antérieurs et en cours des géologues des entreprises, du gouvernement et des universités sont résumés dans le présent rapport et dans une carte d'accompagnement (Martel *et coll.* 2018). De plus, la CGTNO a commandé une étude de modélisation des ressources, dont l'ébauche se trouve à l'annexe A. L'ébauche de l'étude montre la délicatesse des estimations des ressources par rapport à la sélection de la teneur limite, qui fournit une estimation de modèle de 17 Mt pour le total en ressources minérales (veuillez noter qu'il ne s'agit pas d'une « ressource minérale » aux fins de l'instrument national 43-101) de minerai titrant 0,969 % de $WO_3$ et de 0,078 % de Cu pour une teneur limite de 0,5 % par rapport à 10 Mt de minerai titrant 1,21 % de $WO_3$ et de 0,117 % de Cu pour une teneur limite supérieure de 0,8 %. L'or et le bismuth sont anormaux au moins dans quelques parties du gisement (Gebru 2017); seulement quelques échantillons ont été analysés pour ces métaux.

Le gisement Mactung est situé dans la ceinture de chevauchements de l'avant-pays de l'orogène de la Cordillère, dans une succession qui va d'une strate terrigène et carbonatée déposée sur le cote est la pente du bassin Selwyn, datant de la fin du Néoprotérozoïque au début du Dévonien précoce, à une strate terrigène clastite d'un bassin successeur datant du milieu à la fin du Dévonien. Cette succession a été déformée principalement par des chevauchements et des plissements pendant l'ère Mésozoïque et a été coupée par l'ensemble de plutons post-compressifs 'Tungstène' vers la fin de l'ère du Crétacé. Le métamorphisme régional associé à la déformation a produit de la biotite dans l'argilite et a converti des roches carbonatées en marbres, ce qui a produit une foliation micacée dans l'argilite et un clivage dans les marbres.

Deux intrusions à Mactung, le stock du lac Cirque au nord du gisement et le stock de la montagne Rockslide au sud du gisement, comprennent diverses phases de biotite granitoïde datée de 97,1 à 97,6 Ma (± 0,2 à 0,4 Ma; Gebru 2017) sauf pour une phase du stock du lac Cirque daté à 92,1 ± 0,2 Ma (Selby *et coll*. 2003). Les stocks se sont cristallisés d'un magma de type I fortement réduit et dérivés de la fusion partielle de la croûte ignée métamorphisée, bien qu'une phase tardive leucogranitique ait incorporé du matériel

supracrustal (Gebru 2017). La cristallisation du stock du lac Cirque a eu lieu sur un grand éventail de profondeurs d'au moins 22 km à 8 km. Les intrusions ont causé un métamorphisme thermique, qui a engendré la conversion d'argilite terrigène en cornéennes, d'argilite calcaire en roches calcaires-silicates, et des marbres en marbres recristallisés.

L'intrusion a engendré une altération métasomatique dans les roches environnantes, mais pas dans les intrusions mêmes. Dans les roches environnantes, les processus métasomatiques ont causé la formation de divers types de skarn concentrés de scheelite et des skarns en faible teneur de scheelite dans les cornéennes de calcaire, de marbre et de calcaires-silicates, et le blanchiment et l'invasion de veines de quartz et calcaires-silicates dans les cornéennes terrigènes. Deux zones de minerais, connues sous le nom zone de minerai supérieure et zone de minerai inférieure en ont découlé. Dans la zone de minerai inférieure, l'intensité de l'altération métasomatique augmente à l'échelle d'une série de zones intergradationnelles, d'un calcaire blanchi à la limite est du gisement, en passant par un skarn de marbre en faible teneur de scheelite, puis un skarn de pyroxène concentrée de scheelite, et enfin un skarn pyrrhotite riche en scheelite dans le cœur de la zone de minerai inférieure (Atkinson et Baker 1986; Harris 1980). Le tungstène est principalement situé dans la scheelite, le cuivre dans la chalcopyrite, et l'or principalement dans le bismuth natif. La minéralisation du skarn est de la même époque que la cristallisation des phases les plus anciennes des deux stocks [97,2 ± 0,2 Ma par le rhénium-osmium de la molybdénite dans les veines de quartz, par Gebru (2017) et 97,1 ± 4,1 Ma par l'uranium-plomb de la titanite dans le skarn par Selby *et coll.* (2003)].

La formation des skarns et la minéralisation sont de la même époque que la cristallisation des phases les plus anciennes des stocks du lac Cirque et de la montagne Rockslide. On convient que le pluton de source se trouve en dessous le gisement de minerai, bien que pas encore découvert, on postule que le pluton enfoui a provoqué les fluides (Atkinson et Baker 1986). On a également suggéré que le pluton du lac Cirque s'étend vers le sud en dessous des zones de minerais (Gebru 2017).

Les zones de minerais inférieure et supérieure s'étendent un peu vers le sud, conforment avec la stratification. Les plis sur la propriété sont ouverts en grande partie, bien que deux plis serrés sont reconnus (un sur la montagne Fold, et un qui est souterrain et qui a une incidence sur la formation de Sekwi). Les plongements sont peu profonds vers l'ouest ou l'ouest-nord-ouest dans la partie ouest de la carte, peu profonds vers l'est dans la partie est de la carte et peut-être peu profonds vers le nord-est sur la montagne Fold. Une faille chevauchante vers le nord passe au nord du gisement, tronqué par le stock du lac Cirque. Quelques failles profondes se dirigeant vers le nord traversent la zone de la carte et une d'entre elles déplace une partie du stock de la montagne Rockslide mais est tronquée par le stock du lac Cirque (Abbott 2013), ce qui sous-entend que la faille précède un pluton et suit l'autre. Un certain nombre de failles se dirigeant vers le nord-est et le nord-ouest sur la face nord du mont Allan montrent des déplacements d'une longueur qui peut se mesurer en mètres.

La minéralisation a initialement été contenue par des roches carbonatées de la formation de Sekwi du début de l'ère cambrienne dans la zone de minerai inférieure et la formation de Rabbitkettle de l'ère cambro-ordovicienne dans la zone de minerai supérieure. L'hôte de la formation de Sekwi était une débrite calcaire d'une épaisseur variable qui a probablement été créée par la défaillance de la pente de boues calcaires nodulaires semi-lapidifiées. L'hôte de la formation de Rabbitkettle consiste en trois couches consécutives qui forment collectivement la zone de minerai supérieure. La couche la plus basse coïncide avec le membre D, le membre basal de la formation, qui est un conglomérat de calcaire phosphatique et de quartz sableux à une pierre de taille calcareuse interstratifiée dans une couche mince de calcaire limoneux et des équivalents de skarn et calcaires-silicates. Le membre D a probablement été créé par le vannage prolongé du courant de fond, des débits de sédiments par gravité peut-être causés par des événements sismiques et une entrée fluviale épisodique sur une couche de carbonate où la phosphogénèse était un élément contributif considérable sur la formation des sédiments. Les couches moyennes et supérieures de la zone de minerai supérieure coïncident avec des intervalles épais de protolites interstratifiés avec des protolites d'argilite dans le membre EF de la formation de Rabbitkettle. Elles ont été déposées sur une pente profonde assujettie à des événements mineurs d'écoulement par gravité.

Les autres unités stratigraphiques reconnues sur la propriété comprennent le méta-siltstone de la formation de Narchilla de l'ère protérozoïque tardif à cambrienne en dessous des horizons de minerais. À l'extérieur de la zone de minerai, la formation de Sekwi a une épaisseur et une lithologie variables à l'échelle de la zone de la carte. Il s'agit principalement d'un dépot de pente à eau profonde de calcaire nodulaire et mince et de calcaire limoneux, de brèches d'effondrement et de débrites chaotiques, mais qui comprend de l'argilite lamellaire et non calcaire. Entre les deux formations qui contiennent des minerais, la formation de Hess River de l'ère cambrienne est principalement composée d'argilite, de méta-argilite ou de cornéennes. Au-dessus des horizons de minerais, on reconnaît les unités suivantes : dolomie résistante, schiste talc-trémolite et pierre calcaire-silicate du membre G au haut de la formation de Rabbitkettle; un membre inférieur d'argilite rouge-brun et un membre supérieur noir de schiste graptolitique de la formation de Duo Lake, datant de l'ère ordovicienne à silurienne; argilite bioturbé de la formation de Steel, datant environ de la fin de l'ère silurienne; argilite et calcaire limoneux graptolitique de la formation Sapper, datant de la fin de l'ère silurienne au milieu de l'ère dévonienne; diverses roches clastiques terrigènes de la formation de Portrait Lake, datant de l'ère dévonienne (membres Niddery Lake et Macmillan Pass).

Deux échantillons pris en 2016 de l'argilite rouillée en voie de météorisation des formations de Rabbitkettle et Hess River avaient de faibles teneurs en métal. Les analyses géochimiques des échantillons du membre D ont permis de confirmer la présence de minerais de phosphate. Le traitement pour les conodontes d'un échantillon du haut du membre D de la formation de Rabbitkettle est en suspens.

L'étude actuelle évoque les pensées suivantes pour nous :

- Des skarns minéralisés à Mactung ont le meilleur développement dans les gisements des débits de sédiments par gravité de la formation de Sekwi et dans le membre D de la formation de Rabbitkettle. Une compréhension de l'emplacement paléogéographique et tectonique de Mactung durant le développement des formation de Sekwi et de Rabbitkettle et surtout les aspects qui ont engendré le dépôt des conglomérats devraient donc être cherchés à l'aide d'une cartographie détaillée et des études stratigraphiques.
- Le membre D, en particulier, est complexe et mal compris. Les processus qui entraînent la génération de clastes de phosphates ainsi que les processus qui les ont mélangés avec des clates d'argilites calcaires, ont rebréchifié les brèches et ont transporté les clastes au site final de déposition devraient faire l'objet d'une étude, afin de prévoir où des conglomérats susceptibles aux skarns peuvent se trouver.
- Il est intéressant d'établir la source des fluides minéralisants à Mactung, qu'il s'agisse d'un pluton enfoui qui n'a pas encore été découvert ou d'une extension profonde du pluton du lac Cirque, tel qu'il a été suggéré par Gebru (2017). L'élucidation de l'emplacement et de la géométrie du pluton source aura des retombées importantes pour la prédiction de l'emplacement de ressources minérales supplémentaires.
- Si les structures qui ont contrôlé la mise en place du pluton source sont des failles de l'ère dévonienne ou néoprotérozoïque qui ont été réactivées lors de la mise en place du pluton, des structures réactivées de manière semblable sont donc prometteuses. Les conduits traversés par des fluides minéralisants doivent être identifiés, afin de rechercher d'autres unités susceptibles aux skarns le long de ces conduits.
- Une étude structurale ou stratigraphique devrait permettre de déterminer si des failles post-minéralisation ont eu une incidence considérable sur la distribution de minerais, si la géométrie du pli en forme de Z dans la zone de minerais inférieure, tel qu'il a été illustré dans des sections de mines est exacte et comment la géométrie du pli en forme de Z change en allant vers l'ouest.
- Des travaux supplémentaires devraient permettre de mettre à l'essai le potentiel aurifère à Mactung et d'évaluer le potentiel du membre D en tant que ressource de phosphate.

# Table of Contents

# Introduction

The Mactung deposit is a W-(Cu-Au Bi) skarn that straddles the border between Northwest Territories (NWT) and Yukon, 275 km southwest of Norman Wells and 200 km northest of Faro (Figure 1). The deposit lies 7 km northwest of the Canol Road, a historic route maintained as a trail in NWT and a seasonally passable road in Yukon. The Mactung deposit contains an indicated mineral resource of 33.0 Mt grading 0.88% $WO_3$ and additional inferred resources of 11.9 Mt grading 0.78% $WO_3$ (Narisco 2009). The indicated resource includes a probable mineral reserve of 8.5 Mt grading 1.18% $WO_3$ (*ibid*.). Mactung compares well with other deposits, such as the Los Santos Mine, Spain (3.0 Mt grading 0.30% $WO_3$; Wheeler 2012) and the recently opened Drakelands Mine, United Kingdom (58.6 Mt grading 0.17% $WO_3$ and 0.02% Sn; Wolf Minerals 2015).

In 2015, the Government of the Northwest Territories (GNWT) acquired the Mactung deposit from North American Tungsten Corporation Ltd. (NATCL). Subsequently, the Northwest Territories Geological Survey (NTGS) of the GNWT contracted Kirkham Geosciences Ltd. to review the available Mactung drill data for completeness and conduct a confirmatory (non-NI 43-101 compliant) resource evaluation (Appendix A). In August of 2016, the NTGS undertook a small field program at Mactung with the goals of clarifying correlation of mine units with formally defined stratigraphic units, improving map-unit contact locations using Global Positioning System (GPS), and developing a list of questions whose answers would best guide future work on the property. The results of that work are summarized here and in Martel *et al.* (2018). These works focus on the stratigraphy and structure of the Mactung area, as observed in 2016 and as described by previous workers. The igneous geology, and the mineralogy and chemistry of the skarn, have been studied in detail by Gebru (2017).

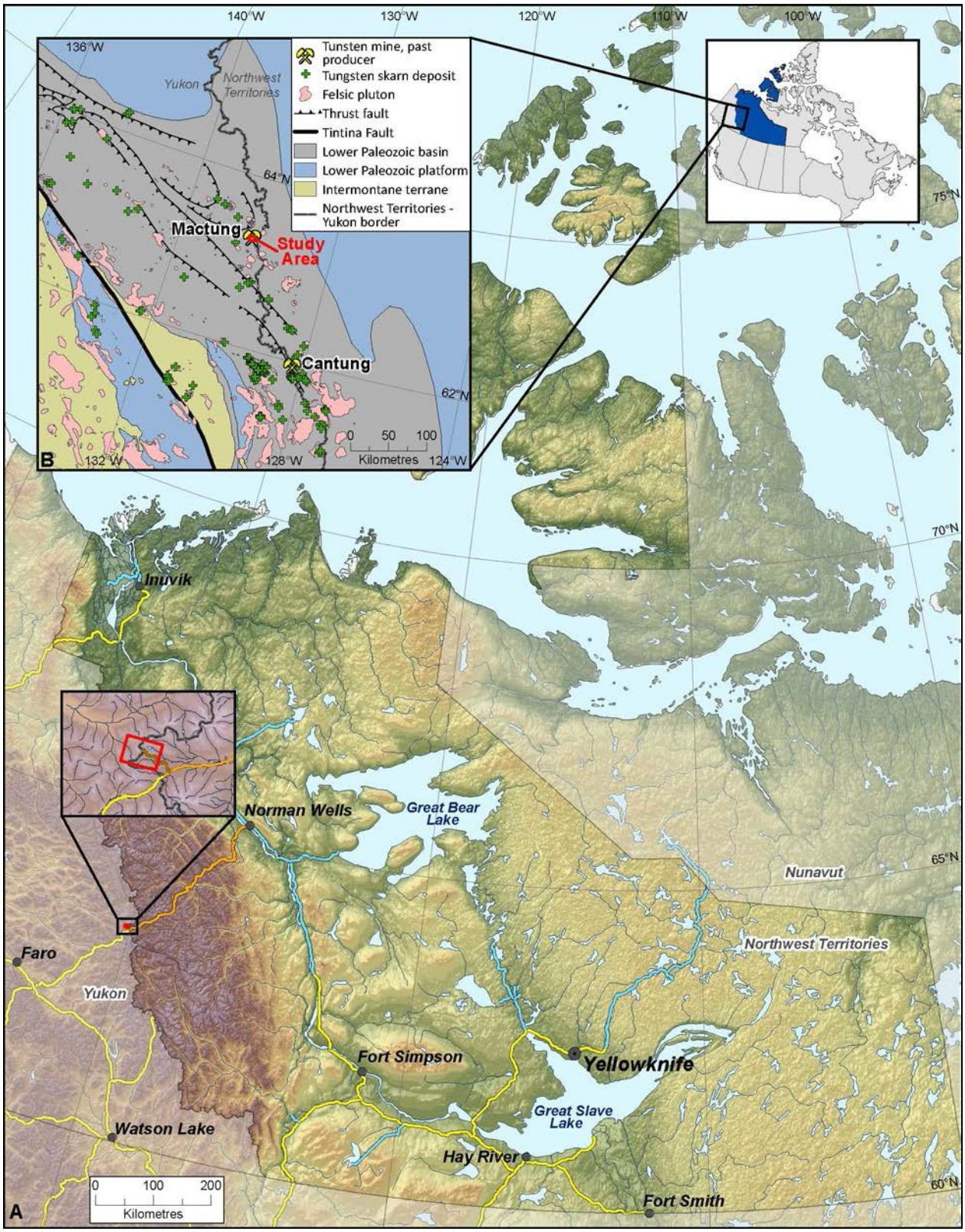
140°W
130°W
120°W
110°W
100°W
75°N
70°N
65°N
60°N
136°W
132°W
128°W
124°W
64°N
62°N
Yukon
Northwest Territories
Tunsten mine, past producer
Tungsten skarn deposit
Felsic pluton
Thrust fault
Tintina Fault
Lower Paleozoic basin
Lower Paleozoic platform
Intermontane terrane
Northwest Territories - Yukon border
Mactung
Study Area
Cantung
0 50 100
Kilometres
B
Inuvik
Norman Wells
Great Bear Lake
Nunavut
Northwest Territories
Faro
Yukon
Fort Simpson
Yellowknife
Great Slave Lake
Watson Lake
Hay River
Fort Smith
0 100 200
Kilometres
A

Figure 1. Location of the Mactung tungsten deposit on the border of Northwest Territories and Yukon. [A] The Mactung study area, communities, and roads (Yellow: all-season road; Blue: winter road; Brown: unmaintained road; Orange: Canol Heritage Trail) on a topographic background. Inset shows study area in more detail. [B] Generalized tectonic and paleogeographic setting of the study area, showing major faults, felsic plutons, and tungsten skarn deposits. Areas designated as Lower Paleozoic basin and Lower Paleozoic platform are autochthonous parts of the ancestral North American craton, dominated by basinal and platformal or shelf settings respectively, and include rocks of late Neoproterozoic age. The location of [B] is shown on a map of Canada with the Northwest Territories emphasized. Data from Colpron and Nelson (2011), Yukon Geological Survey (accessed 2017), and Okulich and Irwin (2014), except showings are from NORMIN (2016) and Yukon MINEFILE (accessed 2017).

## History

The Mactung deposit was discovered in 1962 by J. Allan for Southwest Potash Company, a subsidiary of American Metals Climax which was subsequently re-named AMAX Inc. (Atkinson and Baker 1986). AMAX and its subsidiaries investigated the deposit from the 1960s until the 1980s, while the first government reconnaissance work (Blusson 1971, 1974) and subsequent systematic mapping (Abbott 1983, 2013; Cecile 1982, 1996, 2000) documented the regional geology.

Work done on the Mactung property by 1972 included geological mapping, a small magnetometer survey, soil and rock geochemical sampling, and diamond drilling of 10 782 m of core in 74 holes. Access to the site was improved through the construction of an 11- km access road from the property to the Canol Road in 1970 (Narisco 2009). Encouraging results from the drilling prompted the collaring of an adit into the Lower ore zone at 1890 metres elevation, followed by 726 metres of lateral development and 27 metres of raising, all of which was completed in 1973. A 295-tonne bulk sample was extracted for metallurgical testing and 43 underground holes (1653 m) were drilled from the adit to further test the Lower ore zone (*ibid*.). In 1979, eight holes (688 m) were drilled underground and the workings were extended by 49 metres, enabling collection of nine 45- gallon drums of mineralized skarn for further metallurgical testing. In 1979 and 1980, 17 holes (3418 m) were drilled from the surface (*ibid*). During the early 1980s, most of the Mactung core was re-logged, and project feasibility studies and environmental studies were undertaken. The adit was re-opened, and additional bulk samples were taken, including surface bulk samples from the Upper ore zone in 1982 and in 1983 (*ibid)*. However, the recession of 1981 to 1982 resulted in the collapse of tungsten prices, and by 1985, work on the project had been suspended.

Studies of the chemistry, petrography, and age of the Cirque Lake stock (also known as the Mactung pluton) carried out in the 1980s are summarized by Anderson (1982) and Gordey and Anderson (1993). Dick and Hodgson (1982) made a detailed study of the skarn, reporting results that are, in some respects, at odds with descriptions written by company geologists (Harris and Godfrey 1975; Harris 1977, 1980; Atkinson and Baker 1986).

The property was acquired by Canada Tungsten Mining Corporation in 1985 and by NATCL in 1997. In order to upgrade the resource and to better define its western extent, in 2005, NATCL drilled 25 surface diamond drill holes (6639 m), rehabilitated the adit, and extracted a 79-tonne bulk sample for metallurgical tests. By 2009, NATCL had drilled an additional 76 surface holes. NATCL also supported a detailed petrochemical, mineralogical, and geochronological examination of the granitoids and skarns at Mactung (Gebru 2017). The records of much of the work by AMAX and NATCL are now housed with the GNWT, who acquired the property in 2015. Most of the drill core from the 1960s to 1980s is stored at the Cantung mine site, whereas the core drilled more recently by NATCL is stored at the Mactung site.

## Regional Setting

The Mactung deposit is located within the foreland fold-and-thrust belt of the Cordilleran orogen, in a region underlain by Proterozoic through Triassic sedimentary (and minor mafic volcanic and intrusive) rocks, and Late Cretaceous granitic intrusions (Abbott 2013, 1983; Gordey *et al.* 2012; Martel *et al.* 2011; Cecile 1996, 2000; Gordey 1992; Gordey and Anderson 1993). The strata can be subdivided into a number of tectonostratigraphic packages (Figure 2). Of interest here are the late Proterozoic to middle Paleozoic Selwyn Basin, the broadly co-eval Mackenzie Platform, and a Middle to Late Devonian successor basin. The following information is summarized from the above references, except where noted.

The strata of the Selwyn Basin were deposited in a subsiding basin on the western margin of ancestral North America that was created by Late Proterozoic rifting of the Rodinian supercontinent. In the Mactung region (Figure 2), these strata comprise shale, siltstone and sandstone of the Proterozoic Yusezyu, Narchilla and Vampire formations, shale of the Cambro-Ordovician Gull Lake Formation, chert and shale of the Ordovician Elmer Creek Formation, and a succession of strata previously mapped as the Road River Group, comprising variably calcareous shale, mudstone, lime mudstone, and minor chert and skeletal limestone of a number of Middle Cambrian to Early Devonian formations as well as silty limestone and mudstone of the Cambro-Ordovician Rabbitkettle Formation. The Mackenzie Platform grew on the continental shelf, east and northeast of Mactung, comprising latest Proterozoic to Cambrian fluvial and deltaic sandstone, the Early Cambrian Sekwi Formation carbonate ramp and shelf, and numerous overlying carbonate- dominated units ranging to Middle Devonian in age. Deposition of Selwyn Basin and Mackenzie Platform strata was punctuated by episodes of crustal extension and mafic alkalic magmatism, including the incipient rifting that created the northwest-trending Misty Creek Embayment (Cecile 1982; Figure 2).

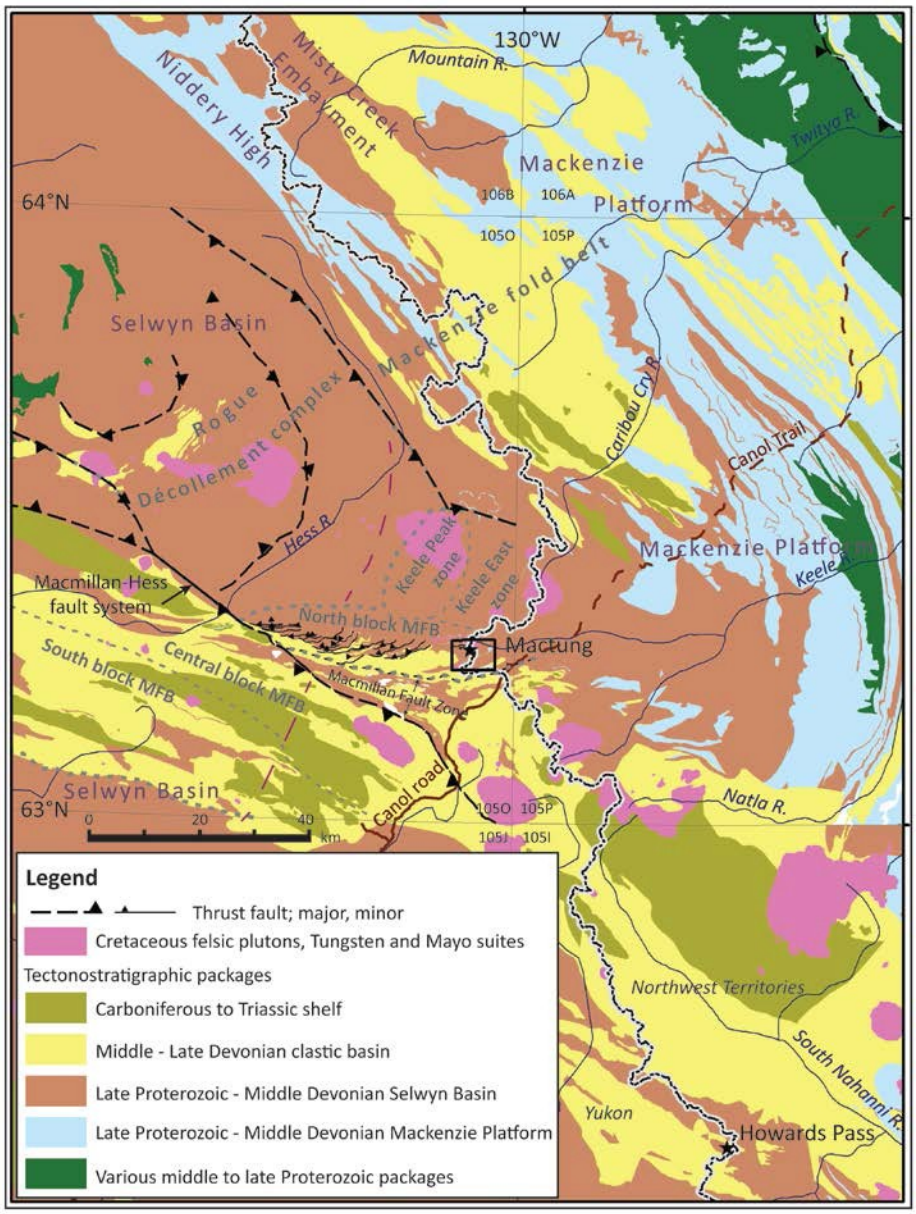


Figure 2. Regional geological setting of Mactung, showing major tectonostratigraphic packages and regional-scale thrust faults. Components of the Macmillan-Hess fault system are labelled. The grey lines are boundaries of structural domains, which are also labelled in grey: the North, Central and South blocks comprise the Macmillan Fold Belt (MFB) as defined by Abbott (2013); other domains are from Cecile (2000). The dashed magenta line separates plutons of the Tungsten suite, east of the line, from those of the Mayo suite (Hart *et al*. 2004). The black box around Mactung is the outline of the accompanying NWT Open File map (Martel *et al*. 2018). The dark purple labels are for paleogeographic features referred to in the text, including the southern end of the Misty Creek Embayment, and the Niddery High, a positive paleobathymetric feature that separated the embayment from the Selwyn Basin (Cecile 1982).

The Mactung deposit is hosted within the Sekwi and Rabbitkettle formations, in strata deposited on the slope of the Selwyn Basin in the Early Cambrian and the Ordovician. Although the Sekwi Formation is dominantly a platformal unit, it includes sediment gravity-flow deposits that came to rest on the slope.

In the Middle to Late Devonian, the region underwent extension, compression and transtension in response to initiation of orogenesis on the western and northern edges of the continent (Gordey and Anderson 1993; Nelson *et al.* 2013), and terrigenous clastic deposits of a foredeep basin came to blanket the former Selwyn Basin and Mackenzie Platform. Syn-depositional faults and aerially restricted volcanism mark a dominantly extensional regime in the Mactung area during this time (Abbott 1983; Cecile 2000). Chert, shale, sandstone, and chert-pebble conglomerate were deposited in submarine fans, interrupted by background muds and minor mafic volcanism. These rocks belong to the Portrait Lake, Prevost and other formations of the Earn Group (Abbott 1983, 2013; Gordey and Anderson 1993; Cecile 1996, 2000).

Northeast-directed folding and thrusting in the Jurassic and Cretaceous formed the existing arcuate mountain belt, which trends northwest and is convex to the northeast. Regional metamorphic grade is mostly sub-greenschist. Early Late Cretaceous felsic plutons were emplaced shortly after the main fold-and-thrust deformation. The plutons generated contact aureoles, and locally, skarn.

The Mactung deposit lies within a structural domain 60 km long that trends west- northwest, at variance to the regional grain, which is north-northwest (Abbott 1983, 2013; Cecile 2000). This variance was caused by the influence of Devonian faults on Mesozoic deformation (Abbott 1983). The west-northwest -trending domain is referred to as the Macmillan fold belt[1] (Abbott 1983), and consists of three sub-domains, of which only the North and Central blocks concern us here. The North Block, referred to as the Macmillan Zone by Cecile (2000), includes Mactung at its eastern end, and is characterized by closely spaced, south-southeast-directed, imbricate thrust faults (Abbott 1983; Figure 2). The Central Block is characterized by tight, upright folds, north-directed reverse faults, and steeply dipping tear faults in a complex pattern that is thought to derive from thickness changes in the Devonian clastic strata that are due to syn-depositional faulting (Abbott 1983). The two blocks (North and Central) are separated by a zone 5 km wide of dominantly north-verging thrust faults (Abbott 1983) whose western end links into the northwest-trending Macmillan-Hess dextral strike-slip fault system (Cecile 2000).

The timing of deformation in the Mactung area is constrained by the Early Norian (Late Triassic) age of the youngest deformed strata in National Topographic System (NTS) mapsheet 105O/NE, and the early Late Cretaceous age of felsic plutons that cut the older rocks and all fabrics (Cecile 2000). In other parts of the foreland fold-and-thrust belt, the compressional deformation is more tightly bracketed between the Early Jurassic and late

[1] Cecile (2000) applies the name Macmillan Fold Belt to a much larger domain. The usage of Abbott (1983) is adopted in this report.

Early Cretaceous (Staples *et al*. 2014; Gordey *et al.* 2011). Late transcurrent movement on strike-slip fault systems such as the Macmillan-Hess fault system, as well as re-orientation of fold axes, are attributed to the Laramide phase of the Cordilleran orogen (Cecile 2000). This phase postdates 92-91 Ma and is thought to be associated with mid-Cretaceous to Eocene transcurrent movement along the Tintina fault (Roddick 1967; Gabrielse *et al*. 2006).

## Local Geology from Previous Work

The Mactung deposit is exposed on the steep north face of Mount Allan (Figure 3), and consists of two scheelite-bearing skarn zones separated by 100 m of hornfelsed mudstone. The deposit is hosted in a Lower Paleozoic succession of mudstone and limestone that has been affected by metamorphism and metasomatic alteration associated with Late Cretaceous pluton emplacement. This section describes the geology as it is known from previously recorded information.

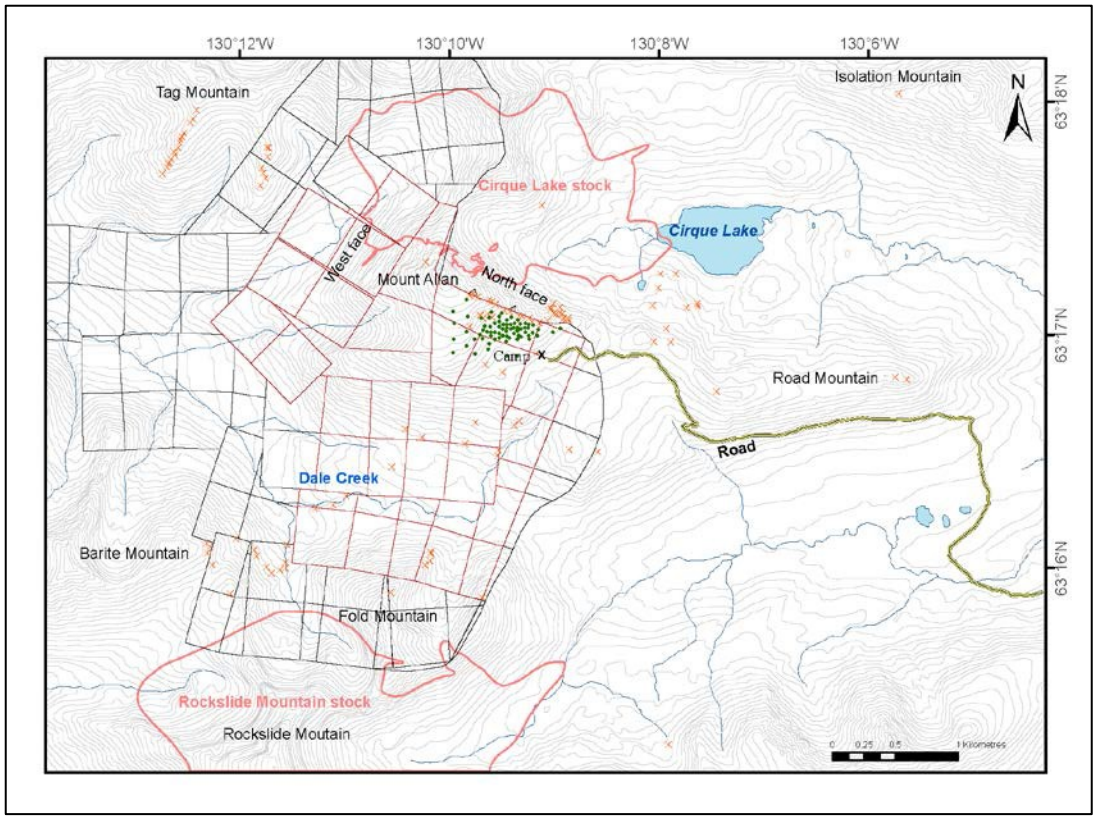


Figure 3. Key geographic features and felsic stocks in the area mapped for this project. Mountain, lake, and valley names are informal. Isolation, Road, Barite, and Tag mountains were named informally during this project; other features were named by Amax Inc. geologists. The Cirque Lake stock has also been referred to, in published literature, as the Mactung pluton. The line labelled as Road and highlighted in yellow represents an unmaintained trail. The green dots on Mount Allan represent drill collar locations, and the orange x's represent station locations from this project. The burgundy boxes outline the mineral leases and black boxes outline the mineral claims owned by the Government of Northwest Territories (http://mapservices.gov.yk.ca/GeoYukon/). Contours lines are 20 m apart.

## Stratigraphic Summary

The stratigraphy of the Mactung area is summarized in Table 1, which shows the units identified by exploration and mine geologists, as well as their formal counterparts The following summary is distilled primarily from Atkinson and Baker (1986), Harris (1977, 1980), Findlay (1969c), and this project. Descriptions of mineral assemblages are given by Gebru (2017) for samples of each unit taken from inside and outside the thermal metamorphic aureole and inside the skarn zone.

The oldest unit consists of Proterozoic to Cambrian, fine-grained terrigenous clastic rocks with minor greywacke (mine unit 1; Narchilla(?) Formation). A lower Cambrian limestone dominated by slump breccia of highly variable thickness (mine unit 2B; Sekwi Formation) hosts the Lower ore zone. This unit is intergradational with an overlying unit of middle Cambrian calcareous mudstone and mudstone (mine unit 3C; Hess River Formation) that is barren, and is in turn overlain sharply by a series of limestone debrites, calcareous sandstone, and mudstone (mine unit 3D; Rabbitkettle Formation, member D) that hosts the lowest horizon of the Upper ore zone. The overlying units are intergradational with member D and each other, and comprise interbedded mudstone and limestone that host the middle and uppermost horizons of the Upper ore zone (mine units 3E, 3F, and 3EF; Rabbitkettle Formation, members E, F, and EF). A resistant dolostone caps the ore-bearing succession (mine unit 3G; Rabbitkettle Formation, member G) and is overlain sharply by a reddish brown weathering mudstone to siltstone (mine unit 3H; Duo Lake Formation, Lower member) which is in turn overlain sharply by black, graptolitic shale (mine unit 4; Duo Lake Formation, Upper member). Rabbitkettle Formation is Early to Middle Ordovician aged in this region (Abbott 2013) and Duo Lake Formation is Ordovician to Early Silurian.

The Upper Silurian Steel Formation is a thin, regional marker unit of orange to grey weathering, light grey mudstone with characteristic centimetre-scale, dark, wispy structures identified as deformed burrows (Gordey and Anderson 1993). The Steel Formation was not recognized by mine geologists. The Upper Silurian to Lower Devonian Sapper Formation (mine units 8 and 9) consists of buff weathering, silty limestone and black calcareous shale. The youngest strata are a complex succession of shale and conglomerate (mine unit 10; parts of Portrait Lake Formation).

Table 1. Stratigraphic units in the Mactung area, correlating formally defined units and mine units. Member names are informal and from this project, except those of the Portrait Lake Formation, which are informal and defined by Abbott (2013). Map symbol refers to the accompanying NWT Open File map (Martel *et al*. 2018). The thicknesses in the map area are rough estimates of possible ranges, except for the Hess River Formation and Rabbitkettle Formation D, E, F, G members, which are from Atkinson and Baker (1986). Mine units 1974 and 1969 are from Harris and Godfrey (1974) and Findlay (1969a, b, c), respectively.

| Stratigraphic age | Unit name | Sub-unit name | Map symbol | Thickness in map area (m) | Mine unit 1974 | Mine unit 1969 | Lithology |
|---|---|---|---|---|---|---|---|
| **LATE CRETACEOUS** | | | | | | | |
| | Felsic dykes and sills | | Kgd | | 8 | 12 | Felsic dykes and sills |
| | Granitic stocks | | Kg | | 7 | 11 | Granitic (*sensu lato* ) stocks |
| **MIDDLE TO UPPER DEVONIAN** | | | | | | | |
| | Portrait Lake Formation | MacMillan Pass member | DPM-ss<br>DPM-sh | >100 | 6 | 10 | ss: Sandstone and shale, minor conglomerate.<br>sh: Shale and siltstone, minor conglomerate and sandstone. |
| **LOWER TO MIDDLE DEVONIAN** | | | | | | | |
| | Portrait Lake Formation | Niddery Lake member | DPN<br>DPN-b | 50-150 | 6 | 10 | Chert, argillite, shale, mudstone, minor bioclastic limestone.<br>b: Barite horizon. |
| **UPPER SILURIAN to MIDDLE DEVONIAN** | | | | | | | |
| | Sapper Formation | | SDS | 100 -200 | none | 8 | Silty limestone, black calcareous shale; mudstone at base; locally graptolitic. |
| | | bioclastic limestone | SDS-bl | | 5 | 9 | bl: Light grey crinoidal limestone. |
| **UPPER SILURIAN** | | | | | | | |
| | Steel Formation | | SS | 20-50 (possibly up to 100) | none | none | Mudstone to siltstone, wispy structures. |
| **LOWER ORDOVICIAN to LOWER SILURIAN** | | | | | | | |
| | Duo Lake Formation | Upper member | OSDu | 5-50 | 4 | 5 | Black, graptolitic shale. |
| | | Lower member | OSDl | 90-200 | 3H | 3H | Rusty weathering mudstone and siltstone, minor limestone. |
| **LOWER TO MIDDLE ORDOVICIAN** | | | | | | | |
| | Rabbitkettle Formation | G member | CORg | 20 | 3G | 3G | Calc-silicate hornfels and schist, minor marble; dolostone. |
| | | EF member | COREf | 50-120 | 3EF | 3EF | Mudstone, siltstone, minor limestone; locally metamorphosed. |
| | | F member | CORf | 30 | 3F | 3F | Mudstone, siltstone, hornfels, up to 40 % interbedded calc-silicate rock. |
| | | E member | CORe | 60 | 3E | 3E | Mudstone, siltstone, hornfels, up to 20 % interbedded calc-silicate rock. |
| | | D member | CORd | 20 | 3D | 3D | Phosphatic-clast sandstone to conglomerate; silty limestone. |
| **MIDDLE CAMBRIAN** | | | | | | | |
| | Hess River Formation | | CH | 100 | 3C | 3C | Mudstone, siltstone, hornfels. |
| **LOWER CAMBRIAN** | | | | | | | |
| | Sekwi Formation | | CS<br>CS-a | 20-50 | 2 | 2 | Limestone, silty limestone, limestone breccia, pale yellow mudstone.<br>a: Breccia facies. Limestone slump breccias and debrites, nodular silty limestone. |
| | | | CS-b | | 2B | 2B | b: Banded facies. Interbedded brown siltstone/hornfels and pale limestone/calc-silicate rock, minor breccia. |
| **PROTEROZOIC to CAMBRIAN** | | | | | | | |
| | Narchilla(?) Formation | | PCN | >200 | 1, 2-1 | 1, 2-1 | Phyllite, schist, meta-siltstone, minor meta-greywacke. |

## Magmatic Summary

Upper Cretaceous felsic plutons (mine unit 11) and dykes and sills (mine unit 12) have intruded and altered the stratigraphic rocks. Two granitic stocks are exposed in the map area. The 2.7 km x 1.4 km Cirque Lake stock (Figure 3) is an oval, southeasterly-elongate body underlying an area of 2.9 km$^2$ west of Cirque Lake, adjacent to the mineralized skarn on the north face of Mount Allan (Figures 3, 4, and 5; also called the Mactung and the Mactung North pluton; Anderson 1993; Gebru 2017). The Rockslide Mountain stock is a slightly larger body, the northern part of which is within the map area (Figures 3 and 4). This stock is referred to as the Mactung South pluton by Gebru (2017).

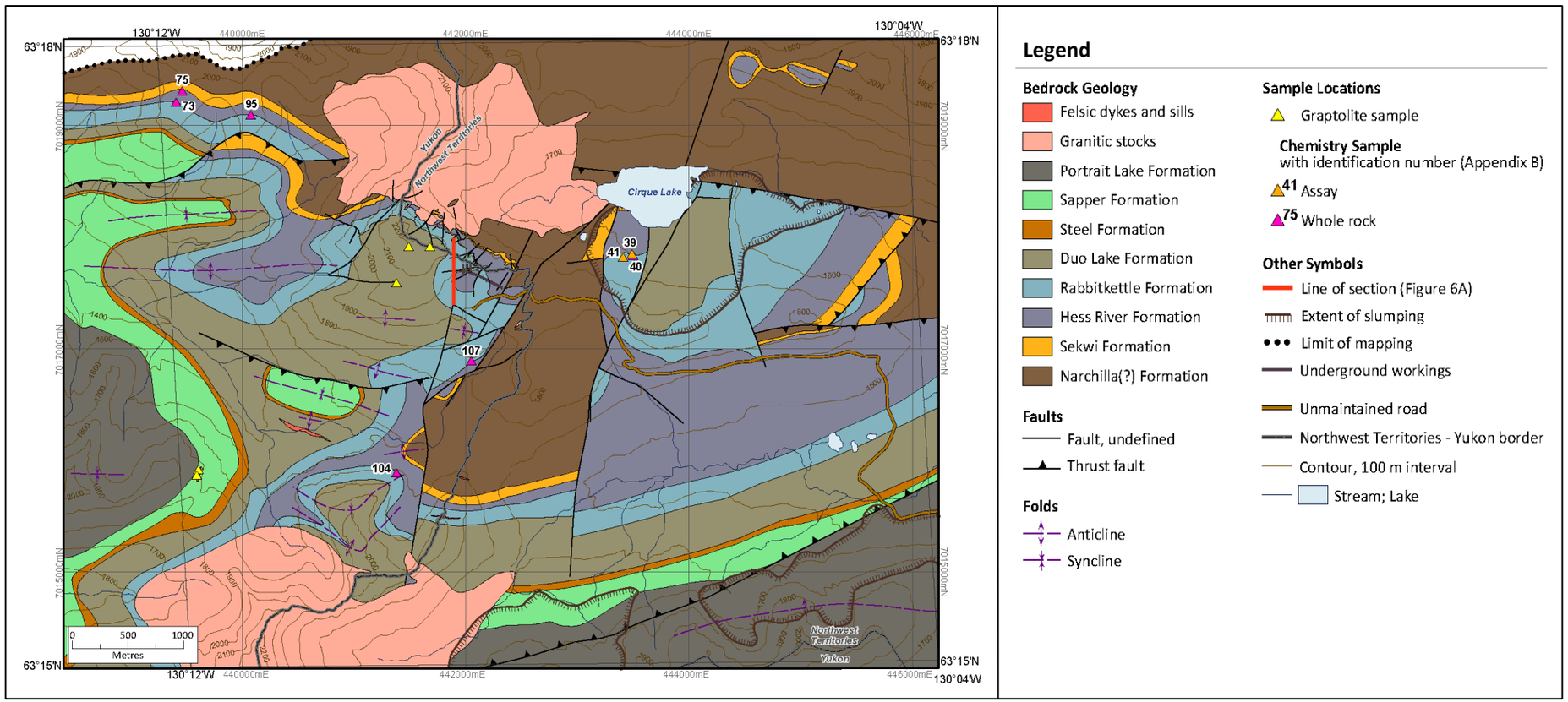


Figure 4. Simplified bedrock geology of the Mactung area. Known mineralization is within the Sekwi and Rabbitkettle formations south of the Cirque Lake stock. The adit is at the eastern end of the underground workings. Locations are shown for dated graptolite populations from the Duo Lake and Sapper formations, and for samples submitted for geochemical analyses (Appendix B). Contour lines are 100 m apart. Modified from accompanying NWT Open File map (Martel *et al.* 2018).

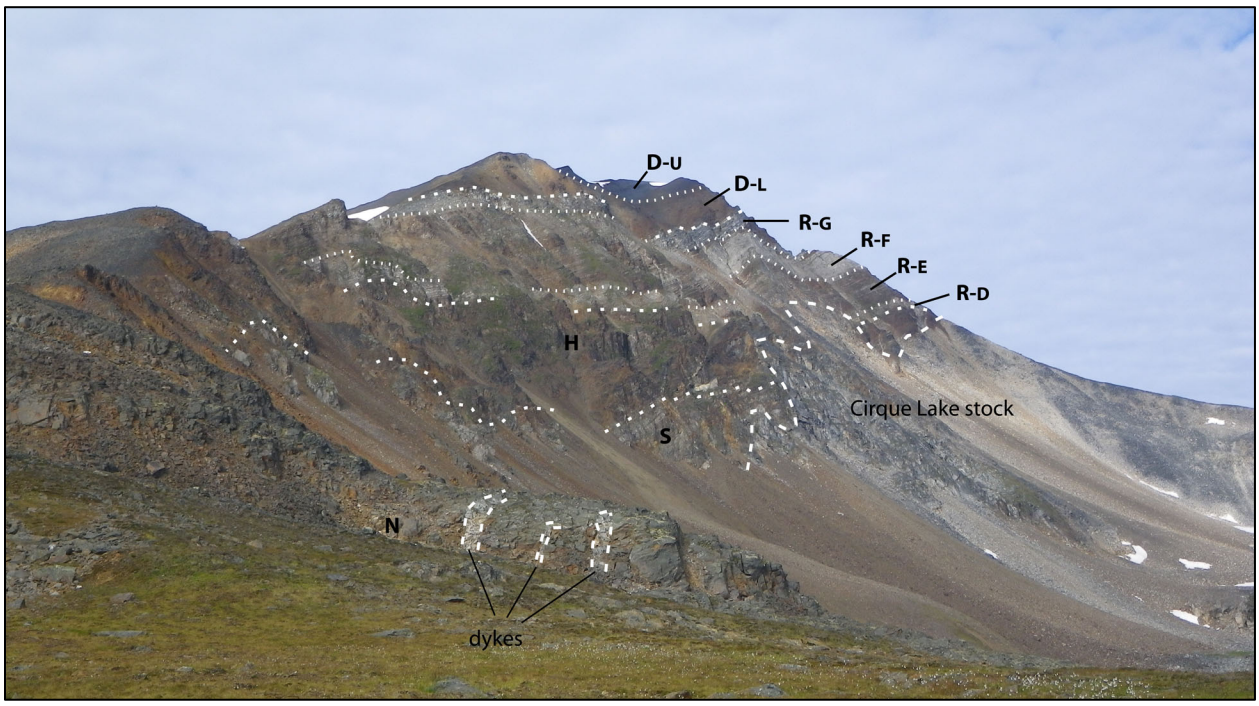


Figure 5. Looking west at the north face of Mount Allan, from a point south of Cirque Lake. Contacts are shown in white; longest dashes for intrusive contacts, medium for formation contacts, and shortest for member contacts. The low ridge in mid-ground is Narchilla Formation (N) cut by a few granitic dykes. The skylined saddle in the background, and the grey rock reaching halfway up the face, is granitic rock of the Cirque Lake stock. Strata on the face of Mount Allan are heavily altered to hornfels and skarn. The lowest light grey bands on the face are skarn of the Lower ore zone, belonging to the Sekwi Formation (S). Higher light-grey bands are skarn of the Upper ore zone, belonging to the Rabbitkettle Formation members D (R-D), E (R-E), and F (R-F). The highest, more resistant, blue-grey band is member G, the unmineralized top of the Rabbitkettle Formation (R-G). The two divisions of the Duo Lake Formation are clear above it: the rusty brown weathering Lower member (D-L) and the black, graptolitic Upper member (D-U). Between the ore zones is the brown weathering colour of the Hess River Formation (H).

The stocks at Mactung belong to the Tungsten plutonic suite, which forms a belt of plutons at the eastern end of the Tombstone-Tungsten gold belt (Figure 2; Mortensen *et al.* 1997; Hart *et al.* 2004; Rasmussen 2013). The three component suites of the belt were originally defined based on lithological characteristics and geographical distribution (Hart *et al.* 2004). Two of the three suites, the Tungsten and Mayo suites, are within the eastern Selwyn Basin near Mactung. Both of these suites consist of small, biotite-bearing, reduced, subalkaline intrusions containing accessory allanite, apatite and zircon. The two suites differ in that plutons of the Tungsten suite are ilmenite-bearing granite to monzogranite, weakly peraluminous, and may contain primary muscovite and accessory garnet or tourmaline, whereas those of the Mayo suite are titanite-bearing granodiorite to monzonite, metaluminous (to weakly peraluminous), and contain hornblende and clinopyroxene but no muscovite, garnet, or tourmaline (Hart *et al.* 2004). By of a variety of isotopic and geochemical evidence, Rasmussen (2013) interprets both suites to have derived by crustal anataxis of the same meta-igneous protolith, with the Tungsten suite comprising a smaller melt fraction or possibly deriving from a slightly more felsic source. The metallogenic associations of each suite, once believed to be distinct (Hart *et al.* 2004), are now known to

overlap (Rasmussen 2013). Plutons of both the Tungsten and Mayo suites are spatially associated with Ag-Pb-Zn bearing veins, and Bi-Te-As-Sb enrichments. Plutons of the Mayo suite are associated mainly with gold, including intrusion-related Au- Bi-Te-W in sheeted quartz-feldspar veins, Au ± W skarns, Au-As in quartz veins cutting intrusions and country rocks, but also with tungsten skarns and tin greisens. Plutons of the Tungsten suite are associated mainly with tungsten skarns, but small enrichments of tin, molybdenum, and gold are present around some.

The Cirque Lake stock is a multi-phase, (garnet-) muscovite-biotite granite with margins that are chilled against the sedimentary country rock. The stock comprises three mutually intergradational and locally cross-cutting phases (Harris and Godfrey 1975): a porphyritic phase, an equigranular phase, and an aplitic phase. The porphyritic or megacrystic phase consists of granite, quartz syenite, and quartz monzonite containing 7% to 20% megacrysts 1 cm to 4 cm long of alkali feldspar and local phenocrysts of quartz and biotite up to 5 mm (Anderson 1983, 1993; Harris and Godfrey 1975; Gebru 2017). This porphyritic phase is cut by a massive, medium-grained, equigranular phase consisting of granite and minor granodiorite. Both lithologies of this equigranular phase are cut by aplitic quartz syenite (Anderson 1982). Gebru (2017), on the other hand, identifies four phases: a biotite-poor leucogranite phase interpreted as an S-type granite that interacted with host rocks during emplacement; a chemically homogeneous biotite granite with an I-type, arc-like composition; and an "undivided granite" and a plagioclase-rich granodiorite, both thought to derive from high-temperature, metasomatic alteration of the biotite granite. The leucogranite phase is present on the northwest and southeast margins of the Cirque Lake stock, and in dykes cutting the southeast margin. The distribution of the other phases was not determined.

Accessory minerals of the Cirque Lake stock visible in hand specimen are muscovite, garnet, andalusite, and locally tourmaline. Minerals visible in thin section include apatite, zircon, monazite, allanite, and scheelite (Anderson 1993; also, Harris (1980) mentions fluorite). Tourmaline coats fractures in the stock, forms halos around dykes and quartz veins in the country rock (Atkinson and Baker 1986), and accompanies quartz in veins that cut the stock (equigranular and porphyritic phases) as well as the hornfelsed country rock. Sheeted veins of quartz-tourmaline-muscovite-arsenopyrite-pyrite-stibnite invade parts of the equigranular phase of the Cirque Lake stock; a sample of one of the veins contained elevated amounts of Au, Bi, W, As, Sb, Cu, Pb, and Zn (Baker and Lang 2001). The stock itself, however, is minimally altered (Gebru 2017).

Felsic dykes are mineralogically similar to the Cirque Lake stock and include porphyritic, massive, aplitic and locally pegmatitic phases, the latter associated with quartz veins (Anderson 1993; Atkinson and Baker 1986). Leucocratic aplite dykes south of Mount Allan have a higher anorthosite content of plagioclase than the leucocratic phases of the Cirque Lake stock (Gebru 2017). Gebru (2017) describes dykes of plagioclase-rich granodiorite and biotite granite cutting the ore zone, and dykes of muscovite-tourmaline leucogranite cutting the southeast margin of the Cirque Lake stock. The Rockslide Mountain stock is at least locally a biotite granite (Gebru 2017). The stock has not been studied in detail; other phases may be present.

On the basis of mineral chemistry and Sm-Nd and Rb-Sr isotopic data, Gebru (2017) infers that the granitic rocks at Mactung derive from a strongly reduced, I-type magma generated by partial melting of old continental crust, which is consistent with Rasmussen's (2013) conclusion that the Tungsten suite derived from crustal anataxis. The less-evolved biotite granite has arc-like chemistry, whereas the leucogranite was sourced from anatexis of buried supracrustal material (Gebru 2017). The biotite granite is estimated to have begun crystallization at depths of 22 km or more, and to have crystallized muscovite at about 15 km, whereas muscovite in the leucogranite crystallized at much shallower depths of 7 km to 8 km.

## Structural Summary

Bedding on the property dips 10° to 40° to the south and strikes northwest (Harris and Godfrey 1975; Harris 1977). Both of the mineralized skarn zones (the Lower and Upper ore zones) dip gently to the south, concordant with bedding. A north- verging, recumbent, tight Z-fold (looking west) has been identified in the Lower ore zone by drilling and underground mapping (Figure 6; Harris and Godfrey 1975; Harris 1980). This fold has elevated the southern limb of the ore zone 60 m with respect to the northern, lower limb (Harris 1977; Figure 6A). The fold plunges gently to the west at the west end of the deposit, and gently to the east at the eastern end (Atkinson and Baker 1986). The ore zone in the central section of the fold is only one metre at the thinnest point (Harris 1977). According to Atkinson and Baker (1986, page 236), "thickening of Unit 2B in hinge zones and abrupt attenuation in the intermediate asymmetric limb are indicative of plastic deformation. …Although this structure is considered a systematic part of the regional strain pattern, it may have resulted, at least in part, from soft sediment stresses." Drill data are insufficient to ascertain if the Upper zone is also folded, but most drawings from the literature show a fold in the Upper zone that is more open than that in the Lower zone (Harris and Godfrey 1975; Harris 1977, 1980; Dick and Hodgson 1982). Some small folds and numerous crenulations on the property plunge 5° to 10° southwest (Harris 1980). Gebru (2017, Chapter 6.4.4) has attributed the structures observed on the property to four, and possibly five, distinct deformation events.

A broad, open syncline at the head of Dale Creek valley, between the Cirque Lake pluton and the Rockslide pluton, is thought to have resulted primarily from doming caused by intrusion of the plutons (Figure 3; Harris and Godfrey 1975). A regional, north-verging thrust fault strikes east just north of the deposit and does not appear to offset the Cirque Lake stock (Abbott 2013). Two main sets of normal faults, an older, north-side-down set that trends east and a northeast-trending set with west side down, both cut intrusive contacts (Atkinson and Baker 1986). The faults also post-date skarning and displace contacts from 1 m to 45 m (Harris 1980).

## Alteration Summary

The history of metamorphic, metasomatic, and retrograde alteration at Mactung is summarized by Atkinson and Baker (1986), and the metasomatic alteration is also described by Harris (1977, 1980), Atkinson (1982), and Dick and Hodgson (1982). A recent dissertation addresses both the metamorphic and metasomatic alteration (Gebru 2017). Tungsten mineralization, which occurred during the metasomatic event, is discussed separately.

## *Regional and Contact Metamorphism*

Deformation and regional metamorphism associated with Jurassic to Cretaceous orogeny produced biotite and generated micaceous foliations in fine-grained terrigenous rocks, and converted carbonate rocks to marbles with cleavage (Atkinson and Baker 1986). Mineral assemblages suggest a temperature of 420 °C was attained during regional metamorphism (Gebru 2017). The Late Cretaceous intrusion of plutons produced the following thermal metamorphic effects in different rock types: biotite ± andalusite ± cordierite hornfels in terrigenous mudstones, calc-silicate hornfels in calcareous mudstones, and a coarsening of grain size and local garnet growth in marbles (Gebru 2017; Atkinson and Baker 1986). Contact metamorphic temperatures of 635 °C to 813 °C were estimated using various mineral assemblages and the plagioclase-amphibole geothermometer (Gebru 2017).

## *Metasomatic Alteration*

Metasomatic alteration subsequent to the contact metamorphism was also dependent on rock type: skarns of various types developed in the limestone, marble, and calc-silicate hornfels, whereas in the terrigenous hornfels, there was bleaching, invasion of quartz veins, and growth of distinctive biotite clots, especially in Narchilla(?) Formation just below the Sekwi contact (Atkinson and Baker 1986).

### Hornfels

Quartz veins in the hornfels contain variable amounts of calcite, dolomite, pyrrhotite, tourmaline, and scheelite (Harris 1980), and the bleached halos commonly contain pyroxene-garnet (Harris 1980). The removal of sulfides and carbonaceous matter from the mudstones and the addition of calcium was concurrent with the removal of calcium from the carbonate rocks, which created a zonation in both the mudstones and carbonate rocks (Dick and Hodgson 1982). In the mudstones, the zonation is from unaltered hornfels to so- called light brown hornfels, in which carbonaceous material has been lost, through dark brown hornfels to green hornfels, marked by progressive losses of muscovite, K-feldspar, and rutile, and formation of amphibole, pyroxene, titanite and plagioclase (*ibid*.).

### Skarn

Metasomatic alteration at Mactung is expressed predominantly as exoskarn: it is best developed in the country rock. Within the granitic stock, skarn-related alteration is restricted to minor sulfidation, formation of pyroxene and titanite, and quartz veins (Gebru 2017). The best-developed skarns, including skarns in the Upper and Lower ore zones, are exposed on the north face of Mount Allan (Figure 3) and extend southward beneath Mount Allan (Atkinson and Baker 1986). The Lower ore zone pinches out about 360 m south of the north face (Harris 1977). The surface area of hornfelsed rock on existing maps (*e.g.,* Findlay 1969a; Harris and Godfrey 1974) is roughly one square kilometre, however, findings from this project suggest that a larger area has been affected, and Gebru (2017) infers a larger area of contact metamorphism based on the widespread occurrence of calcic plagioclase in Narchilla(?) Formation.

The skarn-altered rocks of the Lower ore zone can be classified based on colour (light green, dark green, and brown), grain size (fine grained and fine-to-medium grained), and mineralogy (Atkinson and Baker 1986; Harris 1977; Dick and Hodgson 1982; Gebru 2017). The intensity of metasomatic alteration increases across a series of intergradational zones, from bleached limestone on the eastern periphery of the deposit, through scheelite-poor pyroxene-marble skarn to scheelite-bearing pyroxene skarn and finally to scheelite-rich pyrrhotite-pyroxene skarn in the core of the deposit (Atkinson and Baker 1986; Atkinson 1982; Harris 1977, 1980). The Lower ore zone is about 70% pyroxene skarn and 10% pyrrhotite-pyroxene skarn (Harris 1980), with minor amounts of other skarn types and up to 20% barren, grey marble skarn in blocks up to 3 m wide consisting entirely of calcite (Atkinson 1982). The pyrrhotite-rich core of the zone occupies part of the upper limb of the Z-fold in Sekwi Formation under the east end of Mount Allan (Figure 6A). Adjacent to the core zone is pyroxene skarn, which grades eastward into pyroxene-marble skarn (Harris 1980; Narisco 2009). No description of zonation is available for the Upper ore zone, although Narisco (2009, Figure 7-1) implied that the zonation is present in the Upper ore zone as well.

The name of each skarn type in the detailed descriptions below is emphasised in bold font. The limestone or calc-silicate rock of the outermost **bleached skarn** zone (Atkinson and Baker 1986) was "bleached" by the removal of carbonaceous matter and sulfides (Dick and Hodgson 1982). The **pyroxene-marble skarn** consists of fragments of barren marble in a calc-silicate matrix made of fine-grained, green pyroxene, tremolite, ±garnet, remnant calcite, minor scheelite, and trace pyrrhotite (Atkinson and Baker 1986; Atkinson 1982; Harris 1977, 1980). Wollastonite may also be found in the pyroxene-marble skarn (Gebru 2017). **Pyroxene skarn** is the dominant skarn in the Lower and Upper ore zones, and consists of fine-grained (locally medium- to coarse-grained), dark green pyroxene, quartz, <15% pyrrhotite, minor scheelite, chalcopyrite, garnet, and remnant calcite, and traces of wollastonite, tremolite and sphene (Atkinson and Baker 1986; Atkinson 1982; Harris 1977, 1980). The most altered skarn is **pyrrhotite-pyroxene skarn**, which is coarser grained and carries the best scheelite grades. Pyrrhotite-pyroxene skarn consists of fine- to medium-grained quartz, pyroxene, 15% to 50% pyrrhotite, scheelite, and minor chalcopyrite. Although the pyrrhotite-pyroxene skarn appears massive, relict banding and breccia fragments are outlined by concentrations of scheelite. Wollastonite is mostly restricted to the Upper ore zone. Anorthic plagioclase, which accompanies quartz, apatite that is associated with scheelite, and titanite and rutile are also present in the skarn (Gebru 2017).

**Garnet skarn** consists of veins and pods within the limestone up to 1.5 m long of red garnet, minor quartz, and local traces of scheelite. Atkinson and Baker (1986) assign garnet skarn to an outer zone, whereas Harris (1977, 1980) and Atkinson (1982) indicate that it forms isolated patches within other skarn types. Gerstner *et al.* (1989) and Dick and Hodgson (1982) interpret garnet skarn to result from chemical variations in the protolith, based on fluid-inclusion studies and petrology, respectively. Gebru (2017) identifies garnet as an early metasomatic product that was destroyed progressively during pyroxene formation. **Quartz skarn** or cherty skarn was generated by quartz flooding of pre-existing skarn. Atkinson and Baker (1986) describe the quartz skarn as pods and rootless veins of milky quartz with large scheelite crystals and high grades of $WO_3$. Coarse-grained scheelite has developed adjacent to the veins (Atkinson and Baker 1986). Harris (1977, 1980) describe quartz skarn as hard,

microcrystalline, light green rock made of quartz, pyroxene, and minor garnet, pyrrhotite, and scheelite. **Skarn veins** of pyroxene-garnet ± calcite ± quartz cut both calc-silicate rock and hornfels within the skarn zones. Calcite veins with clay alteration halos cross-cut the quartz and other skarn types.

**Hydrous skarn**, represented by isolated masses of coarse-grained amphiboles, or of biotite, and minor **chlorite skarn** have been interpreted as products of retrograde alteration based on spatial relationships (Harris 1980; Atkinson and Baker 1986 for the amphibole skarn). Later work, however, failed to support this idea. Spatial relationships and petrological evidence were found to suggest that chemical variations controlled the formation of the biotite skarn (Atkinson and Baker 1986; Dick and Hodgson 1982; Gebru 2017). Gerstner *et al.* (1989) similarly invoked chemical variations in the host rock to control skarn mineralogy, based on inferences from fluid-inclusion studies, and Gebru (2017) showed that amphibole formation preceded pyroxene formation.

Fluid-inclusion results have been interpreted to mean that the bulk of the pyroxene skarn formed at 410 °C to 480 °C, and that garnet, amphibole, some of the biotite, and more pyroxene formed as fluid temperatures fell through 430 °C to 350 °C (Gerstner *et al.* 1989). All of those temperatures are deemed to be retrograde by Gebru (2017), who estimated that temperatures during prograde skarn formation ranged from 512 °C to 675 °C. The pressure at which the Mactung skarn formed has been estimated at 2.1 kbar to 2.5 kbar using fluid inclusion and mineral assemblage data (Gerstner *et al.* 1989) and at 2 kbar (7 km to 8 km depth) using iron-in-sphalerite and aluminum-in-hornblende geobarometry (Gebru 2017).

## Mineralization Summary

The main commodity at Mactung is tungsten, however anomalous copper (Atkinson and Baker 1986), gold (Baker and Lang 2001; Gebru 2017) and bismuth (Gebru 2017) are present. Resources of tungsten are given in the Introduction, and results of a resource study commissioned by NTGS are provided in Appendix A.

Tungsten is hosted mainly in scheelite. Wolframite (as ferberite) is a minor component of the ore, replacing scheelite during late quartz flooding or retrogression (Dick and Hodgson 1982). Scheelite is present as disseminations in the skarned rock, as coarse grains in selvages mantling quartz veins or in fractures cutting them (Gebru 2017), and concentrated along bedding planes and around clasts in the pyrrhotite-pyroxene skarn (Atkinson and Baker 1986). Scheelite is associated with pyrrhotite, minor chalcopyrite, and very minor sphalerite and molybdenite (Dick and Hodgson 1982; Atkinson and Baker 1986; Selby *et al.* 2003). The best grades have been found in the quartz skarn (commonly >5% $WO_3$) and in the pyrrhotite-pyroxene skarn (to 1.5% $WO_3$ and to 0.2% Cu; Atkinson and Baker 1986). Good grades are present in the pyroxene skarn (>1% $WO_3$), whereas garnet-pyroxene skarn averages less than 1% $WO_3$, and garnet skarn contains only traces of scheelite. The summary provided by Narisco (2009) and the studies of Gebru (2017) agree that scheelite grains are markedly smaller in the pyrrhotite-pyroxene skarn than in the pyroxene skarn, which implies that the former would provide poorer scheelite recovery, however Atkinson and Baker (1986) noted that scheelite grains are coarser in the pyrrhotite-pyroxene skarn than in the other skarn types, thus there may be some variability in scheelite grain size within a single skarn type.

Atkinson and Baker (1986) also noted that coarse scheelite is commonly present wherever biotite is associated with quartz or pyrrhotite. Scheelite was precipitated in two stages (Gebru 2017). Early scheelite and pyroxene formed at temperatures of 550 °C to 650 °C, based on mineral compositions and assemblages. The second stage of scheelite formation was co-eval with pyrrhotite overprinting, but neither stage was dependent on sulfidation (*ibid*.).

Copper is hosted by chalcopyrite, which is intimately associated with pyrrhotite. Chalcopyrite is more abundant in the Lower ore zone than in the Upper ore zone (Gebru 2017). Copper and gold mineralization were controlled by sulfidation (Gebru 2017).

Gold values in the deposit are erratic and do not correlate with tungsten values, although tungsten-rich ore locally contains up to 1.74 g/t Au (Gebru 2017). Gold correlates directly with bismuth, and is present within native bismuth and, to a lesser extent, within tellurium-bearing bismuth phases, both of which are among the latest, retrograde additions to the skarn (Gebru 2017). The presence of sheeted quartz veins in some Tungsten-suite plutons similar to those hosting gold in association with Mayo-suite plutons, as well as the similarity of the Au-As-W-Sb±Bi geochemical signature in stream sediments coming from plutons of both suites, has led to speculation that the Tungsten suite may be prospective for gold (Mortensen *et al.* 1997; Baker and Lang 2001). The importance of gold in the Mactung deposit has never been systematically examined, however the sulfide-rich skarn of the Lower ore zone was sampled on the adit walls at 5-m intervals, where it was demonstrated to contain an average 0.38 g/t Au over an estimated true thickness of 25 m to 35 m (Gebru 2017). A sample from sheeted quartz veins cutting the Cirque Lake stock returned 110 ppb Au, as well as 2560 ppm Cu, 1440 ppm Pb, and As and Sb in excess of detection limits of 10 000 ppm and 1000 ppm respectively (Baker and Lang 2001).

Early speculations on the source of ore-forming fluids at Mactung were that the fluids derived from the Cirque Lake stock (*e.g.,* Harris 1977). Fluid inclusion studies show that the mineralizing fluids were highly reduced, and confirm a magmatic source (Baker and Lang 2001), with a sedimentary influence suggested by high sulfur-isotope ratios ($\delta(^{34}S/^{32}S)$; Gebru 2017). Examination of field relationships suggested to Atkinson and Baker (1986; Figure 6A) that the source pluton could not be the Cirque Lake stock and must be buried south of the ore zones. The following observations were key to this conclusion: no ore is developed in contact with the stock; metasomatic alteration zones are not parallel to the stock edges; metasomatic alteration within the stock margin is rare, even near the ore zones; pegmatite and other felsic dykes are abundant in deep drill holes south of the deposit, implying a source that is yet deeper; and the stock has steeply dipping contacts adjacent to the ore, and an apex, where ore fluids would be expected to accumulate, hundreds of metres up-dip from the ore zones (*ibid*.).

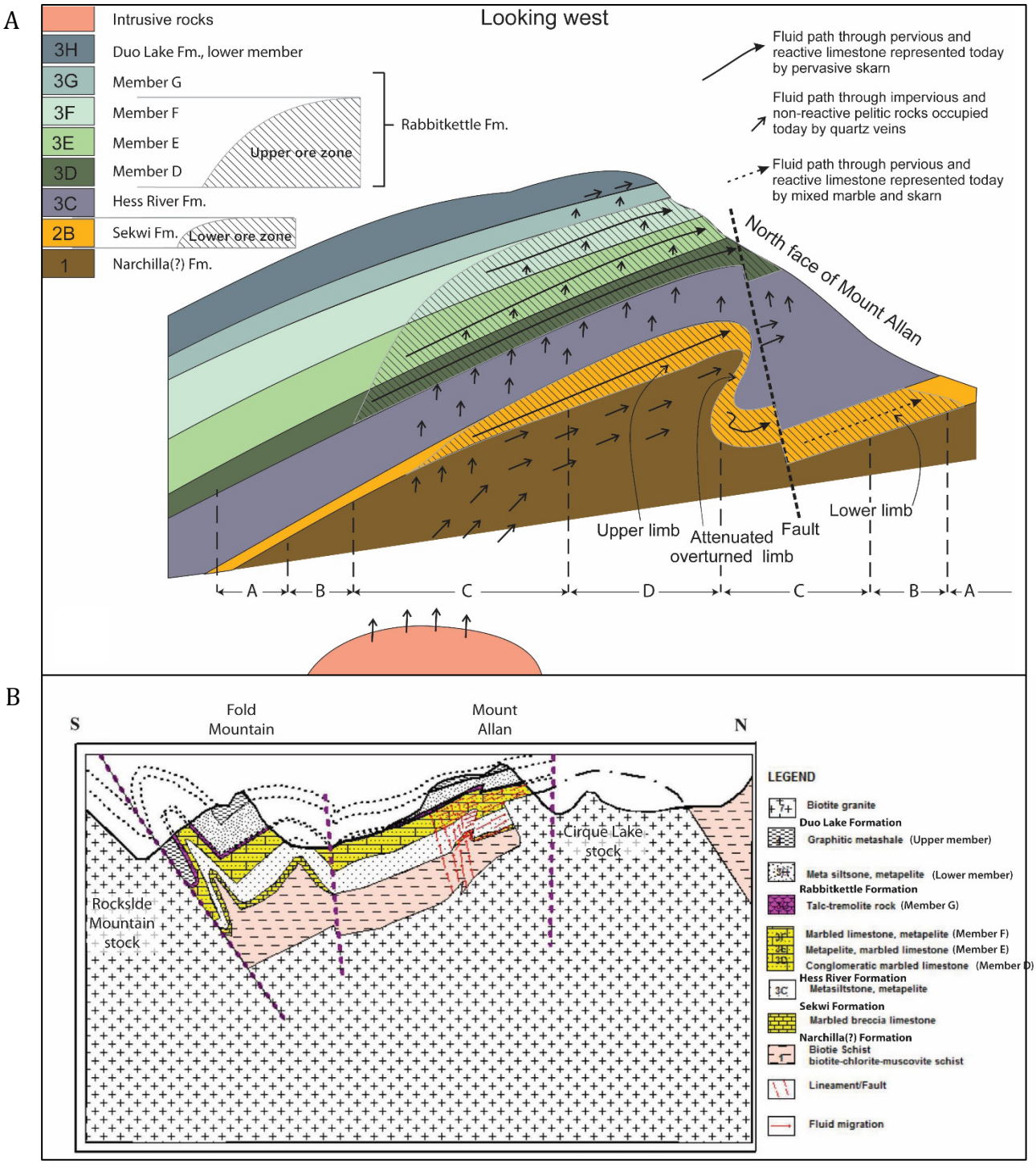


Figure 6. Mineralization models for Mactung, showing hypothetical migration patterns of metasomatic fluids on schematic cross-sections looking west. [A] Mineralizing fluids arise from an undiscovered pluton presumed to lie buried south of the deposit. Note the Z-fold in the Sekwi Formation. The alteration zones A to D within ore-bearing units (the Sekwi Formation and members D, E and F of the Rabbitkettle Formation) are as follows: A = Marbles variably bleached and cross-cut by garnet and garnet-pyroxene skarn, B = Garnet-pyroxene skarn (local remnant

bleached marble), C = Pyroxene skarn, no remnant marble, D = Pyrrhotite-pyroxene skarn, no remnant marble (Narisco 2009). Drawing from Atkinson and Baker (1986) except zones from Narisco (2009) and stratigraphic names and colours from this project. Presumed location of section is shown on Figure 4. [B] Mineralizing fluids arise from the Cirque Lake stock, which joins the Rockslide Mountain stock underneath the Mactung deposit. Cross-section extends from north of the Cirque Lake stock to the north face of Rockslide Mountain in the south, presumably at about the same easting as the section in [A]. After Gebru (2017). Fm = Formation.

Gebru (2017; Figure 6B) shows that the biotite granite of the Cirque Lake stock, skarn, and mineralization were essentially co-eval, and proposed that this phase of the Cirque Lake stock is the source of the mineralizing fluids. He suggests that the stock extends south under the ore zones, where the contact becomes shallowly dipping, and may even join with the Rockslide Mountain stock at depth. Faults and fractures formed by doming as the stock was emplaced may have been utilized as pathways by the mineralizing fluids, which had separated from the source pluton prior to emplacement (Gebru 2017). Regardless of the source pluton, the mineralizing fluids rose from directly beneath Mount Allan.

## Geochronology

Isotopic ages for intrusive and other thermal events at Mactung are compiled in Appendix C. Early work generated K-Ar dates of 89-90 Ma, with errors of 1-4 Ma, for biotite from the Cirque Lake stock and muscovite from a nearby monzogranite dyke (Hunt and Roddick 1987; Anderson 1993). Recent Ar-Ar ages for biotite and muscovite from the Cirque Lake and Rockslide Mountain stocks and two felsic dykes range from 91.8 to 98.1 Ma (± 0.3-2.0 Ma; Gebru 2017), overlapping with U-Pb zircon ages of crystallization for the stocks and dykes, which range from 92.1 to 97.6 Ma (± 0.1-0.4 Ma; Selby *et al.* 2003; Gebru 2017). The youngest published age for the granitic rocks, 92.1 Ma, is from a late leucogranite phase of the Cirque Lake stock (Selby *et al.*, 2003). The other ages, including one from the Rockslide Mountain stock, one from an aplite dyke in Dale Creek valley, two from the Cirque Lake stock, and one from a dyke adjacent to the Cirque Lake stock, all fall within a narrow range from 97.1 to 97.6 Ma (Gebru 2017). Two dates for the mineralization and two for the skarning also fall within this range: 97.2 ± 0.2 Ma for the mineralization by Re-Os of molybdenite from a skarn-related quartz vein (Selby *et al.* 2003), 97.1 ± 4.1 Ma by U-Pb of titanite from the skarn (Gebru 2017), and 97.1 to 97.6 Ma (± 0.6-1.9 Ma) for biotite in the hornfels by Ar-Ar methods (Gebru 2017). A younger date of 89.9 Ma was obtained for biotite in the skarn (Gebru 2017). Additional Re-Os ages were obtained from molybdenite in quartz veins cutting the Cirque Lake stock and the hornfels on the north face of Mount Allan; these Re-Os ages are older, ranging from 99.1 to 100.7 Ma (± 0.4-3.5 Ma) with the large variation in ages ascribed to $^{187}$Os or $^{187}$Re heterogeneity in the sample grains (Gebru 2017).

The geochronology data have been interpreted as follows (Gebru 2017; Rasmussen 2013): The Cirque Lake and Rockslide Mountain stocks were emplaced largely at about 97 Ma, essentially concurrent with skarning and mineralization. Cooling of the stocks lasted for at least 1.5 m.y. and possibly 3.0 m.y. Emplacement of a leucogranite phase at 92 Ma re-set the Ar-Ar chronometer and extended the total duration of the magmatic system to between 5 and 6 m.y. The younger dates from muscovite and biotite reflect this younger thermal event (or series of events). Gebru (2017) discards the older Re-Os dates, and interprets one date that is

sensitive to assumptions on initial osmium ratios as a maximum age of 97.3 Ma for granite intrusion and sulfide mineralization (Appendix C).

# Methods

Existing bedrock geology maps were used as a basis for validating and updating geological interpretations. The maps used were:

- Abbott's (2013) 1:50 000 scale map of NTS 105O/1, 105O/2, the southern half of 105O/8, and parts of adjacent sheets;
- Cecile's (1996) 1:50 000 scale map of the northern half of NTS 105O/8 and points north; and
- A number of unpublished maps of the property, at scales from 1:2400 to 1:15 840, by Amax geologists (mainly Lodder and Harris 1974; Harris and Godfrey 1974; Findlay 1969c; to a lesser extent, Findlay 1969a, b).

Government maps were scanned and georeferenced. Industry maps, already digital, were georeferenced as accurately as possible, but discrepancies between the base topographic datasets of the 1970s and today are significant in places.

A two-person team visited outcrops on Mount Allan and a number of nearby areas (Figure 3) between July 31 and Aug 10, 2016, with the assistance of a helicopter for three of those days. A number of samples were collected, some of which were thin sectioned. Two samples of rusty mudstone were sent for assay and six samples of phosphatic rock were sent for geochemical analyses. Stratigraphic ages were interpreted from graptolite populations in a number of samples by M. Melchin at St. Francis Xavier University (Nova Scotia).

Names of geographic and features and plutons are largely informal names taken from existing company reports. Precedence is given to the names first used. Named features are located on Figure3. The names of Barite, Tag, Isolation, and Road mountains were assigned during this project.

# Results

The updated bedrock geology is published in an accompanying NWT Open File as a PDF map at 1:10 000 scale and a geographic information system (GIS) database (Figure 4; Martel *et al.* 2018). Bedrock exposure ranges from absent on broad valley floors, through poor on gentle slopes, to good on steep slopes. Figure 5 shows the well-exposed north face of Mount Allan, including the major stratigraphic units from the Narchilla(?) Formation to the Duo Lake Formation. South of Cirque Lake, large exposures of rock on gently sloping land have been displaced by slumping (Figure 4).

Pre-existing maps were found to be largely reliable. The presence of calc-silicate rock and minor marble interstratified with the slump breccias and debrites of the Sekwi Formation on the southern spurs of Tag Mountain, as well as overlying them, suggests that the contact-metamorphic hornfels zone extends over a kilometre farther west than the western boundary of the mine map. Open Z-folds at centimetre to decametre scale on the north face of Mount Allan (Figure 7) are compatible with the tight Z-fold inferred by mine geologists to have affected the Lower ore zone.

Figure 7. Looking west at the north face of Mount Allan, from a point south of Cirque Lake. Bedding form lines in yellow highlight open Z-folds. Yellow star shows the location at which photos in Figures 9Q and 23E were taken. The part of the face in this photo is about 200 m to 300 m high.

## Resource Model

A three-dimensional digital model of the Mactung deposit, including solids for the ore zones in the Sekwi Formation and members D, E, and F, was created by member G. Kirkham using data from 249 drill holes (Appendix A). The exercise was conducted primarily to ensure the completeness of the digital database. Further aims of the study were to calculate quantities and grades using a combination of open pit and underground mining approaches that would optimize the extraction of tungsten without the influence of political and economic

constraints. This contrasts with the most recent published resource calculations for Mactung (Narisco 2009), which consider only an underground mine utilizing a combination of long-hole blast and mechanized cut-and-fill mining methods. A final aim of the Kirkham study was to test the sensitivity of the resource model to the selection of cut-off grade.

The reader is cautioned that the values in Appendix A and this paragraph should not be misconstrued as a "Mineral Resource" or "Mineral Reserve" for National Instrument 43-101 purposes. The tonnage and grade of the calculated mineral resource are sensitive to the selection of cut-off grade, which is shown by presentation of resource estimates for cut-off grades ranging in increments of 0.1% from 0% to 1.0% $WO_3$ (Appendix A). For a cut-off grade of 0.5%, Kirkham has estimated an indicated resource of 14.0 Mt at 1.008% $WO_3$ and 0.082% Cu, and an additional inferred resource of 3.4 Mt grading 0.81% $WO_3$ and 0.06% Cu.

## Stratigraphy

The correlations made in this study of mine units with formally defined stratigraphic units largely agree with pre-existing correlations by mine geologists (Table 1). Details of the correlations are discussed by unit, below. Each unit description begins with a summary of previously available information, and then continues with observations made during the 2016 field program. Where relevant, observations from the field program are divided into those made of the unaltered rock and those made of the hornfels and skarn in that unit.

In contrast to previous work, the oldest strata are assigned to Narchilla(?) Formation instead of Vampire Formation, and not only mine unit 4 but also mine unit 3H is assigned to the Duo Lake Formation. Steel and Sapper formations were identified on the south face of Mount Allan and on Tag Mountain. Intervals of calc-silicate rock and patches of skarn in the Sekwi Formation on Tag Mountain suggest that the extents of both hornfels and skarn are greater than shown on previous maps. A view of the north face of Mount Allan from near Cirque Lake (Figure 5) shows strata from the Narchilla through Duo Lake formations, and the Cirque Lake intrusion. In the following descriptions, silty where used as an adjective of limestone refers to silt-sized particles of siliciclastic silt in the limestone.

### Narchilla(?) Formation, Late Neoproterozoic to Early Cambrian

The oldest rocks on the Mactung property are terrigenous clastic strata assigned to the late Neoproterozoic to early Cambrian Vampire Formation by Abbott (2013). Similar rocks 5 km north of Mactung are assigned to the Arrowhead Member of the Narchilla Formation by Cecile (1996). In this report, the rocks are assigned to the late Neoproterozoic to early Cambrian Narchilla Formation, which was defined by Gordey and Anderson (1993) with a type section in NTS 105I/6 (62° 15.7' N, 129° 13.2' W).

On the Mactung property, the Narchilla(?) Formation (mine unit 1) is a heterogeneous package about 750 m thick (Harris 1980) of thin to medium bedded, brown to grey mudstone, shale, siltstone, and greywacke metamorphosed to mica phyllite (Atkinson and Baker 1986). It consists of quartz, muscovite, biotite, chlorite (Harris 1980; Gebru 2017), ilmenite, zircon (Gebru 2017), and altered porphyroblasts of andalusite (Harris 1980). The upper part of the unit is calcareous, which may represent a transition into the overlying

Sekwi Formation (Gebru 2017). The contact metamorphic assemblage includes oligoclase, K-feldspar, cordierite, andalusite, tourmaline, ilmenite, monazite, zircon, and pyrite (Gebru 2017). Where the Narchilla(?) Formation is in contact with Sekwi Formation within the hornfels zone, it has been altered to a spotted biotite hornfels (previously mine unit 2-1) with pronounced layering parallel to the contact formed by 3- to 4-mm clots of biotite concentrated into very thin (1 cm to 2 cm) layers (Harris and Godfrey 1975). Near the Cirque Lake stock, the unit is tourmalinized and consists of up to 50% acicular black tourmaline crystals up to 2.5 cm long.

### *Observations*

Narchilla(?) Formation is semi-resistant and appears dark brown or lichen-covered greyish brown from a distance (Figure 8A). Closer up, the outcrop surfaces weather dull, dark, rusty or orangey brown to creamy grey or beige (Figure 8B), commonly with an orange stain. Lithologies are dominantly micaceous phyllite, but include mica schist, poorly foliated meta-siltstone, and fine-grained meta-sandstone. The fresh surfaces of rocks of the Narchilla(?) Formation are pale to medium grey, usually with a greenish, yellow-greenish, or purplish cast in the better-foliated rocks. A greenish yellow platy mineral, probably sericite, defines the foliation. Black, prismatic porphyroblasts up to 1 mm long are scattered throughout the phyllite and sub-millimetre cordierite(?) and biotite porphyroblasts are present locally. On Isolation Mountain, 3.5 km northeast of Mount Allan, the Narchilla(?) Formation is a pale grey weathering, light grey siltstone and blockier silty mudstone, not obviously metamorphosed.

Bedding is identified by sparse interbeds of blockier, less phyllitic meta-siltstone, probably containing less sericite, and centimetre-scale, planar, parallel, compositional layering (Figure 8C). Locally, beds 10 cm to 15 cm thick are defined by alternations of phyllite and meta-sandstone. Other bedding is expressed by colour differences, consisting of purplish *versus* greenish medium grey bands on fresh surfaces, and dark *versus* pale brown bands on weathered surfaces (Figure 8B). The unit is a metamorphosed mudstone to siltstone with minor fine-grained sandstone.


Figure 8. The Narchilla Formation. [A] Outcrop appearance; planar-, parallel-, thin-bedded phyllite between steep faults south of Cirque Lake. Looking north. [B] Bedding and foliation in phyllite. [C] Bedding and cleavage, looking east from a point east of the south slope of Mount Allan. Outcrop faces are bedding planes, cleavage is the fabric of breakage, which runs from top left to bottom right of the photo. Hammer is 40 cm long.

### *Correlation*

Assignment of the oldest rocks at Mactung to Narchilla Formation as opposed to the Vampire Formation is tentative. The two lithologically similar units are regarded as products of separate depositional systems. The Vampire Formation derived from a source area east of the study area, whereas the Narchilla Formation derived from a source to the west or northwest (Gordey and Anderson 1993). No paleocurrents were measured during the 2016 project, nor are any reported in the map area from prior to this project, and no sedimentary structures were observed. Therefore, the only basis for correlation is lithological.

At the type section in map sheet 105I/6, Narchilla Formation is a recessive, dark blue-grey slate locally with green laminae, and a pale green weathering slate laminated in shades of green. A thick middle member consists of fine-grained, orangey grey wreathing, quartzose sandstone (Gordey and Anderson 1993). In western NTS 105I, the same lithologies are present but the weathering colours are a distinctive maroon with minor pale green, including pale green sandstone beds (*ibid*.). In NTS 105O, the Narchilla Formation consists of two

members, the Senoah and Arrowhead members, that are distinguished primarily on the basis of colour (Cecile 2000). The lower member is the Senoah Member, a drab-brown weathering siltstone and shale with minor quartzite concentrated near the top, and very minor limestone. The Senoah Member is correlated with the lower slate and middle sandstone members at the type Narchilla Formation section in NTS 105I. The upper member is the Arrowhead Member, a bright maroon and green weathering argillite with minor quartzite, correlated with the dull-coloured, upper part of the type Nachilla Formation (Cecile 2000). The Narchilla Formation sedimentary structures include Bouma turbidite divisions and amalgamated beds with scoured bases, suggesting a submarine fan depositional setting (Gordey and Anderson 1993).

The Vampire Formation, at the type section on the southern border of NTS 105I (62° 21.5' N, 127° 56.5' W; Fritz 1982), consists of dark brownish grey weathering, thin to medium bedded siltstone with interbedded, fine-grained quartzose sandstone that locally forms thick-bedded members. Sedimentary structures include planar laminae, load casts, ball and pillow structure, soft-sediment folds, and rare cross-bedding, and indicate an off- shelf depositional environment, possibly on a slope (Gordey and Anderson 1993).

The lithologies in the exposures examined during 2016 are dominantly mud- and silt- grade. On this basis, the oldest rocks in the map area are assigned tentatively to the Narchilla Formation, and are referred to as the Narchilla(?) Formation to emphasize that future work may require re-assignment of these rocks to the Vampire Formation.

## Sekwi Formation, Early Cambrian

Lower Cambrian strata at Mactung (mine unit 2B) are assigned to the Sekwi Formation (Handfield 1968; 63° 33' N, 128° 44' W). The Sekwi Formation at Mactung is described as being highly variable in thickness and composition, ranging from 0 m to 35 m thick on the north face of Mount Allan, where it consists of slump breccias interbedded with well- bedded, fine-grained limestone and shale in 1-m intervals (Harris 1980; Atkinson and Baker 1986). These are correlated down-dip with 35 m of chaotic slump breccia exposed in the underground workings, and farther down-dip, with breccias that thin abruptly to a few centimetres of calcareous mudstone. Clasts in the slump breccias consist of limestone, limestone breccia, phosphatic nodules, and various siliciclastic rocks (Atkinson and Baker 1986). The phosphatic nodules consist dominantly of crystalline apatite, with minor "collophane" (Odekirk 1979b). The great variation in bed thickness over short distances and polylithic nature of the breccia was used to infer an origin as coalescing debris fans (Atkinson and Baker 1986).

Industry maps of the north face of Mount Allan show a sub-unit of the Sekwi Formation that includes horizons of calcareous shale and siltstone containing lenses of limestone (Harris and Godfrey 1974). A correlation is made in this study between that sub-unit of Sekwi Formation and the Banded facies of Sekwi Formation defined during this study. The Sekwi Formation hosts the Lower ore zone.

## *Observations*

The Sekwi Formation on Tag Mountain and the north face of Mount Allan (Figure 3) is divisible into a Breccia facies and an overlying Banded facies that is transitional with the Hess River Formation. The Banded facies comprises the bulk of the Sekwi Formation on Mount Allan and east of Mount Allan near Cirque Lake, whereas the Breccia facies dominates west of Mount Allan on Tag Mountain, and at the east end of the north face. Units mapped as Banded facies contain subordinate breccia, and *vice versa*.

The Sekwi Formation elsewhere has not been assigned to either facies. On Isolation Mountain, 3.5 km northeast of Mactung, the Sekwi Formation is no more than 30 m thick and forms an obvious yellow streak on the hillside (Figure 9A). It is exposed only as very thin, platy fragments that have broken along cleavage planes, not bedding planes. The rock consists of pale yellow, light grey, or pink weathering, soft, argillaceous mudstone that is light grey to greenish grey on fresh surfaces (Figure 9B). Cubic molds, a few millimetres across (Figures 9B and 9C), some coated by oxidized iron sulfides and a few filled with pyrite, cross-cut bedding planes and are interpreted to be molds of euhedral pyrite crystals. Very thin, parallel laminations are generally planar at a centimetre-scale but can be rippled or irregular at a millimetre scale. Beds 2 mm to 20 mm in thickness are defined by colour variations and locally by the presence, absence, density, or character of laminations. On Road Mountain, 3 km east-southeast of Mactung, the Sekwi Formation is less than 20 m thick, weathers reddish yellow, and consists of the same platy, greenish yellow weathering mudstone (Figures 9D and 9E) interbedded with 0.2 m to 2.0 m beds of semi-recessive, buff to reddish yellow weathering limestone conglomerate. The conglomerate contains rounded, pebble- to cobble-sized clasts of black lime mudstone, recessive grey lime mudstone, sulfide grains, and possibly an earlier generation of conglomerate, all floating in a recrystallized matrix of calcite cement.

### Banded Facies

The Banded facies expresses itself as thin-banded skarn or interstratified skarn and hornfels, and minor marble breccia. The banded appearance of this unit is caused by centimetric planar bedding that is defined by alternation of laminated and non-laminated beds or by colour differences (Figure 9F). Dark coloured bands are hornfels that weather medium orangey brown, are medium to dark grey or dark bluish grey on fresh surfaces, and have sub-millimetre pyritic laminations. These dark bands are indistinguishable (at the scale of investigation) from the overlying Hess River Formation, which suggests that the Banded facies grades upward into the Hess River Formation. Light-coloured beds and layers weather cream or light brown, and are very fine-grained to microcrystalline calc- silicate rock, commonly siliceous and rarely slightly calcareous. The fresh surfaces of the light-coloured rock are light or medium grey with purplish or reddish overtones (Figure 9G), yellowish orange, or pale apple green. The light-coloured rock is typically very well laminated with sub-millimetre, planar laminations but may also display discontinuous, wispy, black laminations of irregular width, anastomosing seams of dark material, and differentially weathering, wavy laminations. In places, thin beds are distorted, broken, and stacked by mild slumping, and some intervals are made up of stacked lenticular beds with dark seams anastomosing between them (Figure 9I). Light and dark weathering rocks locally grade into each other laterally across a “bleaching” front (Figure 9F).

The Banded facies dominates the Sekwi Formation on the north face of Mount Allan. In the overthrust sheet on Tag Mountain, the strata between the Breccia facies and the Hess River Formation has been assigned to the Banded facies. It comprises a 10-m interval of the Hess River-like, recessive siltstone sandwiched between short intervals of creamy white weathering calc-silicate rock (Figure 9H).

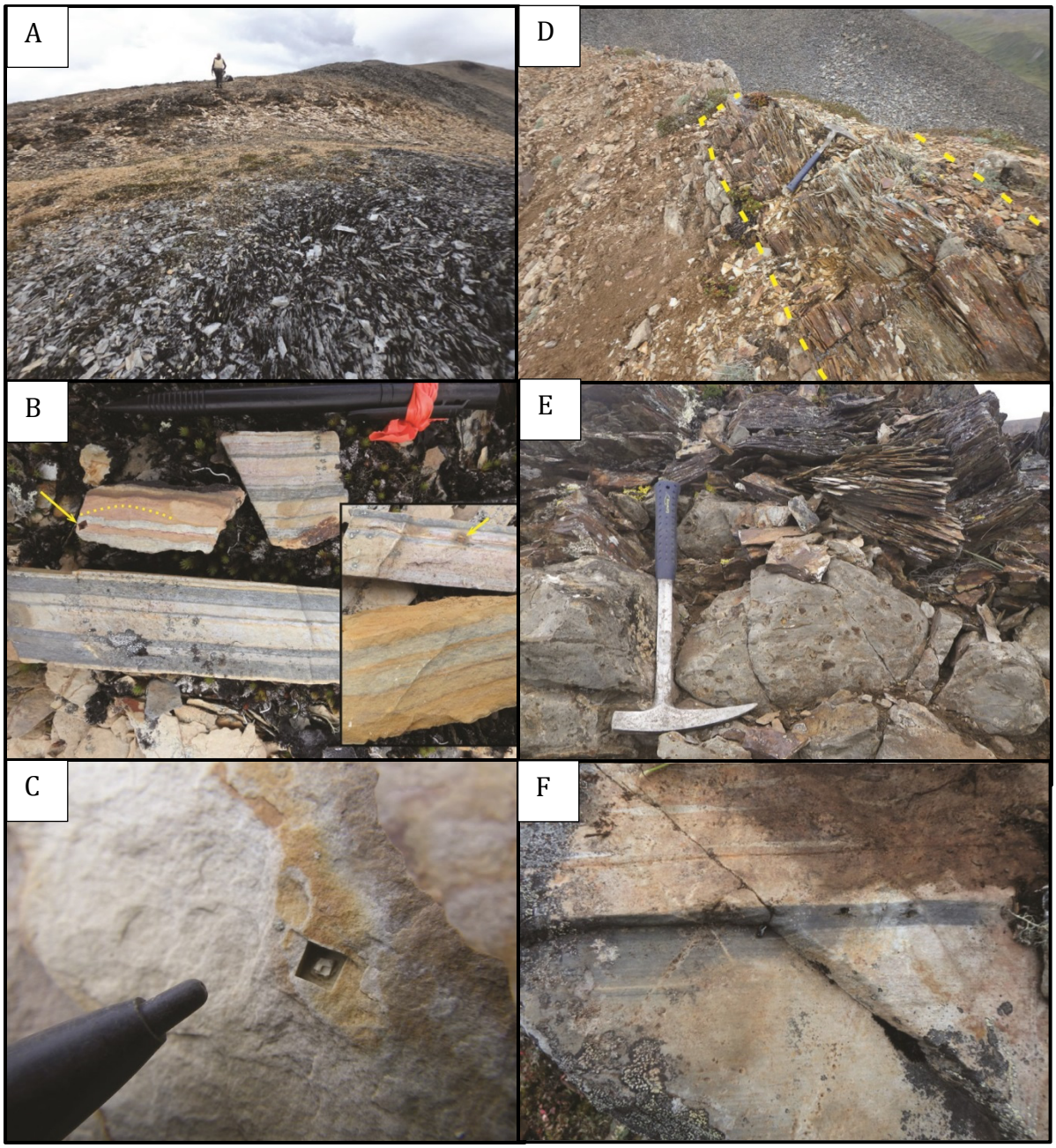


Figure 9 [A]-[F]. The Sekwi Formation; [A]-[C] are from Isolation Mountain, [D]-[E] are from Road Mountain, [F] is the Banded facies. [A] The Sekwi Formation on Isolation Mountain is exposed as rubble that appears pale yellow from a distance. Foreground rubble is of the Hess River Formation and near-

background rubble is of the Narchilla Formation. [B] Selected pieces of rubble from the Sekwi Formation on Isolation Mountain, with a black pencil for scale. Inset is at the same scale. Upper left piece in the main photo shows a cubic mold of pyrite(?) that grew across bedding (arrow), and curved hemispherical laminations (dashed line). In the top piece of the inset photo, a pyrite cube that cuts bedding is surrounded by a dark halo of alteration (arrow). Thin, dark greenish grey beds in the bottom and other pieces consist of a multitude of discontinuous laminations or lenses; similar beds are present in the hornfelsed Sekwi Formation on Tag Mountain. [C] Cubic mold (of metamorphic pyrite?) in pale yellow weathering mudstone and a partial cast at the base of the mold. Pencil tip is 1 mm wide. [D] Mudstone between the dashed yellow lines separates beds of matrix-supported limestone conglomerate to the left and right of the dashed lines. Hammer is 40 cm long. [E] Close-up of conglomerate overlain by mudstone. Hammer is 40 cm long. [F] Weathered surface of calc-silicate hornfels shows "bleaching front" in well-laminated layer, overlain by poorly laminated layer with lenses (boudinaged beds?) of soft, white-weathering mudstone. Field of view is about 20 cm from top to bottom.

**Breccia facies**

The Breccia facies consists mainly of nodular limestone that grades progressively into slumped nodular limestone then limestone debrite. Nodules and lenticular beds of limestone are light grey, 2 cm to 10 cm thick, laminated and cross-laminated. Intervening beds of yellowish grey, silty limestone are thin to medium in thickness, and have wavy, parallel and cross laminations defined by concentrations of siliciclastic silt. Rare black chert beds are 1cm to 2 cm thick. In strata that has slumped gently down-slope, the light grey limestone beds are pulled apart into bedding-parallel boudins, surrounded by yellow siliciclastic-silty limestone that also infills cracks in the boudins. Progressively greater distances of slumping are marked by higher degrees of breakage, from crackle breccias, through mosaic breccias, to various breccias with the chaotic textures of debris flows. Debrites are thick bedded to massive, and have pebble- to boulder-sized clasts of light grey weathering lime mudstone and laminated lime siltstone, in a matrix of yellowish grey weathering, laminated and cross-laminated siliciclastic-silty limestone (Figures 9J and 9L). Less commonly in the debrites are clasts of very thinly interbedded light grey limestone and yellowish grey laminated silty limestone. The debrite is variably clast-supported and matrix-supported, everywhere poorly sorted, with beds of medium thickness defined by different breccia textures, from particulate rubble to crackle packbreccia, to rubble floatbreccia. Clasts are rounded and commonly tabular, but equant clasts are present as well. Some clasts are partly rimmed by a dark grey, submetallic substance (possibly manganiferous or phosphatic). Possible archeocyathans that have been replaced by a phosphatic(?) mineral were noted at one location on the north face of Mount Allan (Figure 9N). Archeocyathans are common in the Sekwi Formation, both *in situ* and in clasts within debrites (Turner *et al.* 2011).

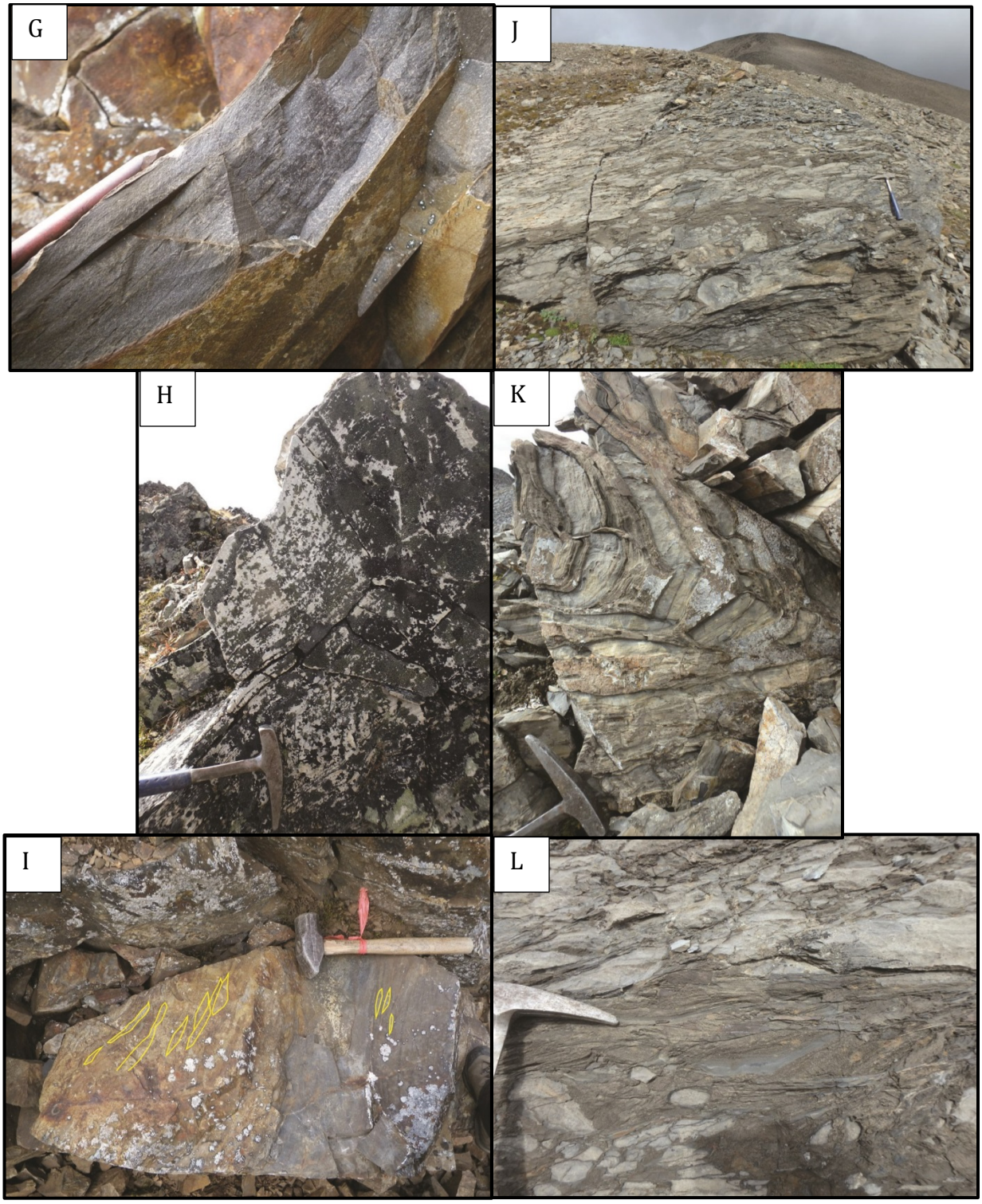


Figure 9 [G]-[L]. The Sekwi Formation; [G]-[I] the Banded facies [J]-[L] the Breccia facies. [G] Fresh surface of very thin-bedded, medium grey, calc-silicate(?) bearing rock probably derived from calcareous mudstone or argillaceous lime mudstone. This rock is interstratified with thin, darker grey layers to give the outcrop a banded appearance. Pencil for scale. [H] White weathering, very thin-bedded calc-silicate rock at the base of the Banded unit on Tag Mountain. Hammer head is 12 cm long. [I] Very thin, slumped

beds are variably broken, lenticular, and distorted (some of the broken beds are outlined in yellow). From north face of Mount Allan. Hammer is 40 cm long. [J] Large boulder of medium-thickness beds of poorly sorted rubble packbreccia (grey, probably debrite) and siliciclastic-silty limestone (brown). From Tag Mountain. Hammer is 40 cm long. [K] Folded nodular silty limestone on Tag Mountain. Hammer head is 12 cm long. [L] Close-up of boulder in [J], showing cross-laminated siliciclastic-silty limestone between beds of limestone breccia. Hammer pick for scale.

Some planar-bedded lithologies are included in the breccia facies. Ten-metre intervals of brown weathering, medium grey siltstone interrupt the carbonate lithologies. Locally, there is considerable sooty, medium-dark grey, finely crystalline limestone (recrystallized?) in single nodular or planar beds, and forming thinly planar-bedded intervals. The finely crystalline limestone is very hard (siliceous?), silty and pyritic, and has graded beds, cross-laminations in silty beds, and centimetre-scale calcareous concretions. Other planar-bedded limestone intervals have been metamorphosed to calc-silicate hornfels.

The Breccia facies on the north face of Mount Allan, where it hosts part of the Lower ore zone, has been extensively altered to marble and skarn, but retains subtle expressions of breccia textures that are assumed to be primary. The other main exposure of Breccia facies is on Tag Mountain, where the rock is unaltered or mildly altered and exposed mostly as rubble (Figures 9J to 9M).

### Sekwi Formation Hornfels and Skarn

Hornfels of the Sekwi Formation is typically affected by a skarn overprint, and belongs to one of three lithologies: marble; microcrystalline, partly calcareous calc-silicate rock; and brown to beige weathering, purplish grey hornfels. These lithologies probably reflect increasing amounts of terrigenous matter in the protolith. The marble, which is present on Tag Mountain and Mount Allan, and the calc-silicate rock, which is present on Tag Mountain with a light skarn overprint and Mount Allan with a heavy skarn overprint, are both thinly to very thinly banded in different colours, and well laminated. The brown hornfels, present southwest of Cirque Lake with a skarn overprint, is also well-laminated, is interbedded with minor brown, diopsidic skarn containing grey nodules of marble that was formed from a nodular limestone protolith, and is cut by microcrystalline calc-silicate veins.

Marbling preferentially affected the slump breccias and debrites, and created a distinctive texture in nodular limestones in which the nodules and calcite bands were preferentially altered (Figures 9M and 9O). Marble selectively affected concretions within the laminated calc-silicate hornfels of the Sekwi Formation. The marble is greyish-white weathering, light grey or white, and finely crystalline in unskarned hornfels (Figures 9P and 9Q), but in the skarn zone it ranges to coarsely crystalline, commonly has a greenish tinge on fresh surfaces, and locally contains scattered, visible garnet and pyroxene crystals. Marble bodies in the skarn zone contain clasts that are difficult to distinguish from the matrix and rare pebbles of non-calcareous mudstone. The marble is easily weathered, which causes it to become friable and crumbly in outcrop, especially within the skarn zone.

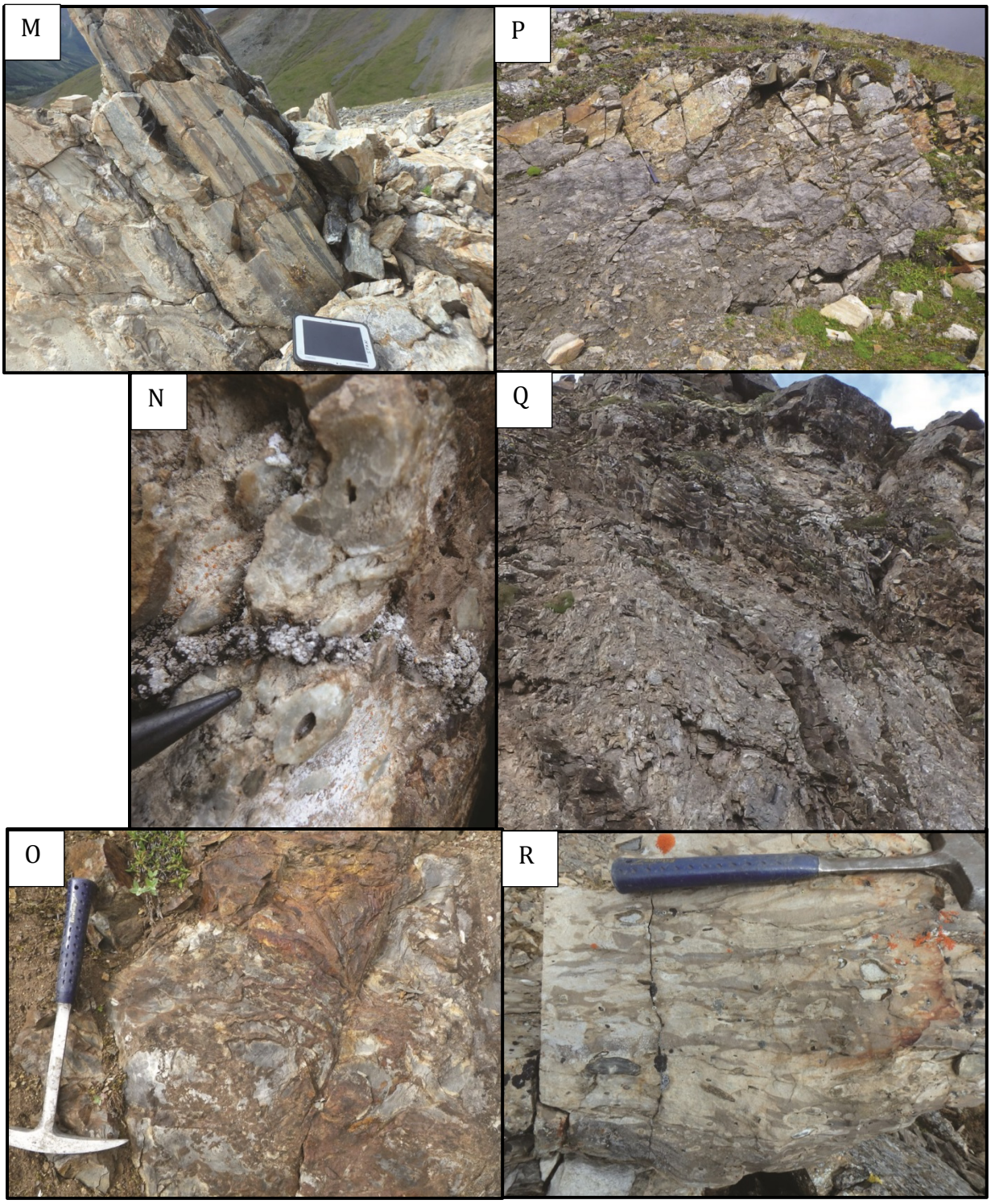


Figure 9 [M]-[R]. The Sekwi Formation; M-N the Breccia facies, O-R alteration. [M] Calc-silicate hornfels derived from very thin bedded limestone (centre) overlying nodular limestone (left), both originally silty or argillaceous. Nodules in the nodular limestone have been altered to light grey marble. From Tag Mountain. Tablet is 20 cm long. [N] Possible archeocyathans, replaced by a hard, non-siliceous, possibly phosphatic mineral. The fossils(?) may be part of a clast in a breccia, although the weathered face of the surrounding rock does not reveal much about what lies underneath. Pencil tip is 1 mm wide. [O] Skarned slump breccia

of nodular limestone. Nodules have been altered to light grey marble. Surrounding silty limestone has been altered to brown weathering skarn. From Banded facies on the south face of Mount Allan. Hammer is 40 cm long. [P] Marble alteration front. Grey marble has preferentially developed in a slump breccia, and only weakly affects the overlying, very thin-bedded limestone, which is now a buff weathering calc-silicate skarn. Looking northeast on Tag Mountain. Hammer is 40 cm long. [Q] The Banded facies overlying the Breccia facies on the north face of Mount Allan. The Breccia facies, at the base of the photo, is a light grey weathering, marble-altered limestone breccia cut by two thick, brown skarn veins, each about 20 cm wide. Immediately overlying strata consist of thin beds of alternating dark and light grey skarn possibly derived from nodular to banded slope-deposited limestone. This is a closer view of the top of the open Z-fold shown in Figure 23E, from a slightly different angle. [R.] Partial skarn (brown) has invaded along bedding planes or laminations in a limestone floatbreccia on Tag Mountain. Hammer is 30 cm long.

The calc-silicate hornfels has, overall, a white-weathering aspect, but on closer inspection shows thin bands of pale greenish cream, green, yellow, light brown, dark purple, light orangey grey, and various shades of grey. Despite the preserved bedding, most of the rock breaks randomly although some will break along bedding planes. On fresh surfaces, beds are purplish grey, light grey, or shades of green or yellow. Sub-millimetre laminations are dark grey and locally pyritic. Beds are parallel and planar at a mesoscale but irregular at a millimetric scale. Pale beds are typically calcareous. Some exposures are entirely calcareous, whereas others are entirely non-calcareous and moderately hard.

Light skarn manifests as patchy alteration that forms irregular, grossly bedding-parallel layers with abundant apophyses that cross-cut bedding (Figure 9R), and thicker bands at angles to bedding, showing that fluid moved first along bedding planes and cross-cutting fractures. Heavy skarn manifests as a calc-silicate rock that weathers rust red, ochre, dark brown, and less commonly, light grey. It has fresh colours of dark green, light greenish grey, apple green, and light and dark grey, with patches or layers of pink. It ranges from microcrystalline to very coarsely crystalline (Figure 9S), and consists primarily of pyroxene and minor pale, orangey pink garnet, although locally garnet is abundant. Pyroxene crystals can be up to 10 mm long and garnets up to 1 mm in diametre. Locally, long green or grey amphibole crystals are present, and rarely, wollastonite(?). Compositional banding a few millimetres to decimetres thick is expressed as variations in colour (on fresh surfaces, greys, greens, and pink). In skarned slump breccias, clasts are cryptic on weathered surfaces. Sulfides are present as inclusions within pyroxene crystals, as millimetric domains of pyrrhotite-pyrite, as centimetric domains loaded with millimetric knots of magnetic pyrrhotite, and as pyrite with rare molybdenite(?) along fracture planes. Sub- vertical veins of sulfide minerals are common and millimetric knots of pyrrhotite are locally abundant.

Brown weathering veins of skarn minerals from a few millimetres to about 20 cm wide are common on the north face. Some are microcrystalline, grey to green, and homogeneous, whereas others are zoned or coarser. Bedding-perpendicular and bedding-parallel veins of very coarse, white quartz, and veins and pods of very coarse, greyish white calcite cut the skarn.


Figure 9[S]. The Sekwi Formation, alteration. Garnet (red), diopside(? green), and pale grey amphibole needles in skarned breccia of the Breccia facies on the north face of Mount Allan. Scale bar is 1 cm.

### *Correlation*

There are two Lower Cambrian formations near Mactung, the carbonate-dominated Sekwi Formation and the shale-dominated Gull Lake Formation (Gordey and Anderson 1993; 62° 23.4' N, 129° 19.2' W). The latter is suggested to be a deeper-water equivalent of the Sekwi, Hess River, and lowermost Rabbitkettle formations, and ranges to Ordovician in age (Cecile 2000). The Gull Lake Formation consists of buff to grey weathering, commonly bioturbated, thin- to thick-bedded mudstone, slate, shale, and siltstone locally grading to sandstone, with variable but minor amounts of limestone, silty limestone, and limestone conglomerate (Abbott 2013; Cecile 1996, 2000; Gordey and Anderson 1993). In NTS 105O west of Mactung, a tongue of the Sekwi Formation is present intermittently at the base (Abbott 2013), and north of Mactung, a basal member of thin-bedded limestone and slump- derived limestone conglomerate has been called the North Keele member (Cecile 1996, 2000). In NTS 105I, there is an intermittent limestone that is commonly a slump or debris- flow conglomerate at the base of Gull Lake Formation (Gordey and Anderson 1993).

The Sekwi Formation in NTS 105O near Mactung is described as massive to thin-bedded oolitic limestone, limestone, and limestone conglomerate, with minor grey and green shale (Abbott 2013). The Sekwi Formation in NTS 105P, northeast of Mactung, ranges from 30 m to >1100 m thick. The formation consists of a lower member of deeper-water nodular silty limestone with intermittent limestone debrites and turbidites, a middle quartz sand-rich carbonate member, and a complex upper member of shallow-water subtidal to peritidal, mainly carbonate lithologies, including minor bright red shale and siltstone interpreted as paleosols (Turner *et al.* 2011; Dilliard *et al.* 2010). The typical weathering colours of the Sekwi Formation are yellow, orange, and grey. The thick debrites in the lower member were generated by movement on syn-depositional faults (Dilliard *et al.* 2010).

The Lower Cambrian carbonate debrite at Mactung has been assigned herein to the Sekwi Formation, based on the predominance of carbonate lithologies and the typical yellow to orangey grey weathering colours, and in agreement with Atkinson and Baker (1986). The outlying exposures in the eastern part of the map area (Road and Isolation Mountains) are

also assigned to the Sekwi Formation rather than the Gull Lake Formation, based again on weathering colours and the presence of a carbonate breccia bed similar to the breccia or debrite of the Sekwi Formation under Mount Allan. The assignment of these strata to the North Keele member of the Gull Lake Formation was rejected as unnecessarily complicated. The Sekwi Formation at Mactung, including the Lower ore zone, probably correlates with the North Keele member, the tongues of Sekwi Formation west of Mactung, and the basal limestone and limestone debrite at the base of Gull Lake Formation in NTS 105I.

### *Interpretation*

The Breccia facies was originally an *in situ* nodular limestone deposited on a submarine slope. The breccias or debrites formed by slumping and collapse of the nodular slope deposits, and range from slightly slumped to chaotic debrites that travelled far enough downslope to completely disrupt internal bedding. Evidence of tensile strain shortly after deposition is found in the boudins that formed from nodular beds. The boudins originated as partially cemented, plastic mud that cracked from brittle strain as the strata slid downslope, while the surrounding silty lime mud, with greater siliciclastic content, remained unlithified and filled the cracks. Cross-laminated silts were deposited from turbulent flow after the main debris flow had passed. The source area for the Breccia facies under Mount Allan included not only nodular limestone but also siliciclastic and phosphatic rocks, suggesting a mixed shelf, and its multi-generational nature (Atkinson and Baker 1986) shows that the source area was subject to repeated disruptions leading to sediment gravity flows.

Slumping and sediment gravity flows may have been caused by gravitational collapse of an over-steepened slope, or by seismic activity. A seismic origin is favored because thick debrites in the Sekwi Formation 40 km to 60 km to the northeast have been interpreted as products of Early Cambrian seismic activity (Dilliard *et al*. 2010), and because the change in thickness and character of the Sekwi Formation east of Mactung can be explained by syn-depositional faults that moved blocks of seafloor to different depths.

The Banded facies was originally, before contact metamorphism and skarning, a calcareous mudstone/siltstone with variable amounts of interbedded limestone, some of it nodular, and local small breccia beds. The Banded facies is both laterally equivalent to and overlies the Breccia facies debrites, and as such represents not only an upslope equivalent of the breccias but also deposition on the slope subsequent to the sediment gravity flow episodes. The Hess River-like lithologies within the Banded facies indicate that the contact between the Sekwi and Hess River formations is gradational.

The Sekwi Formation northeast and southeast of Mactung is relatively thin, which implies quiet conditions, perhaps in a sediment-starved setting or on a topographic high. A few beds of polylithic and probably bi-generational sediment gravity flow deposits, more akin to the breccias under Mount Allan than to the slumped nodular limestone on Tag Mountain, might reflect seismic events.

## Hess River Formation, Middle Cambrian

Mine unit 3C is assigned to the Hess River Formation (Cecile 1982; 62° 42’ N, 130° 47’ W), which is Epoch 2 to Epoch 3 of the Cambrian in age (Cecile 1982). The Hess River Formation

on the Mactung property consists of 60 m to 90 m of fissile, pyritic, carbonaceous, mudstone or argillite and siltstone, with rare limestone beds and lenses in the upper and lower parts of the unit (Atkinson and Baker 1986; Harris 1980). The lower contact is sharp and conformable, whereas the upper is gradational. The Hess River Formation outside of the zone of contact metamorphism contains quartz, muscovite, phlogopite, potassic feldspar, pyrrhotite, titanite, and apatite (Gebru 2017) and local white mica pseudomorphs after andalusite (Harris 1980). Inside the hornfels zone, there are two varieties of the Hess River Formation, brown and green, both of which have lost "dark impurities", muscovite and K-spar, gained silica and calcic plagioclase, and coarsened quartz and pyrrhotite. The brown hornfels has locally gained biotite, whereas the green hornfels has gained tremolite and may contain calcite (Gebru 2017).

Elongate intraclasts of mudstone, siltstone, and phosphatic material form intraformational conglomerates, and also exist as isolated clasts. Thin beds disrupted by syn-sedimentary processes form boudin-like lenses (Atkinson and Baker 1986; Harris 1980), and thin phosphatic beds and lenses are present (Harris 1980). Siliceous sponge spicules point to an early to middle Cambrian age for the unit (Atkinson and Baker 1986).

Metamorphosed Hess River Formation ranges from argillite to hornfels with increasing intensity of metamorphism. Limestone beds within the unit on the north face of Mount Allan are skarned (Harris 1980).

### *Observations*

The Hess River Formation is a meta-mudstone and -siltstone that weathers light grey, medium grey, dark brown or rusty, and locally blue-grey or yellowish grey (Figures 10A, 10B, and 10C). The fresh colour is dark grey, or rarely medium grey. Where the Hess River Formation is hornfelsed, it tends to weather rusty brown to light orangey brown and to have a bluish cast on fresh surfaces. Beds of medium thickness, of blocky coherent meta-mudstone or -siltstone, alternate with medium-thickness intervals of flaggy to irregularly parting meta-siltstone. Thin beds are revealed by colour alternations on both fresh and weathered surfaces. The rock is typically well laminated, with sub-millimetre sulfide laminations, millimetre-scale planar, parallel laminations of dark grey including continuous and discontinuous varieties, and orange weathering, silty laminations and very low-amplitude ripple cross-laminations. Pyrite is concentrated into laminations and beds, and is also disseminated as specks and cubes up to 1 mm and aggregated into millimetric domains. Bedding and laminations are visible in the hornfels, but breakage is random and not affected by bedding planes. The hornfels is locally siliceous. Zoned veins of skarn minerals (garnet, pyroxene) up to a few centimetres wide cross-cut bedding within the skarn zone on Mount Allan and south of Cirque Lake (Figures 10C and 10D).

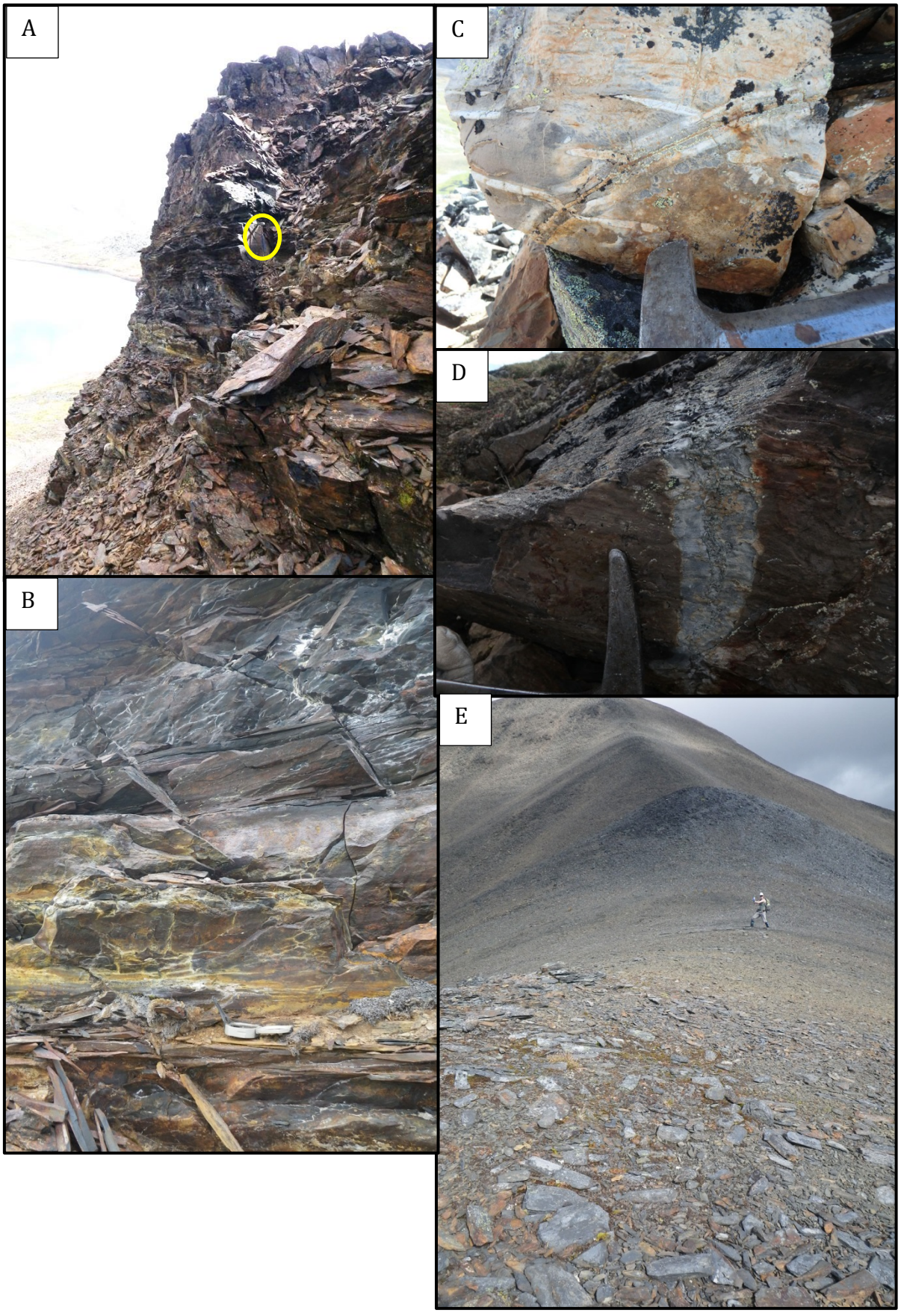
A
C
D
B
E

Figure 10. The Hess River Formation. [A] Outcrop on the south shore of Cirque Lake, looking east-northeast. Hammer 40 cm long [is circled in yellow]. [B] Mudstone and silty mudstone in medium-thick intervals. Photo was taken south of Cirque Lake. Brunton compass for scale. [C] Flat lenses (boudins?) of pale grey, soft mudstone in light brown hornfels. The alteration halo alongside the vein does not affect the lenses. Photo was taken on the north face of Mount Allan. Hammer handle is 2 cm across. [D] Skarn vein with bleached halo a few centimetres wide cuts laminated meta-mudstone south of Cirque Lake. Hammer tip for scale. [E] Looking north on Tag Mountain, from the base of the Rabbitkettle Formation across the mostly covered Hess River Formation. The dark hill behind the geologist is basal Hess River Formation phosphatic(?) siltstone.

The contact between the Hess River and Sekwi formations is not exposed but is presumed conformable. In rubble on Isolation and Road mountains, the contact is a sharp change from yellow weathering rubble of the Sekwi Formation to grey weathering, dark-lichen covered rubble of the Hess River Formation.

A common feature of the Hess River and Rabbitkettle formations is the presence of elongate, flat lenses or nodules, some of which may be boudinaged beds, a few centimetres in length and a half to one centimetre wide, of soft, creamy grey weathering, non-calcareous material (Figure 10C). Local porphyroblasts, too small to identify with certainty, include sub-millimetre, blue-grey prismatic minerals and equant, 1 mm to 2 mm, light grey ones.

A phosphatic interval a few metres thick is exposed as rubble at the base of the Hess River Formation on Tag Mountain (Figure 10E). A bed 10 cm thick of graded phosphatic sandstone is present within the interval. Black, moderately hard, phosphatic grains of coarse sand to granule size and a few rounded granules of rusty pyrite are cemented by calcite. The rest of the interval consists of thin-bedded, dark grey to purplish grey siltstone rubble with a bluish grey weathering colour that is suggestive of the weathering of phosphate minerals. In the overthrust sheet on Tag Mountain, the basal Hess River Formation does not contain a phosphatic interval.

### *Correlation and Interpretation*

The Hess River Formation is a basinal unit that is recognized within the Misty Creek Embayment (Cecile 1982, 1996, 2000; Turner *et al.* 2011; Fischer 2016), where the formation consists of dark grey to black, calcareous mudstone or lime mudstone to lime siltstone containing variable amounts of siliciclastic silt, and very minor siltstone, sandstone, and granule conglomerate, including granule conglomerates dominated by phosphatic grains. The beds are thin to very thin, from 10 mm to <1 mm. The laminations are orange and yellowish orange from the presence of terrigenous silt and pyrite. The packaging of graded millimetric beds of pyrite, quartz silt and lime mud, current-ripple cross-laminations and climbing ripples, and sub-millimetre parallel laminations suggest that the unit is mainly a turbidite deposited from a dilute flow (Chevrier and Turner 2013; Fischer 2016).

Regional correlatives of the Hess River Formation toward the platform are the dark, thin-bedded limestone and minor slump breccias and siltstone of the Rockslide Formation, and the shallow-water dolostone of the Avalanche Formation (Gordey and Anderson 1993).

Correlatives deeper in the Selwyn Basin are the shale and siltstone of the Gull Lake Formation (Cecile 2000; Abbott 1983).

The green hornfels of the Hess River Formation was originally a calcareous mudstone in which the presence of calcite permitted reactions that formed tremolite during the metasomatic event. Assignment of mine unit 3C to the Hess River Formation is supported by the presence of originally calcareous beds, very thin beds, graded beds, abundance of laminated and cross-laminated mud-grade rocks, paucity of limestone beds, and lack of bioturbation. Orange weathering, silty laminations and very low-amplitude ripple cross-laminations are similar to sedimentary structures in the Hess River Formation regionally. The Hess River Formation has been identified in NTS 105P/NW (Turner *et al.* 2011), where its presence can be used to argue that the Misty Creek Embayment extends southeast that far. Identification of the Hess River Formation at Mactung expands the extents of the formation out of the Misty Creek Embayment.

The Hess River Formation at Mactung was deposited below storm wave base, probably on the basin floor or at the toe of the slope, perhaps as turbidites. The basal phosphatic interval indicates that the source region was a carbonate shelf with terrigenous input, on which phosphogenesis took place at least intermittently.

## Rabbitkettle Formation, Early to Middle Ordovician

The Rabbitkettle Formation was defined without a type section, but with a type area in NTS 105I/SE (Figure 2; Gabrielse *et al.* 1973). Cecile (1982) established two reference sections in the Misty Creek Embayment (at 64° 27’ N, 130° 52’ W; 63° 47.7’ N, 130° 27.7’ W). Regionally, the unit may be as old as middle Cambrian (Aitken *et al.* 1973), and certainly is as old as late Cambrian (Cecile 1982, 2000; Gordey, 2013), but conodont and graptolite collections from the Mactung area (NTS105O/7, 105O/8 and 105P/5) range in age from Early to Middle Ordovician (Abbott 2013). The top of the Rabbitkettle Formation is diachronous, and southeast of Mactung, the top of the Rabbitkettle Formation is the same age as the Duo Lake Formation siliceous shale (NTS 105I; Gordey and Anderson 1993).

In the eastern Selwyn Basin around the Mactung area (NTS 105O/SE), the Rabbitkettle Formation is described as a buff to grey weathering, thin-bedded, argillaceous or silty limestone with minor interbeds of limestone and grey shale (Abbott 2013). Southward, in the western part of NTS 105I, the Rabbitkettle Formation consists mostly of thin bedded, colour-banded, locally nodular, silty to argillaceous limestone, or pale weathering, recessive, argillaceous limestone (Gordey and Anderson 1993).

Mine units 3D, 3E, 3F, 3EF, and 3G are collectively correlated with the Rabbitkettle Formation. Figure 11 shows parts of the Hess River, Rabbitkettle, and Duo Lake formations on Fold Mountain, south of Mactung.

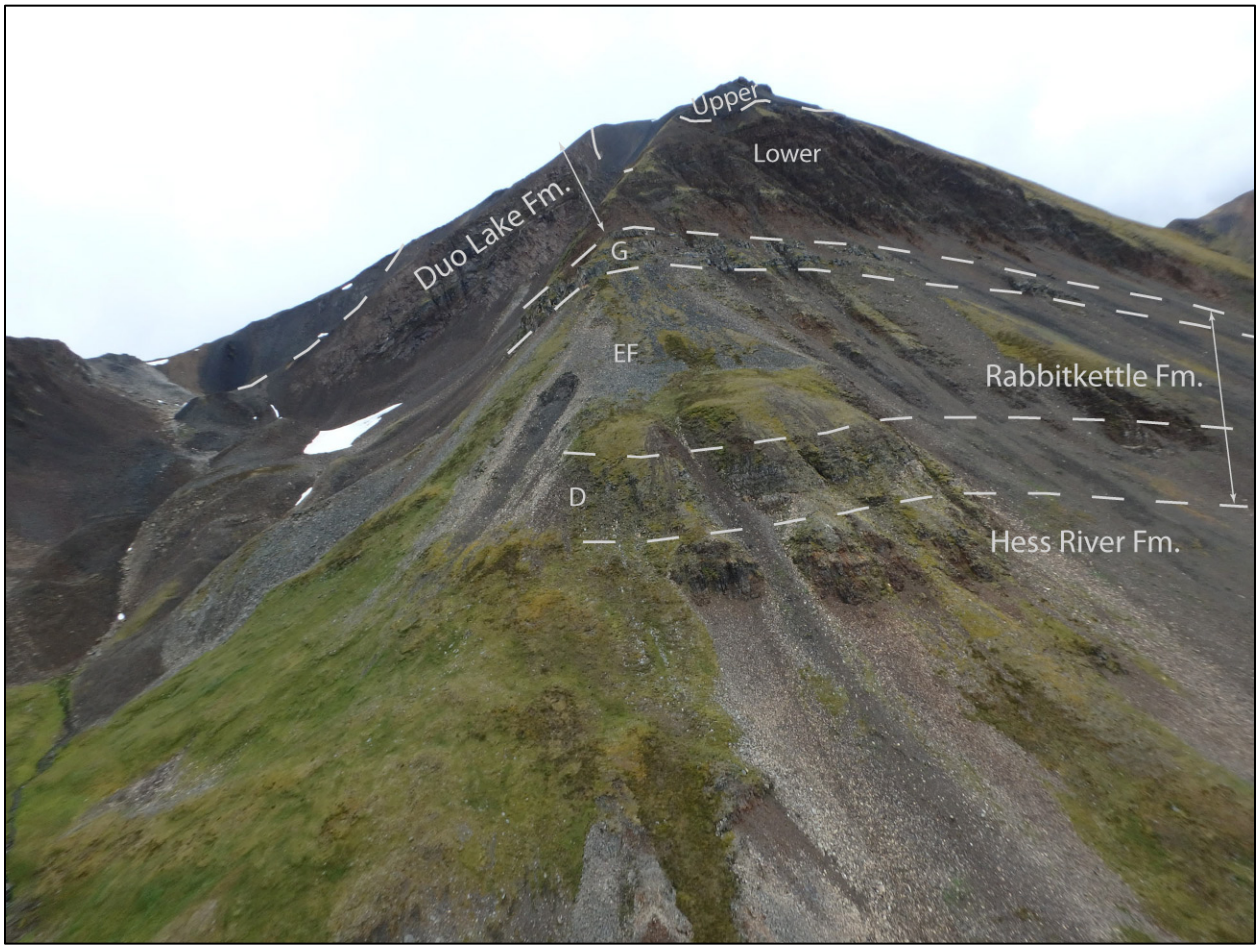


Figure 11. Looking south at Fold Mountain. The Hess River Formation and a felsic dyke form the first resistant outcrop, partway up the slope. The grey band immediately above the Hess River Formation is quartz-sandy phosphatic-clast limestone conglomerate and sandstone of member D of the Rabbitkettle Formation. The upper grey band is member G; between them, member EF is poorly exposed. Above member G, the rusty brown weathering Lower member of the Duo Lake Formation reaches almost to the summit, and just visible capping the summit is the black of the Upper member. The narrow, light band near the base of Lower member is a limestone horizon.

### *Member D – Phosphatic Conglomerate*

On the Mactung property, member D (mine unit 3D) consists of up to 20 m of "repetitively intercalated", beds 2-cm to 100-cm thick of limestone- and phosphatic-clast limestone slump breccias, mudstone, shale and siltstone in conformable contact with the underlying Hess River Formation (mine unit 3C; Atkinson and Baker 1986). The breccia is described as well sorted and well bedded, with clasts of limestone, phosphatic nodules, and siliciclastic rock. The breccia of member D differs from the breccias of the Sekwi Formation in being thinner bedded with smaller, better sorted, less compositionally variable clasts (Atkinson and Baker 1986). The phosphatic nodules are dominated by "collophane", without much crystalline apatite (Odekirk 1979b). Member D outside of the thermal metamorphic aureole contains calcite, quartz, apatite, ±muscovite, ±phlogopite, and minor titanite and pyrite (Gebru 2017).

Where affected by thermal metamorphism, member D includes pyrrhotite ±calcic clinopyroxene, and where skarned, includes Fe-clinopyroxene, calcic plagioclase, quartz, ±garnet (enclosing clinopyroxene), and minor zoisite, calcite, very coarse apatite, and scheelite (*ibid*.).

**Observations, Member D**

Member D is a recessive unit of calcareous, phosphatic sandstone to conglomerate, and limestone or lime mudstone with a variable component of siliciclastic silt. The unit is 1 m to 2 m thick on Tag Mountain below the thrust, <1 m thick south of Cirque Lake, and approximately 10 m thick on the south face of Mount Allan and the north face of Fold Mountain. The contact of member D with the underlying Hess River Formation is covered by a few centimetres to decimetres of overburden where it was traversed during this project. A sample of limestone was taken from the top of member D to test for identifiable population of conodonts; processing of the sample is pending.

Sandstone and conglomerates of member D weather greyish white or dark grey, whereas limestones weather yellowish brown to grey (Figure 12). Fresh surfaces are various shades of grey or black. Clasts in the sandstone/conglomerate consist of phosphatic rock, lime mudstone, quartz sand, and pyrite, as well as conglomerate and microbreccia (Figures 12B, 12C, 12D, and 12E). Clasts range in size from fine sand to cobble, with a predominance of granule sizes in the phosphatic population and pebble to cobble sizes for the lime mudstone. Most clasts are roughly equant and subrounded to rounded, although lime mudstone clasts tend to be elongate to irregular and range from rounded to sub-angular. Phosphatic clasts, which generally dominate the clast population, are described in more detail below. Light grey, lime mudstone clasts are locally the dominant clast type, and well- rounded quartz grains from silt to coarse sand size are abundant in some beds and absent in others. Pyrite grains up to granule size are scattered throughout, rarely comprising 1% to 2% of the rock, and locally are concentrated into thin beds. The matrix of the sandstone/conglomerate is calcareous, and ranges from dominantly particulate, mud-sized particles to dominantly cemented, as seen in thin section. The matrix also contains silt- sized grains of apatite, locally abundant micaceous minerals, and variable amounts, up to 50%, of quartz silt. Grain-supported textures dominate (Figure 12B to 12F). Sorting ranges from good to poor, and the clast population is often bimodal, with packed, well-sorted granules and sparse pebbles (Figure 12D).

Bedding in member D is typically very thin to thin, but ranges up to medium and, locally, thick. Beds are defined by colour, weathering, and the composition, size, packing, and sorting of clasts (Figures 12C, 12G, 12H, and 12I). Beds up to 60 cm thick of laminated limestone, with no or only a few percent phosphatic grains, are interstratified with phosphatic-grain sandstone and conglomerate. Conglomerate beds lack horizontal continuity and can be highly irregular, whereas limestone beds are planar and regular. Conglomerate beds range from one or two granules thick to over 30 cm thick. Conglomerate beds are typically separated from other conglomerates by sandstone or lime mudstone. Graded beds are common in which clast concentration and size change; both normal and reverse grading are present (Figure 12B) although reverse is rare. Laminae and cross laminae are formed by granule- and sand-sized phosphatic grains, locally interlaminated with orangey yellow lime silt. Scours are

present at the bases of beds (Figure 12G), at both hand specimen and microscopic scales, and clasts at the top of some beds were eroded prior to emplacement of the next bed. The unit as a whole fines upward, and beds thin upward.

Phosphatic clasts are black or blue-black on weathered surfaces (Figures 12C and 12D) and black or white on fresh surfaces, except in the skarn zone where both fresh and weathered surfaces are white (Figure 12F). Phosphatic clasts include oblong, tabular and irregular clasts, as well as ovoid nodules(?) or oblate spheroids without apparent cortices. A few clasts have central cavities, possibly from a weathered-out nucleus (Figures 12D and 12F). Phosphatic clasts are a mixture of a cryptocrystalline, high-relief, colourless material (collophane?) and a low-relief, amorphous, dark material (organic matter?), with minor and variable amounts of crystalline apatite, calcite(?), and an opaque mineral (pyrite?). Some of the phosphatic clasts contain ooid-like grains with radial structure amongst the cryptocrystalline material. Coated silt-sized grains of apatite(?) are present in some beds (a thick brown rim in plane polarized light), and rare silt-sized grains have concentric laminations. Most of the phosphatic grains, however, are fragmental and lack the internal concentric laminations characteristic of coated grains.

In drill core, a complex succession of re-working is evident by multiple generations of breccia and numerous small-scale unconformities. Plastically deformed clasts, up to cobble size, of phosphatic sandstone and lime mudstone preserve graded beds and scours. These clasts are intimately admixed with rounded phosphatic clasts cut by abundant veinlets of white calcite that pre-date clast formation (Figure 12E).

Sulfide alteration of member D outside the immediate Mactung area includes millimetric patches of pyrite and pyrite-pyrrhotite that replace the matrix, and gossanous, sulfide-rich domains of centimetre scale. The relationship of this sulfide replacement to skarn mineralization is unknown; it is present in unskarned rock on Tag Mountain. Quartz and calcite veins up to 25 cm thick cut the unit within the skarn zone on Mount Allan and, to a lesser extent, on Tag Mountain.

#### Observations, Member D Skarn

Where skarned, member D is s very finely crystalline calc-silicate rock that weathers pale to medium grey, green, beigey brown, or rusty brown (Figure 12I). Parts of it are banded with green, orange, and white layers 1 cm to 3 cm thick, finely laminated, and locally cross-laminated. The green layers are probably diopsidic and the orange layers garnetiferous (Atkinson and Baker 1986; Harris 1980). Millimetric veins of pale orange garnet(?) and translucent, slightly greenish, grey amphibole(?) form part of the skarn. Clasts are difficult to discern in outcrop of the intensive skarn, but in partially skarned outcrops on the south slope of Mount Allan, beds of phosphatic(?)-clast granule to pebble conglomerate alternate with laminated and cross-laminated limestone. The phosphatic(?) clasts are mostly black weathering but in some beds within the skarn zone, they weather white (Figure 12F). Select beds have been replaced by bundles of similarly oriented, centimetres-long, black amphibole crystals that are clustered with adjacent bundles of differing orientations (Figure 12H).

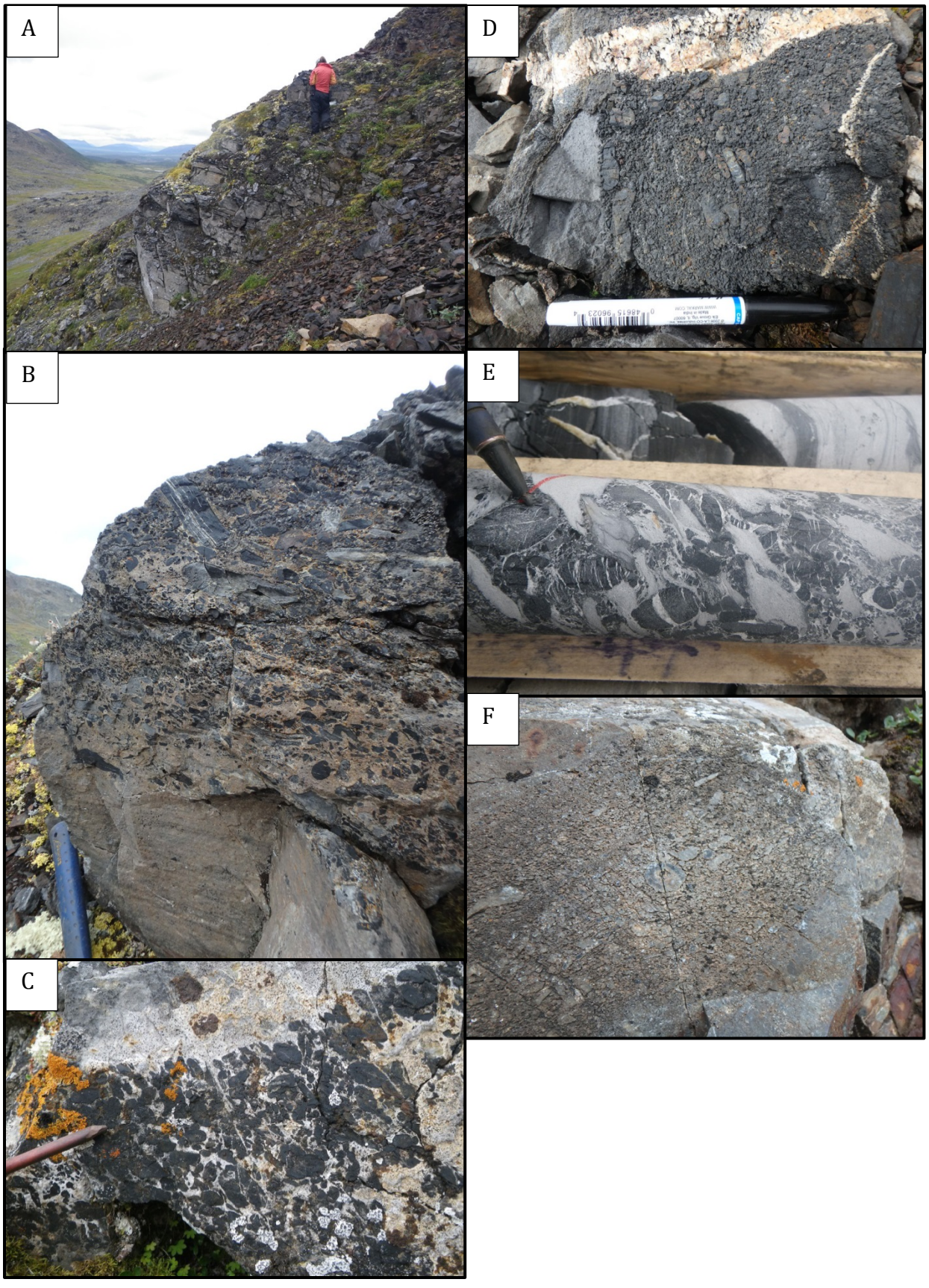
A
D
B
E
F
C

(continued)

Figure 12. (continued)

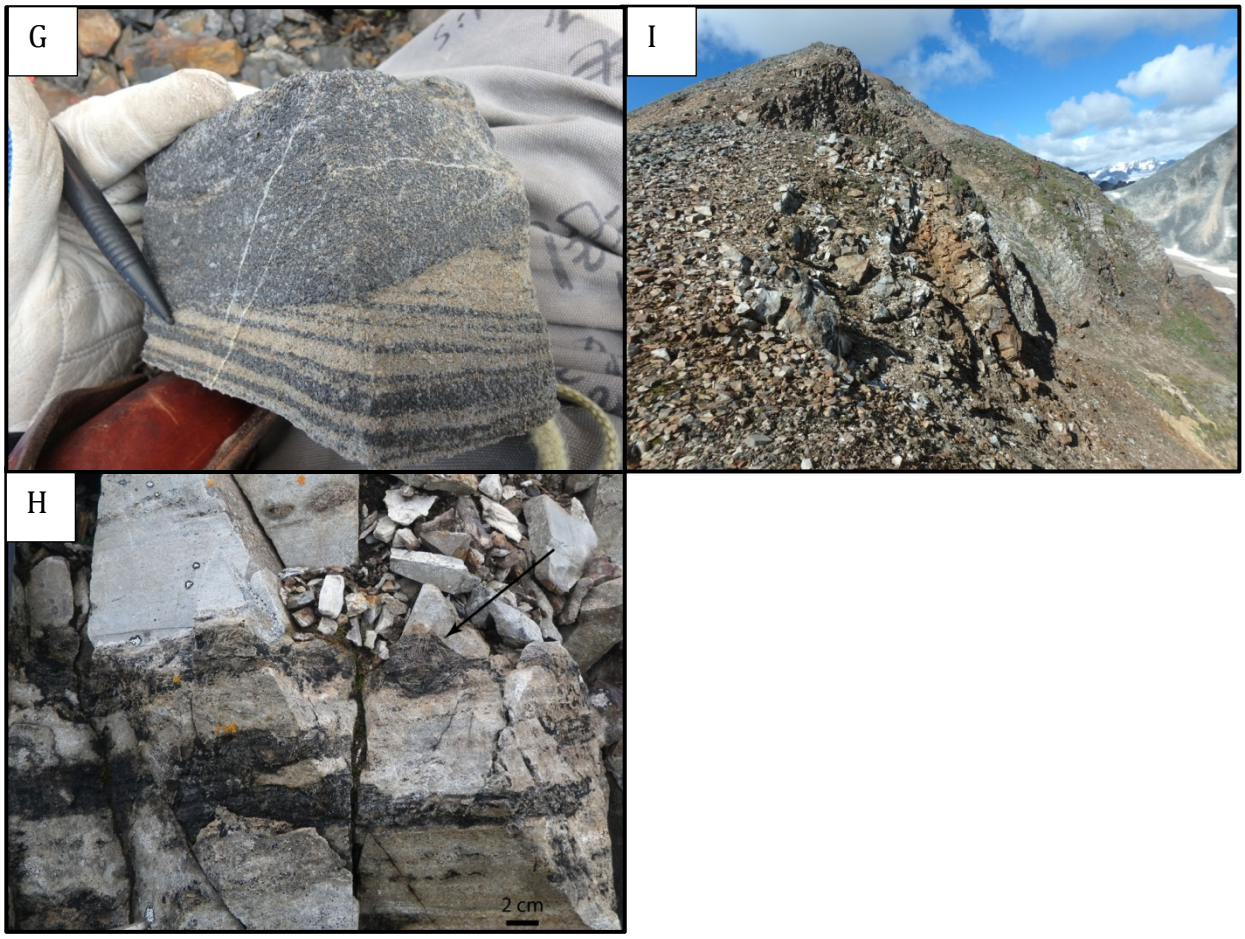


Figure 12. Member D of the Rabbitkettle Formation. [A] Outcrop appearance. Looking southeast on Fold Mountain. [B] A reversely graded bed of phosphatic- and limestone-pebble conglomerate with a quartz sandy limestone matrix, overlying a bed of quartz sandy limestone that is laminated with dark grains that are probably phosphatic. The largest clasts in the conglomerate are limestone, granule-sized ones (difficult to make out in the photo) are phosphatic, and those of intermediate size are a mixture of the two lithologies. Photo was taken on Fold Mountain. Hammer handle for scale. [C] Typical weathered surface of phosphatic-clast conglomerate. A contact with a non-conglomeratic bed is just above the pencil. Clasts weather blue-black and lack internal structure. Many are rounded oblate spheroids. Clasts are moderately densely packed and poorly sorted in this sample. Photo was taken south of Cirque Lake. Pencil for scale. [D] Conglomerate with a bimodal population of densely packed phosphatic clasts (mostly granule size, a few pebbles) and some cobbles of lime mudstone. A few of the phosphatic pebbles have small central cavities – see comment for F. Photo was taken on Tag Mountain. Marker pen for scale. [E] Drill core from a hole drilled under Mount Allan, showing densely packed clasts of lime mudstone (light and medium greys) and phosphatic(?) rock (dark grey) in a calcite matrix that appears to consist largely of cement. Irregular shapes of light grey limestone clasts suggest that these were deformed by transport in a plastic state. Regular shapes of phosphatic(?) clasts suggest re-working prior to incorporation in this final breccia. Veins cutting phosphatic(?) clasts at different orientations may be the remnants of marine cements infilling

cracks in a phosphatic hardground that was subsequently ripped apart by high-energy currents. Pencil tip is 1 mm wide; core is about 4 cm across. [F] A bed of conglomerate with phosphatic clasts that are translucent, pale grey to white on the weathered surface, from within the skarn zone on the south face of Mount Allan. Largest clast (about 7 mm across) has a central cavity that may be the mold of a weathered-out nucleus, but such structures are rare and ambiguous. [G] Piece of rubble from Tag Mountain shows a bed of coarse phosphatic-grain sandstone that has scoured the underlying laminated, phosphatic-sandy limestone. Pencil for scale. [H] Beds of limestone partially altered to calc-silicate minerals on the south face of Mount Allan. Dark, irregular bands were formed by replacement that proceeded outward from selected beds, and consist of clustered bundles of amphibole crystals (*e.g.,* at arrow) up to a few centimetres long. [I] Looking northwest across the north face of Mount Allan. Member D is the grey and locally rusty weathering band in the foreground to midground, crossing from centre to right in the bottom part of the photo; it is roughly 10 m thick. Thin beds in member D show structural undulations. Dark brown overlying rocks are mudstone hornfels of member E.

### *Members E, F, and EF – Interstratified Mudstone and Limestone*

Mine units E and F were both described as argillite, argillaceous siltstone, and siltstone, interbedded on a scale of decimetres with argillaceous limestone that is more abundant in the middles of the units (Findlay 1968; Harris and Godfrey 1975). Those early descriptions do not provide a clear demarcation between units, and the mine units 3E and 3F were eventually mapped and described as a single entity, mine unit EF, at most places on the property (Findlay 1969a, b, c; Lodder and Harris 1974; Harris and Godfrey 1974; Harris 1977, 1980). Where mine units 3E and 3F were distinguished, on the north face of Mount Allan, the distinction refers more to ore zones than to stratigraphic entities. Mine units 3E, 3F, and 3EF are referred to here as members E, F, and EF of the Rabbitkettle Formation, respectively.

Member E (uppermost horizon of the Upper ore zone) consists of 60 m of thinly interbedded, black to brown hornfels of mudstone, shale and siltstone, with scattered skarned limestone beds, and a central part with 20% skarned argillaceous limestone (Atkinson and Baker 1986). Member F (middle horizon of the Upper ore zone) consists of 30 m of thinly to very thinly interstratified mudstone and siltstone hornfels, with a middle interval containing up to 35% skarned limestone beds (Atkinson and Baker 1986). Siltstone of members E and F locally contains pyroxene and garnet, and may have a spotted appearance due to clusters of garnet (Odekirk 1979a). Member E is said to be gradational with members D below and F above. Member F is overlain sharply but conformably by member G (Atkinson and Baker 1986).

Member EF averages 90 m thick, and consists, in an ideal section, of 18 m of black shale with rare limestone intervals, 24 m of interstratified black shale and limestone, another 18 m of black shale with rare limestone, another 27 m of interstratified black shale and limestone, and a final 3 m of pyritic black shale (Harris, 1980).

Minerals in mudstone of members E and F include quartz, tremolite, plagioclase, and K-feldspar; originally pure carbonate rocks consist of dolomite, calcite, quartz, Fe-carbonate, and minor pyrrhotite, pyrite, chalcopyrite, and scheelite; and originally calcareous mudstones contain, among other minerals, clinopyroxene, calcic plagioclase, tremolite, pyrrhotite, and minor alkali amphibole (Gebru 2017).

### Definitions and General Observations

On the north face of Mount Allan, to match pre-existing maps as closely as possible in this study, the base of Member F is defined as the base of the lowest calc-silicate horizon within a thick succession (>10 m) in which calc-silicate rock is more abundant than mudstone or hornfels. Member F was also tentatively identified on Fold Mountain during this project. The division between members E and F in the eastern part of the map (Figure 4; Martel *et al.* 2018) is taken from Lodder and Harris (1974).

Members E, F, and EF are a well-bedded succession of mudstone, siltstone, and limestone. Very thin to medium, planar, parallel beds of interstratified mudstone and siltstone form intervals up to a metre thick that alternate with similar-thickness intervals of thin- to medium-bedded limestone. Members E and EF lie with apparent conformity on limestone conglomerate or calc-silicate skarn of member D. Members F and EF are overlain abruptly but conformably by member G.

### Observations, Members E and EF

Member E is a recessive to semi-resistant, brown or banded brown-and-white horizon, about 60 m thick on the North Face (Figure13A), thinning to 40 m on Tag Mountain below the thrust. Member E consists of medium to rusty brown weathering, locally siliceous, meta-mudstone and meta-siltstone, and subordinate limestone ranging from scattered lenses to abundant beds. Member EF lithologies are identical to those of member E, but the proportion of limestone or calc-silicate is less and there are no intervals more than a metre or two thick that are dominated by limestone or calc-silicate (Figure 13B).

Mudstone, silty mudstone, and siltstone of both members are intergradational and have flaggy to blocky partings (Figure 13B). The mudstone is rarely slightly calcareous, whereas the siltstone is commonly calcareous. Both the mudstone and the siltstone are medium to dark grey with rare, light orangey grey beds, and are typically very finely laminated. The beds are very thin, mostly 0.5 cm to 1 cm but up to 15 cm thick, and the bedding is defined by colour differences, bundling of laminations, greater silt or pyrite content, or preferential silicification. Graded siltstone-mudstone beds are 2 mm to 8 mm thick. Laminations in shades of grey are continuous, planar, and parallel whereas pyrite laminations are discontinuous. Pyrite is also locally abundant as scattered millimetre-scale grains. Gossans have developed along some of the calcareous siltstone intervals.

Limestone in member E ranges from sparse thin beds and concretions in mudstone, to up to 50% limestone in short sections on Tag Mountain. The limestone is typically platy, thinly to very thinly bedded, dark grey weathering with a brown, yellow or blue cast, dark to very dark grey on fresh surfaces, laminated, and very finely to medium crystalline with a component of siliciclastic silt. There are also intervals of siliceous, pyritic limestone and slabby, dull sooty-grey weathering, dark grey, microcrystalline limestone. Concretions are oblong, medium grey weathering, dark grey, finely crystalline, locally laminated, and locally pyritic, and can be over a metre long (Figure13C).

Member EF was traversed only on Fold Mountain, where it consists of silty mudstone interstratified with platy limestone (Figure13D). Beds in the rust-brown weathering mudstone are <1 cm to 15 cm thick, with sub-millimetre laminations in some. Limestone increases toward the top of the member, where it is interstratified with silty mudstone. The platy limestone is a dark grey, siliciclastic-silty lime mudstone that weathers medium grey, is thin to very thin bedded, and locally hosts oblong, calcareous, siliceous concretions a few tens of centimetres long. Soft-sediment deformation structures consist of millimetre-scale distortions in laminae (Figure 13E).

### Observations, Members E Hornfels and Skarn

Member E is a hornfelsed siltstone or mudstone with subordinate but upward-increasing amounts of calc-silicate rock. It is interpreted as skarned argillaceous to silty limestone interstratified with hornfelsed mudstone. The bulk of member E has a brown-and-white banded appearance created by brown weathering, hornfelsed mudstone interstratified on a decimetre scale with white weathering calc-silicate rock. The frequency of white horizons increases upward, until near the top there are a few metres dominated by white calc- silicate rock in which interbeds of brown hornfels are only a few centimetres thick (Figure13A). The very top few metres consist of brown hornfels without calc-silicate beds.

The mudstone and calc-silicate intervals are described further in the following paragraphs. Brown intervals of mudstone hornfels are up to 1 m thick and banded on a centimetre to decimetre scale by alternating yellow-grey *versus* steel-grey bands. The rock is a very fine-grained hornfels, typically well laminated, often with sulfides. The rock is brown weathering, and dark steely grey on fresh surfaces, with a purplish sheen on fractures. Bleaching along fractures and bedding planes is common within the skarn zone. In the lowermost parts of member E, centimetre-scale, rusty-yellow-beige alteration corridors that run alongside fractures form a network around domains of grey, unaltered rock (Figure 13G).

Calc-silicate intervals are 30 cm to 60 cm thick, and consist of hard, non-siliceous, non-calcareous, thinly bedded, microcrystalline (to finely crystalline), pale grey, pale purplish grey, and greenish grey hornfels, and orangey grey or greenish grey skarn (Figure 13H). These rocks locally have a talcy feel. Planar, parallel laminations are common. In areas of heavier skarning, pale green, very fine-grained alteration invades the calc-silicate rock along bedding planes and fractures (Figure 13I), or cuts across and obliterates bedding. Veins of brown and pale green skarn cut the calc-silicate intervals. Abundant veins of coarse quartz, many of them rimmed by sulfides and diopside(?), and veins of coarse calcite cut member E within the skarn zone on the North Face.

A variety of lenticular features are present in both the brown mudstone hornfels and the pale calc-silicate rock. In the mudstone hornfels, there are millimetre-scale, white- weathering lenses of very fine-grained, non-siliceous, non-calcareous material. In the calc- silicate horizons, there are similar, white-weathering lenses, as well as very thin lenses or discontinuous laminations of darker grey (Figure 13J), and black, argillaceous horizons. There are also rare, centimetre-scale, black lenses, reminiscent of the black chert lenses in member F but not siliceous, which may be chert nodules that were de-silicified during metasomatic alteration (Figure 13J).

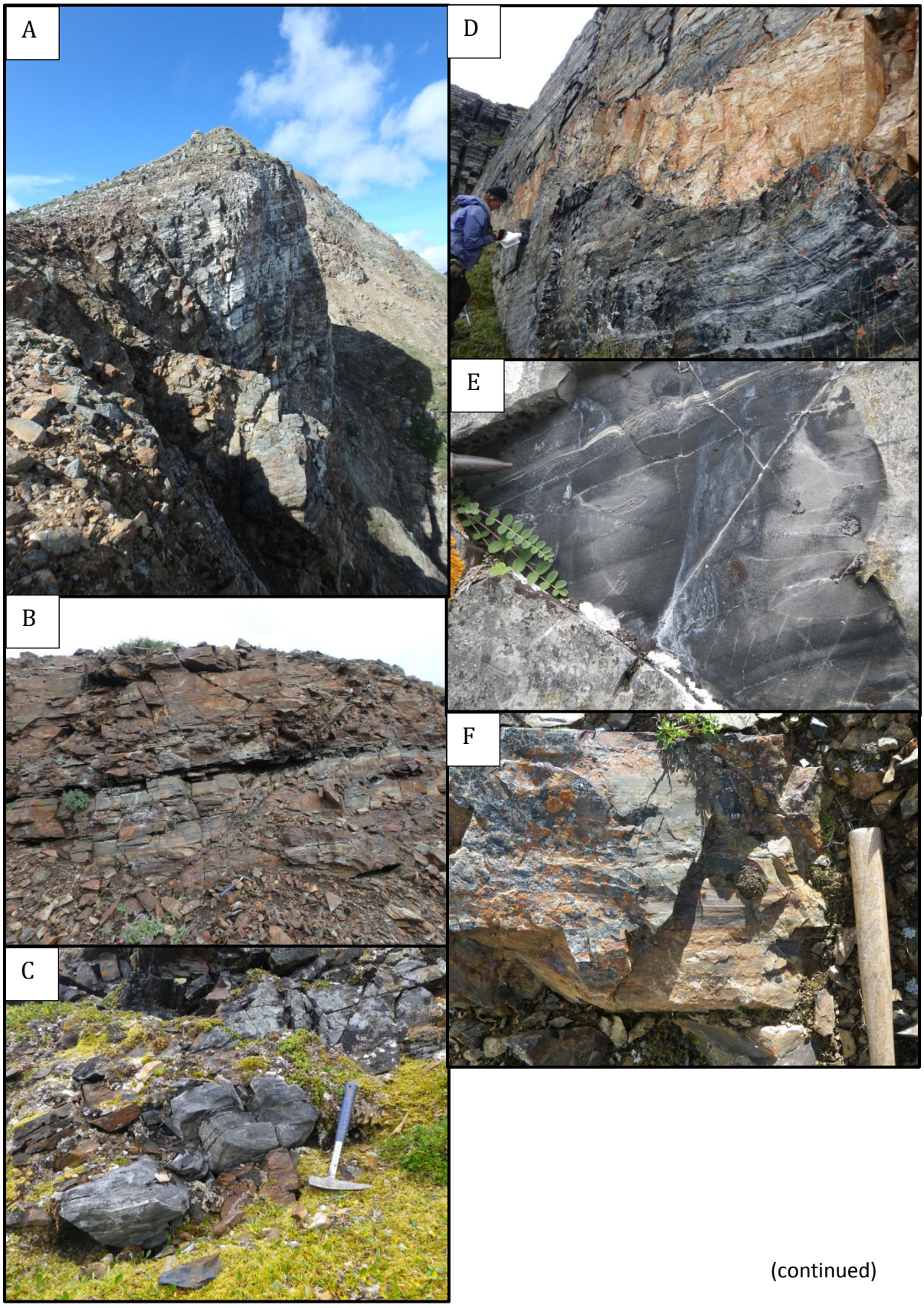


(continued)

Figure 13. (continued)

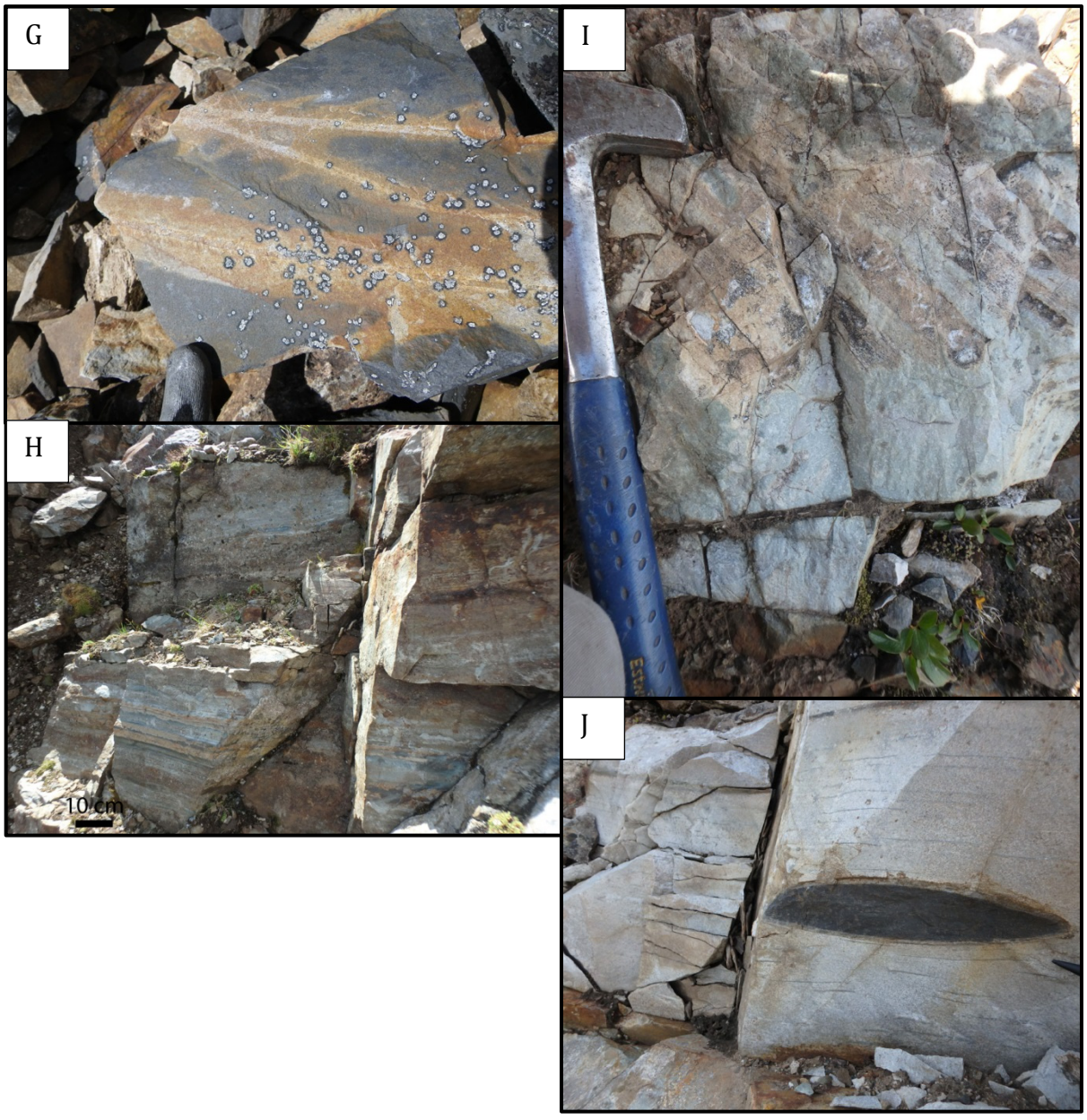


Figure 13. Members E and EF of the Rabbitkettle Formation. [A] Upper member E in the skarn zone on the north face of Mount Allan. Looking southeast. White-banded part of the cliff face is about 6 m high. [B] Mudstone and silicified mudstone of member EF on the south slope of Mount Allan. Hammer in the foreground is 40 cm long. [C] Grey limestone concretion (offset by minor fault) within brown mudstone of member E south of Cirque Lake. Hammer is 30 cm long. [D] Very thin-bedded limestone and mudstone of member EF cut by felsic dyke. Brownish grey beds are silty mudstone, dark grey beds are silty lime mudstone. [E] Soft-sediment deformation in white laminations within thin-bedded lime mudstone. Blue efflorescence obscures part of the rock. Pencil tip is 1 mm wide. [F] Finely laminated, mudstone hornfels from member E within the skarn zone on the north face of Mount Allan. Hammer handle is 3.5 cm across.

[G] Alteration style that is typical of mudstone hornfels within the skarn zone. Yellow alteration halos along fractures separate domains of unaltered, steely grey hornfels. Grey-gloved fingertip at the bottom for scale. [H] Very thin-bedded calc-silicate rock of member E skarn on the north face of Mount Allan. [I] Pale green diopsidic(?) skarn invades a pale brown calc-silicate hornfels along bedding planes. From skarn zone on the north face of Mount Allan. Hammer for scale. [J] Discontinuous, dark grey laminae and a black lens that may be a de-silicified chert nodule, in calc-silicate skarn. Member E, north face of Mount Allan. End of pencil for scale.

**Observations, Members EF Hornfels and Skarn**

Brown intervals of mudstone hornfels are at least 5 m thick and probably much thicker in member EF. Near the edge of the hornfels zone, meta-mudstone of member EF contains tiny, equant, glassy porphyroblasts.

Calc-silicate skarn of member EF contains 10% disseminated, mm-scale, magnetic grains of pyrrhotite (surrounded by magnetite?) in a very finely crystalline, pale grey, buff-weathering, calcareous calc-silicate rock. Where metamorphosed but not skarned, the platy limestone of member EF contains abundant millimetre-long grey amphibole(?) porphyroblasts shaped like needles or slender prisms.

**Observations, Member F**

Member F forms resistant, whitish grey horizons on the steep north and west slopes of Mount Allan (Figure 5), where the unit has a banded appearance from short distances away. Member F is much the same as member E, except that calc-silicate intervals are more abundant than intervals of mudstone hornfels, and are generally thinner bedded and better laminated than those in member E. Beds or lenses of medium grey weathering marble are present but rare in the calc-silicate horizons. Member F, like member E, is cut by numerous veins of calc-silicate minerals, calcite, and quartz.

Rocks assigned to member F on Tag Mountain include a variety of interstratified calcareous and terrigenous lithologies, in intervals ranging from <1 m to 8 m thick. Rock types include: nodular meta-limestone in which thin, light grey marble beds and nodules are separated by yellow, laminated silty limestone(Figure 14A); platy lime siltstone; sooty grey lime mudstone; dark grey, finely crystalline, pyritic marble; and recessive, dark grey, silty mudstone and siltstone. Beds in all of these lithologies are thin, defined by compositional differences or the density of laminations (Figure 14). Laminations are mostly planar or wavy but include cross-laminations in silty beds (Figures 14B and 14C). Rock types also include a grey calc-silicate rock that is resistant, microcrystalline, white to grey weathering, non-calcareous, and locally siliceous, and has planar, parallel layers from less than a millimetre to a few centimetres thick, abundant disseminated pyrite, and rare black chert nodules.

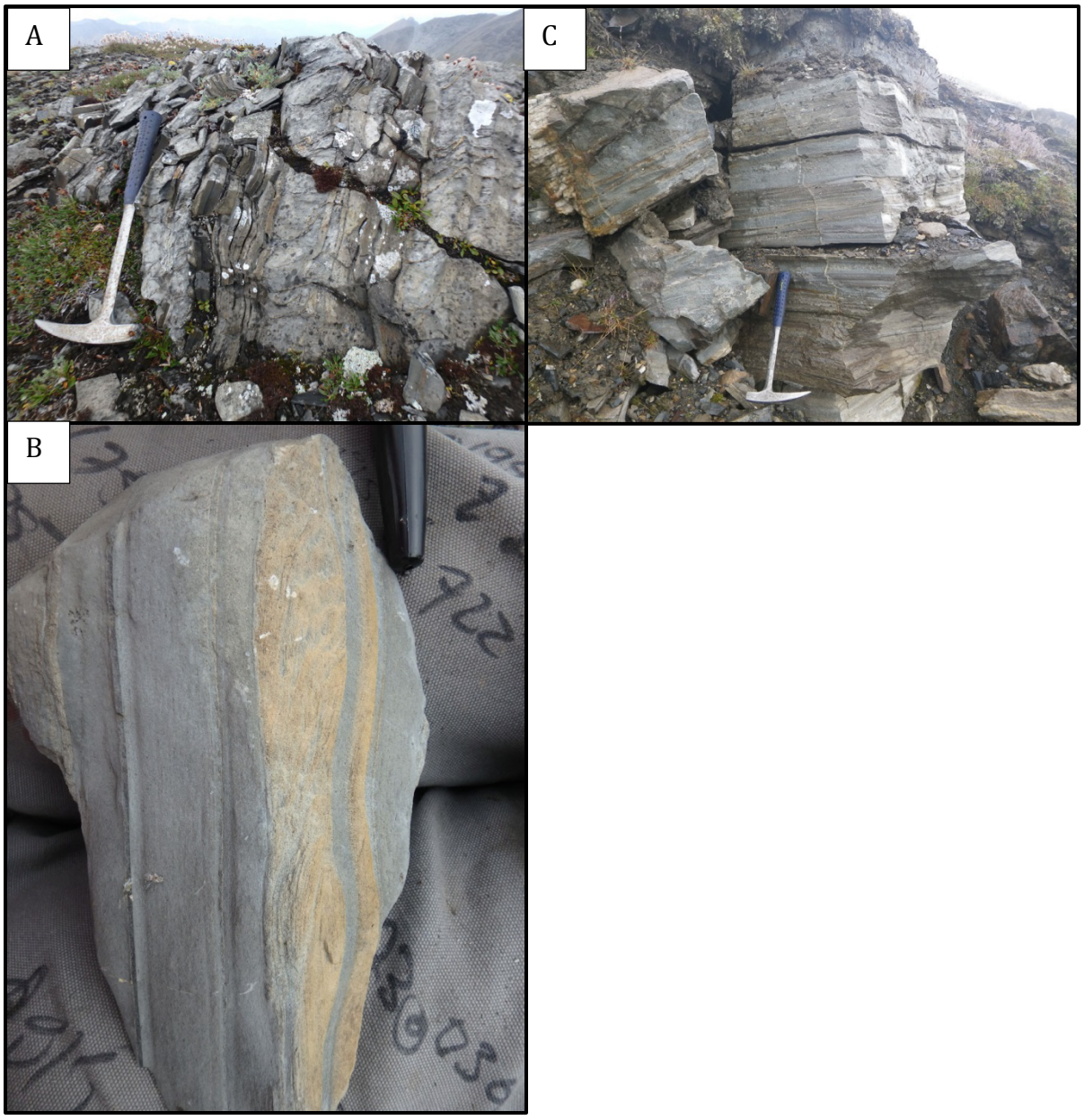


Figure 14. Member F of the Rabbitkettle Formation. [A] Subvertical beds of yellowish grey silty limestone and light grey re-crystallized limestone or marble. Hammer is 40 cm long. [B] Ripple cross-laminated yellow silty limestone and planar-parallel laminated grey lime mudstone. Tip of marker pen for scale. [C] Calc-silicate rock from within the skarn zone, otherwise similar to the rock shown in [A] and [B]. The yellowish/brownish grey, silty layers are cross laminated. Hammer is 40 cm long.

### *Member G – Calc-silicate rock or dolostone*

Mine unit 3G is referred to here as member G of the Rabbitkettle Formation. Member G is described as a 20 m-thick, banded quartz-talc-tremolite hornfels and locally a banded marble within the hornfels zone, and a dolostone outside of it (Atkinson and Baker 1986; Harris

1980; Oderkirk 1979a). Member G is resistant, with thin shale interbeds (Atkinson and Baker 1986), and has sharp but conformable upper and lower contacts. The member forms an upper cap to the ore system, with all but a trace of scheelite mineralization occurring below (Atkinson and Baker 1986; Harris 1980). A recent interpretation suggests that the talc-tremolite rock was produced by contact metasomatism of a quartz-tremolite schist, itself derived by regional metamorphism of a dolostone (Gebru 2017).

### *Observations*

Member G lies conformably but sharply on members E and EF. Member G forms a resistant horizon with a distinctive greenish grey, almost bluish grey, colour as seen from a distance. Member G is 20 m thick on Mount Allan, and 10 m to 20 m thick to the east and west. West of Fold Mountain, member G may be even thinner, and is of very different character. Member G is metamorphosed and skarned on Mount Allan and Fold Mountain, and elsewhere is metamorphosed but unskarned or patchily skarned.

Metamorphosed member G includes resistant, medium crystalline, very light grey weathering, white marble; recessive, platy marble in decimetric intervals; and thin-bedded, siliceous, locally calcareous dolostone to calc-silicate rock (Figure 15A).

Member G skarn is a well-bedded, finely to microcrystalline, calc-silicate rock that can locally be called a talc-tremolite schist. Member G weathers light grey to buff, commonly with greenish grey layers (Figure 15B; also, a photo of this member is used for illustration in the Structure section, Figure 23B), and is white, light grey or medium grey on fresh surfaces. Despite the very fine crystal size, its weathered aspect on Mount Allan is that of a medium or coarsely crystalline rock. Member G skarn is locally calcareous or siliceous, moderately soft to hard, and is commonly schistose with a sub-phyllitic sheen that is probably caused by talc (Figure 15C). Prismatic or acicular porphyroblasts of dark grey tremolite(?) are concentrated in some of the skarned beds, graded in size and abundance (decreasing up). These porphyroblasts are typically <1 mm long and have been weathered out on all exposed surfaces (Figure 15E). Tiny equant porphyroblasts of translucent, pale pinkish orange garnet(?) are present in places. Beds in member G skarn are thin to very thin, typically laminated, and rarely cross-laminated (Figure 15D). Local medium-thickness intervals and interbeds of marble and argillaceous rock interrupt the calc-silicate succession.

In the valley west of Fold Mountain, the top of the Rabbitkettle Formation has been assigned to member G but is atypical. The atypical member G consists of mudstone interbedded with siliceous, slightly calcareous mudstone to siltstone, and sparse, 20-cm beds of finely crystalline limestone. Beds are planar and parallel, ranging from <1 cm to 30 cm thick. The siliceous, slightly calcareous beds contain abundant deformed burrows(?) preserved as irregular, wispy, darker grey laminations and distorted lenses (Figure 15F). The very top of the member is a resistant interval of very dark grey, siliceous, pyritic mudstone containing irregularly shaped, flat, elongate, centimetre-scale clasts or lenses of mudstone with a very thin dimension perpendicular to bedding. Some of the clasts(?) weather a light bluish grey (Figure 15G).

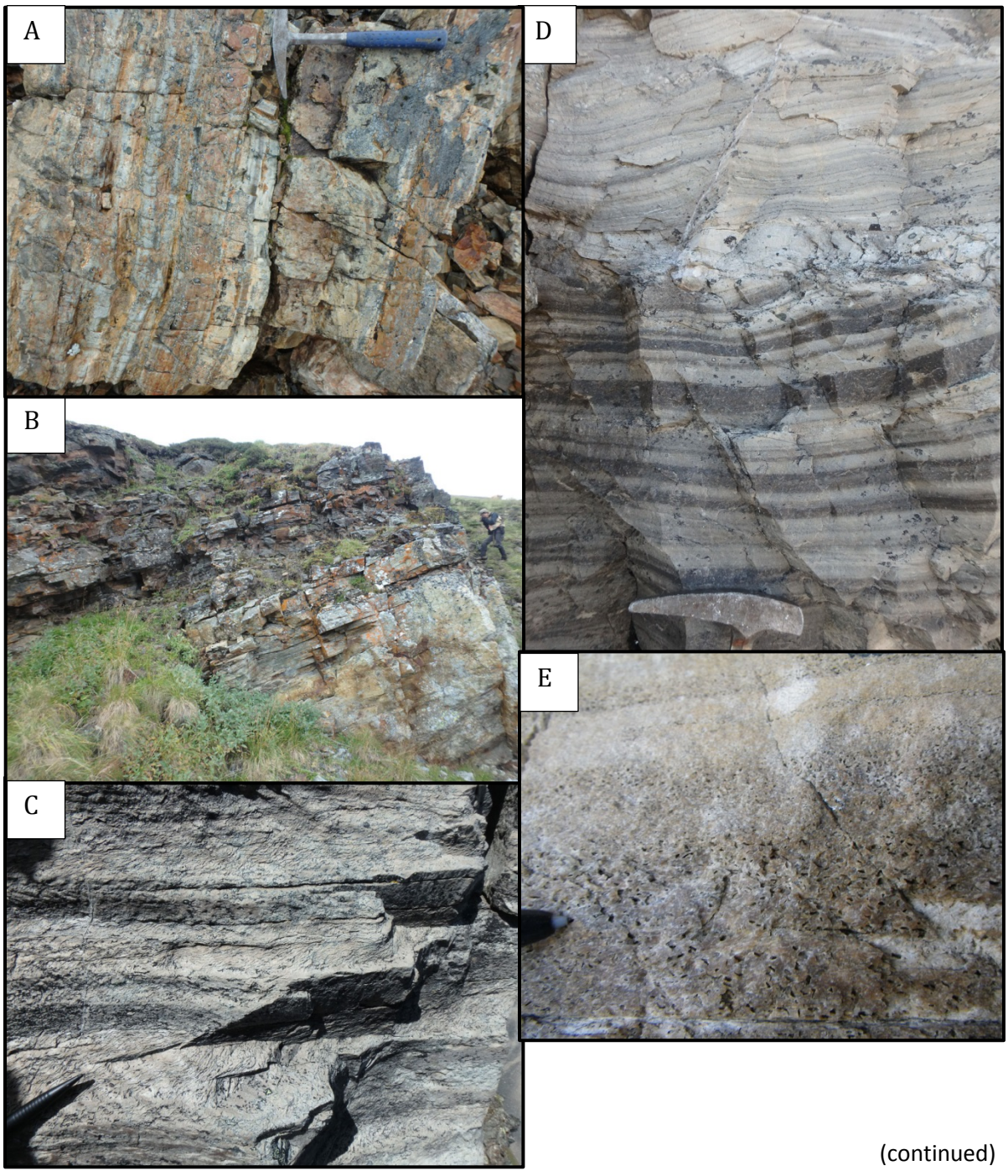


(continued)

Figure 15. (continued)

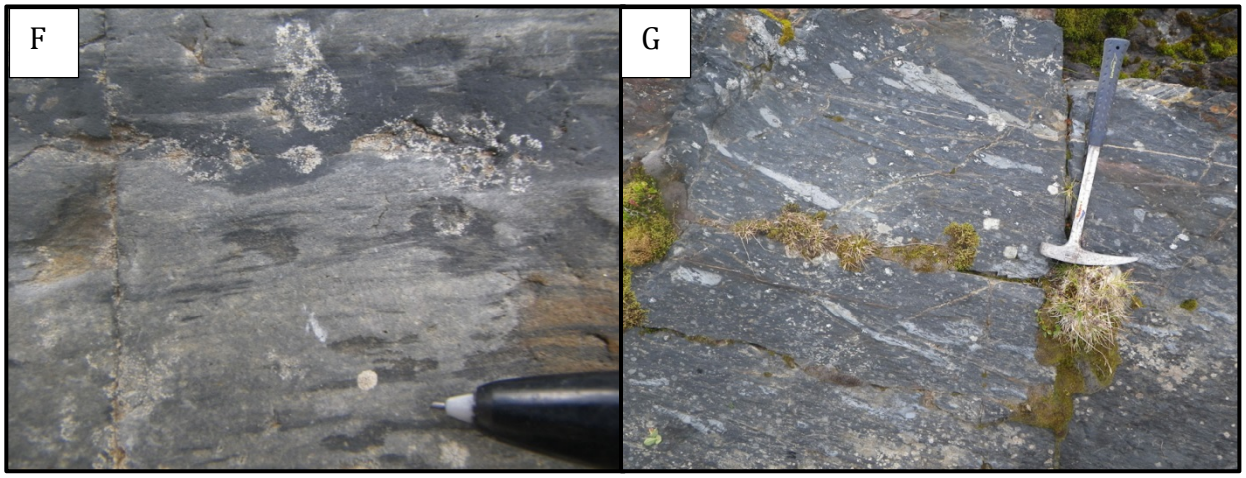


Figure 15. Member G of the Rabbitkettle Formation. [A] Thin-bedded, siliceous, dolomitic calc-silicate rock south of Cirque Lake. Hammer is 30 cm long. [B] Member G (buff coloured) overlain by the Duo Lake Formation (brown). South slope of Mount Allan. [C] Talc-tremolite schist with phyllitic sheen. Foliation intersects thin beds at a low to moderate angle. North face of Mount Allan. End of pencil for scale. [D] Thin-bedded calc-silicate skarn underlies laminated calc-silicate skarn. North face of Mount Allan. Hammer head is about 12 cm long. [E] Pits from weathered-out tremolite(?) crystals are graded in size, decreasing upward. Pencil tip is 1 mm wide. [F] Deformed burrows(?), viewed at an angle to bedding. Pencil tip is 1 mm wide. [G] Elongate, irregularly shaped structures (flat clasts?) within siliceous mudstone weather a pale bluish grey. Hammer is 40 cm long.

## *Interpretation*

### Member D

Rocks rich in phosphatic minerals can form in a variety of ways. Phosphatic laminae can form during very early diagenesis, within the upper few centimetres of sediment on the sea floor, during periods of very low sedimentation rate and upwelling of bottom waters rich in inorganic phosphorus (Follmi *et al.* 2005). Phosphatic material formed in this way can be concentrated by subsequent breakage of the laminae and winnowing by bottom currents (Follmi *et al.* 2005). In places of high primary productivity where organic matter accumulates at a high rate, phosphate minerals form below the sediment-seawater interface through microbial oxidation of organic matter (Follmi 1996). In deltaic and nearshore marine environments with high sediment accumulation rates and vigorous bioturbation, phosphate minerals precipitate as a consequence of phosphate desorption from buried riverine iron and manganese oxyhydroxides (Follmi 1996). The phosphatic minerals at Mactung appear to derive from hardgrounds or lamellae that were broken and re-worked multiple times, thus perhaps the processes responsible for phosphate precipitation were low sedimentation rate and nutrient upwelling, although the process of oxidation of organic matter within the sediment can't be ruled out. Plastically deformed rip-up clasts admixed with veined phosphatic clasts, described above (Figure 12E), support this notion: since at least some of the clasts formed as rip-ups of a still-plastic substrate, the veins, which pre-date clast formation, also must have formed in an unlithified substrate, thus the veins might represent

cracks in a phosphatic hardground that were infilled with marine cement prior to the hardground being ripped up by storm or wave currents.
Graded beds and planar and cross laminations in Member D suggest deposition as tempestites or turbidites (Lowe 1982). The presence of reverse grading suggests that at least some of the succession was deposited from turbidity currents or debris flows (Lowe 1982), which may have been initiated by major storm events, tidal action, or gravitational collapse. The paucity of coated grains in the population of phosphatic grains supports an allochthonous emplacement.

An interpretation of member D that is compatible with the available information is that member D developed by prolonged bottom-current winnowing, repeated sediment gravity flows, and episodic fluvial input on a carbonate shelf where phosphogenesis was a significant contributor to sediment formation. Rivers transported quartz grains up to granule size from a mature hinterland. The thinner beds of phosphate-granule conglomerate conceivably formed *in situ* by storm- or current-driven winnowing of lime muds containing phosphatic lamellae (as has been suggested for parts of the Monterey Formation in California; Follmi *et al.* 2005), however, evidence for transport of sediments is provided by the mixture of phosphatic lithoclasts, fragments of lime mudstone, and mature quartz grains in thicker beds, the scouring at the bases of some beds, and erosion at the tops of others. Transport distances in the initial breccia-forming events may not have been far, permitting repeated re-working and multiple generations of brecciation. Sediment gravity flows caused by mild storm surges may have swept winnowed, fragmental, phosphatic sediments off the shelf, or basinward down a sloping shelf, scouring the underlying muds and forming granule-conglomerate beds a few centimetres to a few millimetres thick. The larger, rounded phosphatic grains, however, were transported in a high-energy flow or for long distances, probably by turbidity currents. In-between sediment-flow events, lime muds were deposited by currents and suspension settling. Although phosphogenesis likely took place during the prior maximum transgression of the sea, the incorporation of quartz grains and limestone clasts in the allochthonous phosphatic beds hints that their formation took place during a lowstand of sea level (Follmi 1995). Although highstand deposition cannot be ruled out (*ibid*.), lowstand deposition is compatible with Gordey and Anderson's (1993) interpretation of the basal Rabbitkettle and Haywire sandy members to the east as intertidal to shallow subtidal deposits.

### Members E to G

Although sedimentary structures are not well-preserved in members E to G, the thin beds and fine-grained aspect show that these units were deposited in deep waters, subject to some current activity indicated by cross-laminations, and minor gravity-flow events indicated by graded beds. Rare soft-sediment deformation structures imply a slope setting in places. Protoliths were mudstone, siltstone, and limestone in members E, F, and EF.

Member G was a dolostone prior to regional metamorphism (Gebru 2017), though it may have locally been a limestone (above). Grading in the size of metamorphic minerals in some beds reflects a primary compositional grading, which, along with rarely preserved cross-laminations, may have been created by sediment gravity flows. Interbeds of medium thickness in a predominantly thin-bedded unit may reflect similar episodic depositional events. If dolomitization was diagenetic, rather than fault-related, member G was probably

deposited in waters of shallow to moderate depth. On Mount Allan, member G has a coarse-grained appearance on weathered surfaces, at odds with its microcrystalline grain size. This appearance may result from textural preservation of medium to coarse quartz sand grains that have been replaced by microcrystalline aggregates of calc-silicate minerals (as described, for example, by Blusson (1968) for contact metamorphism of quartz-sandy dolostones at Cantung). Therefore, parts of member G on Mount Allan may have originated as a quartz-sandy dolostone.

### *Correlation*

The stratigraphic interval occupied by members D to G is no older than early to middle Cambrian (sponge spicules in the Hess River Formation at Mactung; Atkinson and Baker 1986) and no younger than Late Ordovician (the age of upper the Duo Lake Formation at Mactung, below). Units that occupy the same stratigraphic interval regionally include the Gull Lake, lower Elmer Creek (Cecile 2000), Hess River, and Rabbitkettle formations, and the lower parts of the Duo Lake and Haywire formations (Gordey and Anderson 1993; Cecile 2000). The Elmer Creek Formation, exposed ≥30 km northwest of Mactung, is dominated by chert and represents a deeper basinal environment than the Mactung strata. The Haywire Formation is a dolostone with a basal sandstone member exposed 110 km southeast of Mactung. It was deposited in shallower water than the strata at Mactung. Only the Hess River, Rabbitkettle, and Duo Lake formations were deposited in slope or basinal environments and could therefore be matches for members D to G. It is furthermore clear that some of the members D to G must belong to the Rabbitkettle Formation since the Duo Lake Formation is not likely to lie directly on the Hess River Formation.

Member D therefore correlates with either the basal Rabbitkettle Formation or the upper Hess River Formation. The choice of unit is informed by a comparison of the latter two units with member D and the environment of formation inferred for member D. Phosphatic intervals are present regionally in both the Hess River and Rabbitkettle formations: an interval of phosphatic sandstone and quartz-sandy limestone is present near the middle of the Hess River Formation in a section measured 55 km northeast of Mactung (Turner *et al.* 2011); the base of the Rabbitkettle Formation on the Niddery High (Figure 2) consists of 20 cm of limestone conglomerate with black, phosphatic cement; and at another location on the Niddery High, there is a 10 m interval within the Rabbitkettle Formation of thick- bedded limestone containing phosphatic nodules and laminae (Christie and Sheldon 1986). Therefore the presence of phosphorite is not distinctive of either formation. The upper part of Hess River Formation is nowhere remarkably different from the rest of the formation. Likewise, the Rabbitkettle Formation within the Misty Creek Embayment and on the Niddery High (Figure 2; NTS 106B, 105O, and 105P) contains no distinctive basal member (Cecile 1982, 2000; Fischer 2016; Turner *et al.* 2011). However, along the eastern margin of the Selwyn Basin (NTS 105I/NE), the lowermost Rabbitkettle Formation consists of 30 m to 40 m of white weathering, fine-grained, medium- to thick-bedded quartz sandstone with ripple cross-laminations and herringbone cross-stratification, and minor siltstone (Gordey and Anderson 1993). This sandstone member developed during a period of shallowing at the beginning of Rabbitkettle time (*ibid*.). Farther south, in NTS 105I/SE, strata equivalent to the lower Rabbitkettle Formation consist of a quartz sandstone and sandy dolostone with local dessication cracks and raindrop imprints. These strata belong to the basal Haywire

Formation and were deposited on a sandy to muddy tidal flat that intermittently experienced subaerial conditions (Gordey and Anderson 1993). In NTS 105I/SW and parts of NTS 105J, strata equivalent to the basal Rabbitkettle and Haywire formations are absent beneath a pronounced Late Cambrian unconformity (Gordey and Anderson 1993; Gordey 2013). In NTS 105J/NW, the base of the Rabbitkettle Formation is covered, but one of the lowest exposed intervals is a thick conglomerate with limestone and quartz sandstone clasts (Gordey 2013).

At Mactung, member D marks a change in depositional environment from quiet, background sedimentation, interrupted occasionally by minor sediment gravity flows sourced from a muddy shelf, to active deposition dominated by sediment gravity flows sourced from a mixed shelf undergoing prolonged phosphogenesis. Such a change appears to indicate shoaling of the depositional area, which would be expected basinward of the developing unconformity and subaerial exposure 100 km away, in southern NTS 105I. Therefore member D is assigned to the basal Rabbitkettle Formation, correlative with the sandstone members at the bases of the Rabbitkettle and Haywire formations in southern NTS 105I. The remaining members thus belong to the Rabbitkettle Formation or younger formations.

The lithologies and stratigraphic packaging of members E to G can be compared with those of their possible correlatives. The Hess River Formation is a possible correlative only if the assignment of member D to basal Rabbitkettle Formation is wrong. The Rabbitkettle Formation in this type area (NTS 105I/SE; Gabrielse *et al.* 1973) and in the Misty Creek Embayment (NTS 106B and 105O/NE; Fischer 2016; Cecile 1982) is a semi-resistant unit of thinly interbedded, wavy-banded silty limestone and variably calcareous siltstone, with minor shale, dolostone, slump breccias and intraformational debrites. The formation has a distinctive banded appearance at scales ranging from hand specimen to mountainsides, caused by the regular alternation of yellow *versus* grey weathering beds and by thin, rhythmically repeated couplets of limestone grading up into shale. In these areas, the Rabbitkettle Formation lacks the thick intervals of mudstone found in members E and EF at Mactung, however, it bears similarities to member F. On the Niddery High and in places along the eastern margin of Misty Creek Embayment (NTS 105O and 105P; Cecile 1996, 2000; Turner *et al.* 2011), mud-grade calcareous rocks form 30% to 50% of the unit, in intervals <1 m thick; and at one locality in the easternmost Selwyn Basin (NTS 105I/NE), calcareous shale and calcareous siltstone form intervals tens of metres thick (Gordey and Anderson 1993, section 22). The Rabbitkettle Formation at this latter location is comparable to members E, F, and EF at Mactung. Southwest of Mactung (northern NTS 105J), the Rabbitkettle Formation is predominantly argillite, with lesser planar and ripple cross-laminated siltstone (locally sandstone) and silty limestone, local thick intervals of finely crystalline limestone, thin chert interbeds, and a thick, basal conglomerate with limestone and quartz sandstone clasts (Gordey 2013). The Duo Lake Formation lacks thick carbonate intervals, except for the Cloudy member, which is a thick limestone interval at the top of the formation in the heart of the Misty Creek Embayment (Cecile 1982). The bulk of the lithological and stratigraphic evidence support the assignment of members E, F, and EF to Rabbitkettle Formation.

Thick intervals of crystalline dolostone, such as the protolith of member G, have not been recorded in Rabbitkettle Formation. Dolomitic shale is common, as are thin intervals of crystalline limestone. Thin-bedded dolostone is rare. At one locality (NTS 105I/NW), a 60-

metre interval of medium-bedded crystalline limestone is present in the upper part of the section. Member G, despite the scarcity of crystalline dolostone in Rabbitkettle Formationregionally, is more akin to Rabbitkettle Formation. Thus, members D to G are all correlated with the Rabbitkettle Formation.

## Duo Lake Formation, Early Ordovician to Early Silurian

The Duo Lake Formation is a basinal unit that is recognized in the Misty Creek Embayment and eastern Selwyn Basin (Cecile 1982, 1996, 2000; Gordey and Anderson 1993). The type section of the Duo Lake Formation is 163 km north of Mactung (64° 42' N, 130° 47' W, NTS 106B). At that location, the Duo Lake Formation ranges in age from earliest Early Ordovician to Late Ordovician (Cecile 1982). The basal and upper contacts of the formation are diachronous, both being younger to the southeast of the type section. The Duo Lake Formation in NTS 105O ranges from late Early Ordovician to latest early Silurian (Cecile 2000; Abbott 2013). The oldest and youngest ages are both from a section 6 km northeast of Mactung, where the uppermost Duo Lake Formation is latest Llandovery and the base of the unit is latest Early to Middle Ordovician (Abbott 2013).

Mine units 3H and 4 are assigned to the Duo Lake Formation. Mine unit 3H has been described as over 90 m of black, carbonaceous, pyritic, fissile shale with strong limonite stains on surface exposures, and unit 4 has been described as ≥50 m of black, carbonaceous, graptolitic shale and flaggy mudstone (Atkinson and Baker 1986).

### *Observations*

The Duo Lake Formation is subdivided into Upper and Lower members. Both members are present on Mount Allan (Figure 5) and the Lower member alone on Tag Mountain and Fold Mountain (Figure 11). Industry maps show both members on the peak east of Fold Mountain; they have been eastward from there to the map edge for this project (Figure 4). The Upper member is inferred to be present under cover elsewhere. The Lower and Upper members can be distinguished by weathering colours and relative resistance, which are rusty brown and semi-resistant for the Lower member, and black and recessive for the Upper member (Figures 5, 11, and 16).

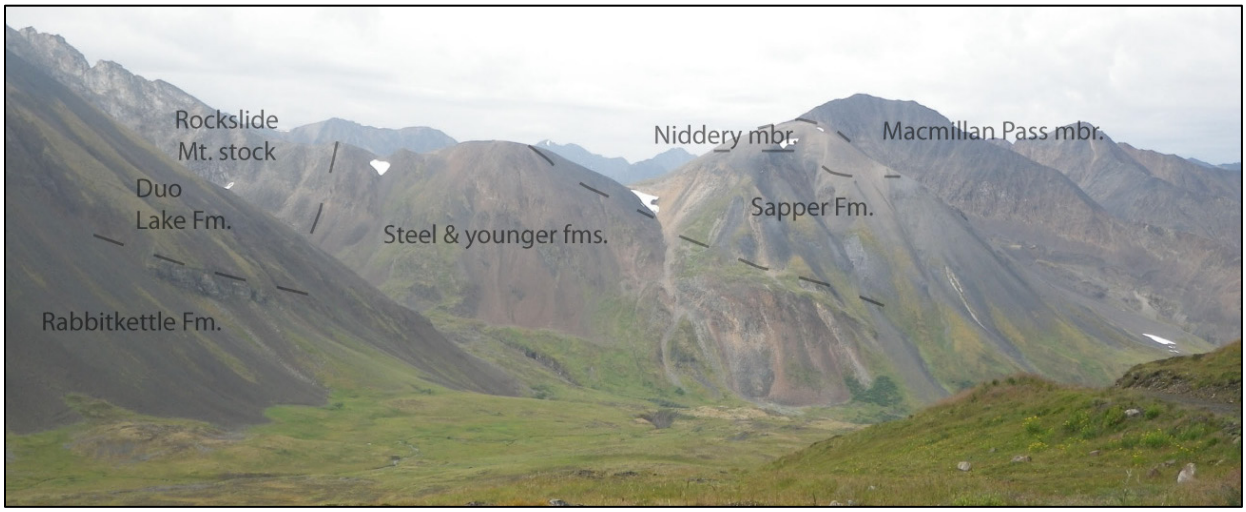

Figure 16. Looking southwest at Barite Mountain. Units discernable at a distance are labelled.

The Lower member of Duo Lake Formation (mine unit 3H) is a very thin- to medium- bedded (rarely thick-bedded), locally siliceous, medium grey to black, fine to medium grained mudstone, silty mudstone, and siltstone, with minor limestone. The Lower member weathers rusty brown, dark greenish grey, yellowish ochre, or black, and is commonly siliceous, pyritic, or both (Figure 17A; a photo of this member is used for illustration in the Structure section, Figure 23F). Beds as thin as a few millimetres are defined by subtle differences in grain size or by concentration of sulfides (Figures 17B and 17C). Monotonous successions of very thin to thin, planar, parallel beds can be over 10 m thick. Lighter coloured beds consist of beige or medium grey weathering, dark grey siltstone with sub- millimetre, pyritic, calcareous laminations that are planar, parallel, and discontinuous. Darker beds consist of dark brown or dark grey weathering, very dark grey, fine mudstone with 0.5 cm to 2 cm lenses of pyrite or pyrrhotite. Laminations in the darker beds, where present, are sub-millimetre in thickness, defined by shades of grey and locally also by concentrations of sulfides, discontinuous to continuous, planar or rarely wavy, and parallel. The Lower member has a fissile to blocky parting, but even where the rock has a blocky parting, it breaks into plates upon being struck. Within the hornfels zone, cordierite(?) and andalusite(?) porphyroblasts are present, some containing pyrite at the core.

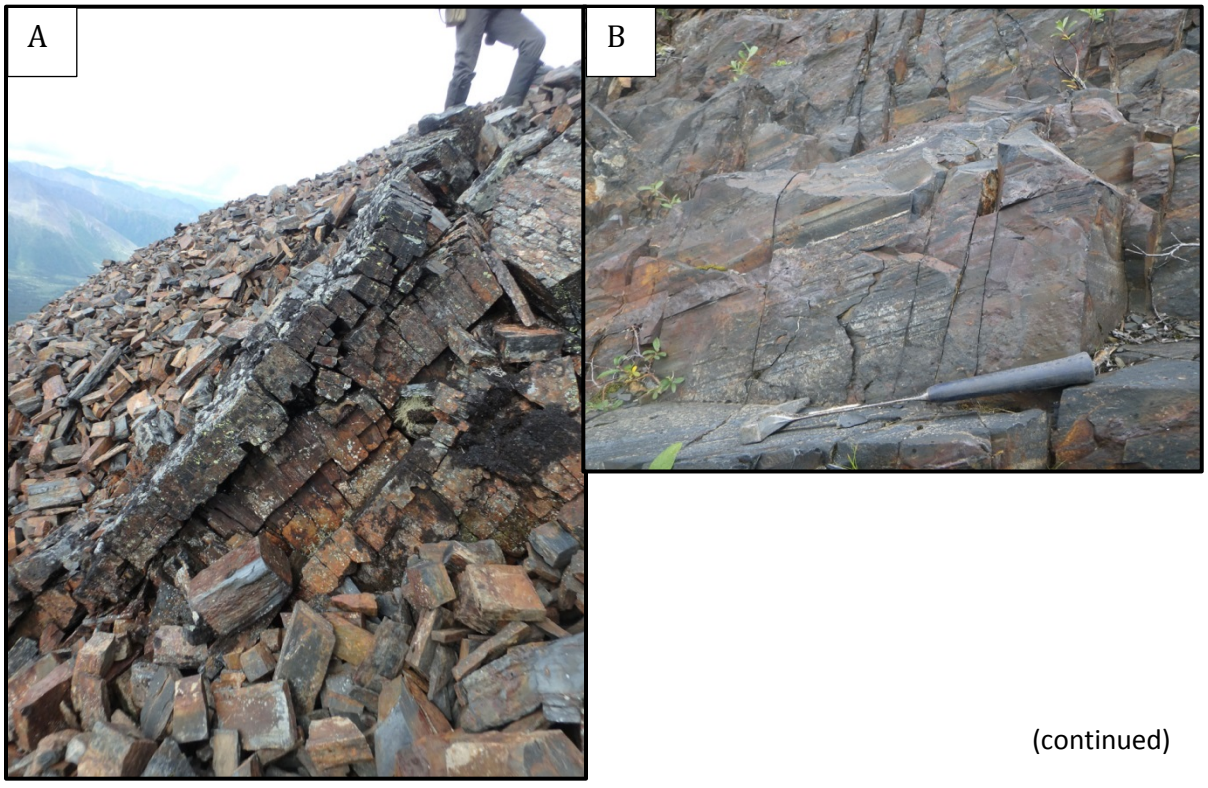


(continued)

Figure 17. (continued)

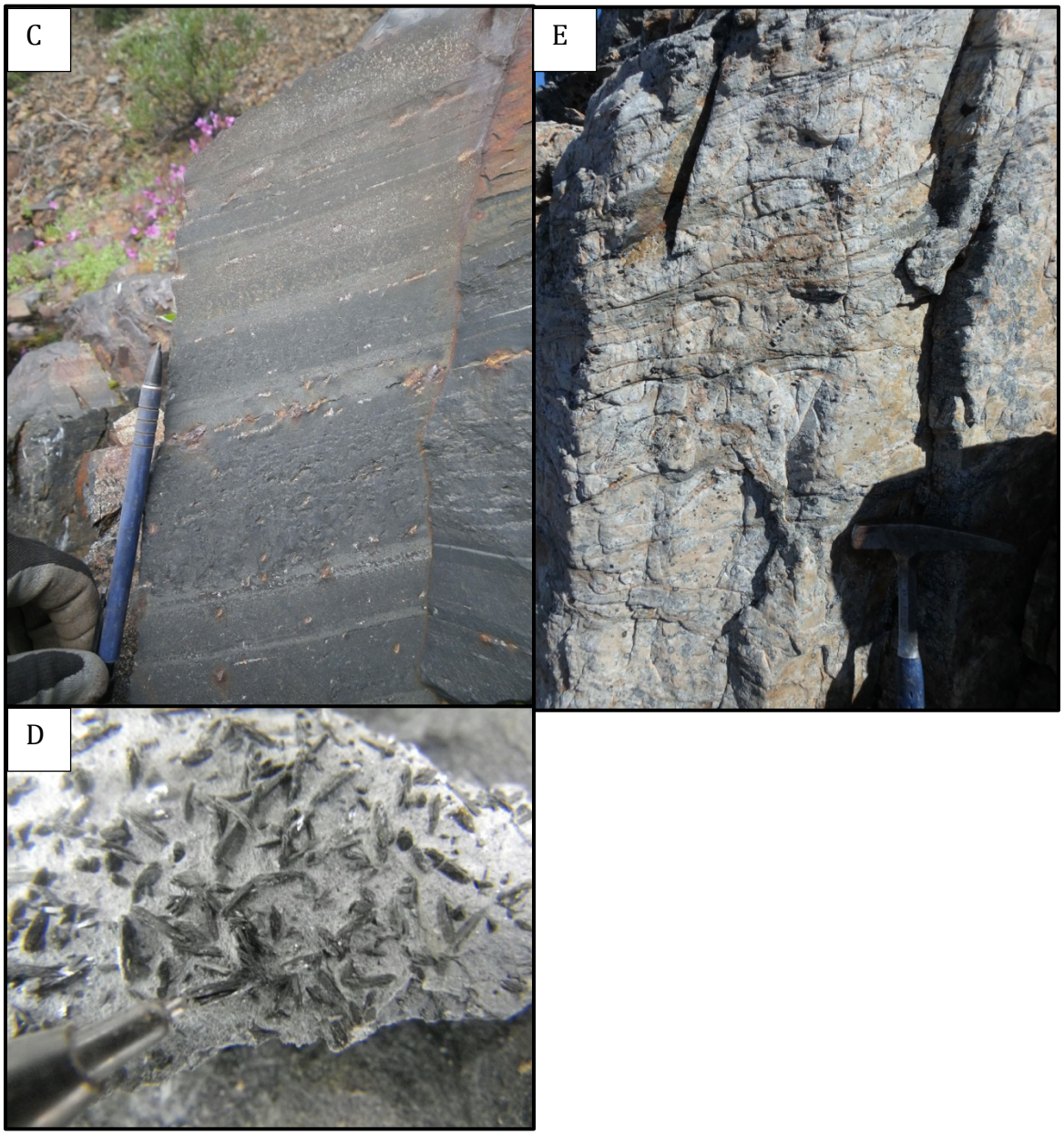


Figure 17. The Duo Lake Formation, Lower member. [A] Typical outcrop appearance. At this location on Tag Mountain, bedding is parallel to the slope, and cleavage is at right angles to it. [B] Very thin, planar mudstone beds. Dale Creek valley. Hammer is 30 cm long. [C] Very thin beds on a relatively fresh face. Dale Creek valley. Pencil for scale. [D] Black tremolite prisms with ragged terminations, from a meta-limestone bed within a succession of silty lime mudstone beds within mudstone. Dale Creek valley. Pencil lead is 0.5 mm wide. [E] Quartz calc-silicate skarn bed within the Lower member on the south slope of Mount Allan. Hammer is 30 cm long; about 20 cm of the hammer is showing.

Limestone beds are locally abundant in the Lower member, weathering various shades of grey and brownish grey. Intervals of limestone up to 1 m thick, but generally less, are dominated by dark grey, finely crystalline limestone and lime mudstone in beds from 1 cm to 20 cm thick,

with subordinate thin interbeds of non-calcareous mudstone. The limestone commonly contains knots and disseminations of pyrite and pyrrhotite. Prismatic black amphibole porphyroblasts (tremolite?) a few millimetres long are abundant in some of the beds (Figure 17D). On Mount Allan, within the skarn zone, the Lower member contains sparse beds of siliceous, quartz-veined, microcrystalline, grey-white weathering calc- silicate rock (Figure 17E).

The Upper member of the Duo Lake Formation (mine unit 4) is a platy to slabby, black to dark grey weathering shale, black to very dark grey on fresh surfaces, that is commonly pyritic and graptolitic (Figure 5). The Upper member is locally siliceous, and rarely ranks as chert. Sedimentary structures include flute casts (Figure 18A), millimetric mud chips, and laminations. The pits left by weathered-out mud chips (or possibly, porphyroblasts) weather a blue colour (Figure 18B). Three collections of graptolites from the Upper member on Mount Allan (Figure 4) were examined by M. Melchin of St. Francis Xavier University, who provided ages of Sandbian to mid-Katian and upper Katian (both Late Ordovician) for two, and a tentative age of Darwillian or possibly lower Sandbian (latest Middle Ordovician or possible early Late Ordovician) for the other (M. Melchin personal communication, 2016).

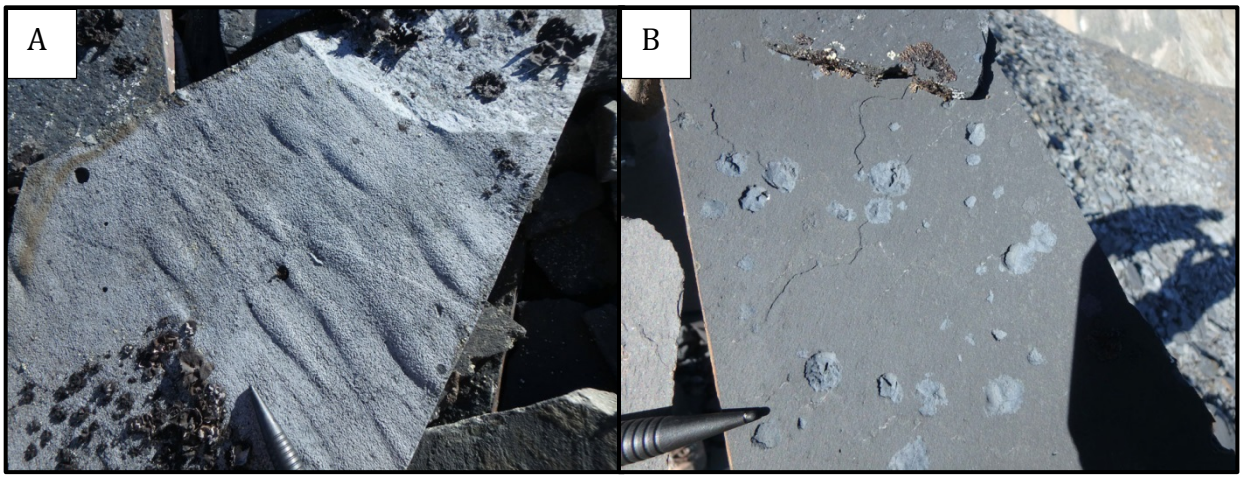


Figure 18. The Duo Lake Formation, Upper member, Mount Allan. [A] Flute casts in black shale. [B] Mud chips(?) in black shale weather light bluish grey. End of pencil for scale.

### *Interpretation and Correlation*

The Lower Duo Lake Formation at Mactung was deposited in a moderately deep, quiet setting, under periodically or episodically alternating influences that produced thick successions of rhythmically varying muds. The absence of sedimentary structures other than laminations suggests a quiet setting below storm wave base. The ubiquity of fine pyrite implies a syn-depositional or diagenetic origin, but without additional information, little can be inferred about oxygen levels or abundance of organic matter in the depositional system. The presence of limestone beds in some parts of the section and the absence of limestone beds in others shows that deposition took place near the carbonate compensation depth (CCD), perhaps above the CCD sometimes and below it at other times.

The Upper Duo Lake Formation was deposited in a deep marine setting where organic matter was either deposited or preserved in abundance, perhaps being starved of terrigenous input. Mud rip-ups indicate that the setting was not always a quiet one, and flute casts show that at least some depositional events were turbulent.

Regionally, the Duo Lake Formation is a highly variable unit without correlateable members, comprising recessive, thin- to very thin-bedded, variably calcareous, black, grey or brown mudstone, shale, siltstone, and chert with locally abundant graptolites, and volumetrically minor but widespread, thin-bedded skeletal limestone and brown sandstone (Cecile 1982, 2000; Fischer 2016; Gordey 2013; Abbott 1983). In NTS 105J south of Mactung, the Duo Lake Formation consists of a thin, recessive, upper interval of black, graptolitic, siliceous shale that overlies a thick interval of presumably biogenic chert (Gordey 2013). Mine unit 3H has been assigned by some workers to the Rabbitkettle Formation but its assignment to the Duo Lake Formation is supported by the its lithological resemblance to the Duo Lake Formation elsewhere, and the probable deepening of depositional environment between member G and mine unit 3H. The similarity of mine units 3H and 4 to, respectively, the thick lower member and thin, recessive, graptolitic upper member of the Duo Lake Formation in NTS 105J provides additional support. Mine unit 4 resembles the black, graptolitic shale of the Duo Lake Formation elsewhere, and the graptolite ages provided by M. Melchin of St. Francis Xavier University (personal communication, 2016), leave its assignment to Duo Lake Formation in little doubt.

## Steel Formation, Late Silurian

The Steel Formation was defined by Gordey and Anderson (1993; 62 °19.5' N, 129 °27.0' W in NTS 105I as a thin unit of orange weathering mudstone lying conformably and gradationally over the Duo Lake Formation. The Steel Formation is Ludlovian (late Silurian) in age, but possibly as old as middle Silurian. The youngest age of the formation is constrained in NTS 105I/6 by the Pragian (middle Early Devonian) age of the overlying Portrait Lake Formation (Gordey and Anderson 1993), and in NTS 105O by the age of the overlying Sapper Formation, which is as old as Ludlovian (Abbott 2013). The upper contact of the Steel Formation with black siliceous shale of the Portrait Lake Formation is presumed conformable from the sharp delineation in scree (Gordey and Anderson 1993). The Steel Formation was not identified on the Mactung mine maps (NTGS collection) but was noted by Abbott (2013) on the east flank of Barite Mountain.

### *Observations*

The Steel Formation was identified on the south face of Mount Allan, on Tag Mountain, and on the east flank of Barite Mountain. Contacts were not observed. The thickness of the Steel Formation is estimated to be 50 m to 100 m.

The Steel Formation weathers orangey grey, light grey, or beige (Figure19A). It is a very fine-grained, medium and light grey mudstone to siltstone with pyrite specks and nodules of pyrrhotite up to 2 mm across. Ubiquitous wispy, three-dimensional structures of darker grey resemble folded or distorted lenses and irregular, discontinuous lamellae (Figure 19B). The rock is locally calcareous, elsewhere moderately hard and probably siliceous. Partings are

slabby to irregular, and locally the rock breaks with a conchoidal fracture. Thin beds are defined by colour differences.

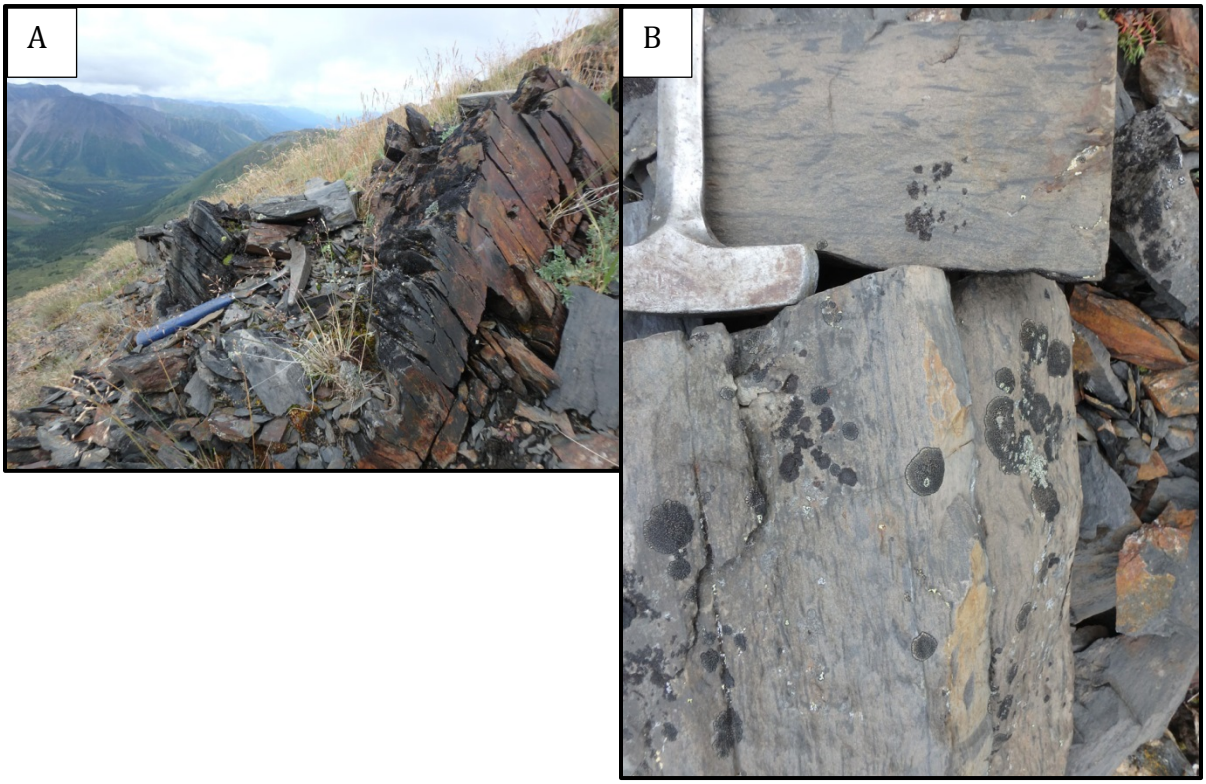


Figure 19. The Steel Formation. [A] Outcrop appearance. Note grey stripes of bedding in the rubble just past the hammer. Looking southwest on Tag Mountain. Hammer is 30 cm long. [B] Pieces of rock placed together to show characteristic deformed wispy structures (burrows?) of darker grey in buff coloured mudstone. Tag Mountain. Hammer handle is 2 cm wide.

### *Correlation*

Steel Formation in its type area is 100 m to 140 m thick, siliceous, locally dolomitic or argillaceous, and light to dark grey on fresh surfaces (Gordey and Anderson 1993). The predominantly orange weathering colour of the formation is due to disseminated pyrite, although members up to ten metres thick are weathered dark grey. The Steel Formation in NTS 105O is described as green shale and mudstone that is orange to green weathering, with intermittent, thick beds of pyritic dolostone (Abbott 2013). The Steel Formation is characterized by ubiquitous wispy laminations. The depositional environment of the Steel Formation has been interpreted as a quiet setting below wave base, with oxygenated bottom waters supporting a community of horizontal burrowers whose burrows are preserved as the characteristic wispy structures (Gordey and Anderson 1993).

The lithology, stratigraphic position, and especially, presence of wispy structures, in the interval of strata above the Duo Lake Formation at Mactung support the assignment of this interval to the Steel Formation.

## Sapper Formation, late Silurian to Middle Devonian

The Sapper Formation (Gordey and Anderson 1993; 62 °42' N, 128° 25.6' W) is a recessive, dark-weathering silty limestone unit that ranges in age from Ludlovian to Eifelian (late Silurian to Middle Devonian; Abbott 2013). In the region around Mactung (NTS 105O), the Sapper Formation ranges from 0 m to 300 m thick, in sharp contact with the underlying Steel Formation but gradational over a few metres with the overlying Niddery Lake member (Abbott 1983).

Mine unit 8, east of Fold Mountain, is a black, argillaceous limestone (Findlay 1969c), at the top of which are two lenses of massive, light grey, crinoidal limestone (mine unit 9; *ibid*.; not shown on Figure 4 but shown in the accompanying map, Martel *et al*. 2018). Both of these units are assigned to the Sapper Formation.

### *Observations*

The strata above the Steel Formation were not traversed from base to top, and neither the upper nor lower contact was observed. Where visited, the strata directly overlying the Steel Formation consist of recessive, dark brown to grey weathering shale, mudstone, siltstone, and silty mudstone, with rare calcareous siltstone. The non-calcareous shale and mudstone-siltstone are moderately hard, light to dark grey, and locally friable, with a greyish blue hue on some weathered surfaces (Figure 20A). Millimetric knots of pyrite are common. Thin, planar, parallel beds and 1-mm laminations are defined by differential weathering, concentrations of pyrite, and colour. Laminations are discontinuous, planar, parallel, and locally lenticular. Rare, thin interbeds of orange weathering mudstone are reminiscent of the Steel Formation. The calcareous siltstone is recessive, light grey weathering, and dark grey on fresh surfaces.

The upper part of the Sapper Formation, directly beneath the shale of the Niddery Lake member on Barite Mountain, consists of platy, fissile, dark grey to black, graptolitic lime mudstone and lime siltstone (Figures 20B and 20C), with rare thin beds of intraformational flat-pebble breccia. Two collections of graptolites (Figure 4) yielded Early Devonian ages, specifically Lochkovian to lower Pragian and upper Pragian to lowest Emsian, as determined by M. Melchin of St. Francis Xavier University (personal communication, 2016).

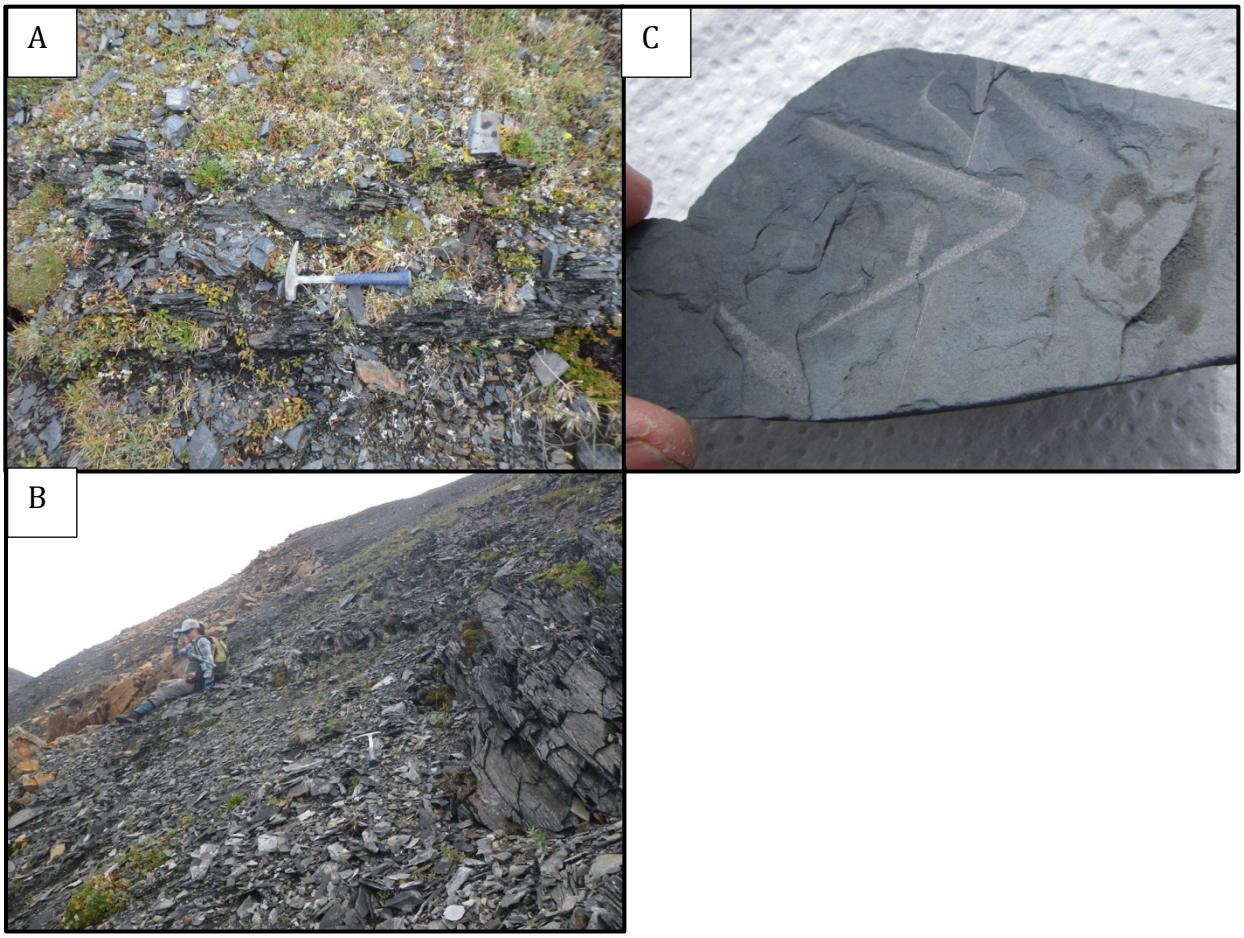


Figure 20. The Sapper Formation. [A] Typically poor exposure of non-calcareous mudstone from the base of the unit. Hammer for scale, 30 cm long. [B] Dark grey, graptolitic limestone from the upper Sapper Formation, cut by a felsic dyke. [C] Pendant, J-curved and straight uniserial graptolites from the upper Sapper Formation. Stipes of pendant graptolite are about 5 cm long.

### *Correlation*

The Sapper Formation in the vicinity of its type section (NTS 105I) is a recessive unit, up to 850 m thick, of dark grey to tan-orange weathering limestone and silty limestone. Dark weathering lithologies include: black, very fine to finely crystalline limestone with very thin, wavy beds; black graptolitic shale; and black, platy, argillaceous limestone. Lithologies that weather buff-orange to tan, and locally pink, are, in most places, confined to the upper part of the unit, and consist of grey-black, laminated, thin- to medium bedded, variably argillaceous to silty limestone (Gordey and Anderson 1993). In many places a lower limestone member and an upper silty limestone (rarely siltstone) member can be distinguished. In NTS 105O, the Sapper Formation ranges from 0 m to 300 m thick and consists of recessive, buff to tan weathering, platy, thin-bedded, dark grey to black silty limestone and calcareous black shale (Abbott 1983). South of Mactung, the unit includes lenses of massive grey limestone (Abbott 1983, 2013). An off-shelf, quiet depositional setting has been inferred for the Sapper Formation by Gordey and Anderson (1993).

The interval of strata immediately above the Steel Formation has been assigned tentatively to the lowermost Sapper Formation, despite the lithologies of this interval being dissimilar to any of those described for the Sapper Formation. The absence of the characteristic Steel-Formation wispy structures supports the assignment, but further study may indicate that inclusion in the Steel Formation is more appropriate. The interval of strata immediately below the Niddery member of the Portrait Lake Formation has also been assigned to the Sapper Formation. The lithology, age, and stratigraphic position of this interval confirm the assignment. The assignment of the crinoidal limestone lenses of mine unit 9 to the Sapper Formation is corroborated by Abbott's (2013) observation of massive grey limestone lenses within the Sapper Formation south of Mactung. The entire formation at Mactung, if assignment of the lower interval to the Sapper Formation is correct, may be equivalent to the upper, silty-limestone member in NTS 105I.

## Portrait Lake Formation, Niddery Lake and Macmillan Pass members, Devonian

The Portrait Lake Formation (Gordey and Anderson 1993; 63° 8.0' N, 130° 1.5' W) was defined in NTS 105I for an interval of Lower to Upper Devonian, fine- to coarse-grained, terrigenous clastic off-shelf strata with a diachronous base from Early to early Middle Devonian in age. A marked basal unconformity in NTS 105I/NE does not extend to NTS 105O, where Abbott (2013) describes an intergradational contact with underlying Sapper Formation. Abbott (2013) proposed the name Niddery Lake for a siliceous shale member at the base of the Portrait Lake Formation that ranges from Early Devonian (late Pragian to early Emsian) to Middle Devonian (Eifelian) in age, and modified the existing definition of Macmillan Pass member to describe an overlying, turbidite fan complex of Middle to Late Devonian age.

Areas mapped as the Niddery Lake and Macmillan Pass members on our map (Figure 4; Martel *et al.* 2018) are from Abbott (2013), except contacts in the southeast have been modified to match more-detailed mine maps. The lower contact of the Niddery Lake member on Barite Mountain was crossed at one location, and the shale facies of the Macmillan Pass member was visited at one location during this project.

### *Observations*

On Barite Mountain, the basal part of Niddery Lake member consists of dark reddish brown weathering, dark grey mudstone in thin, wavy, non-parallel beds (Figure 21). Sedimentary structures include asymmetrical ripples, small intraformational slumps, and laminated thin to very thin beds. The shale facies of the Macmillan Pass member east of Fold Mountain is a grey shale that is thinly bedded and well cleaved.

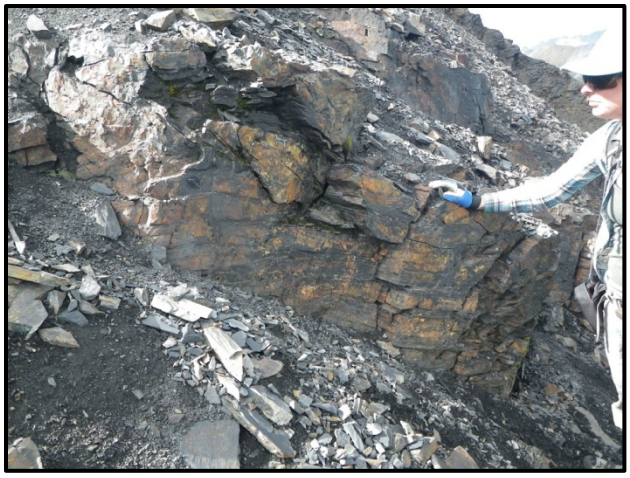

Figure 21. The Niddery member of the Portrait Lake Formation. Thin-bedded mudstone with wavy beds at the base of the outcrop, and slumped and distorted beds at the top. Barite Mountain.

### *Correlation*

The Niddery Lake member is present between the Sapper Formation and the Macmillan Pass member in the north block of the Macmillan Fold Belt (Figure 2). The lower contact of the Niddery Lake member with the Sapper Formation in NTS 105O is gradational over 10 m to 20 m in which black shale is interstratified with thick beds of light grey, crinoidal limestone (Abbott 1983). The bulk of the Niddery Lake member above this consists of black to dark blue-grey weathering, thin-bedded chert, cherty argillite, and siliceous shale. Lenses or intermittent horizons of stratiform barite <1 m thick are common. Rare baritic lenses are up to 30 m thick, in which barite is interbedded with and replaces limestone. Barite and limestone lenses may represent one or a few tectonically dismembered horizons (Abbott 1983, 2013). The uppermost Niddery Lake member locally includes intervals of light grey, bioclastic limestone a few metres thick (Abbott 2013).

The Macmillan Pass member includes a grey weathering, chert-pebble conglomerate facies, a brown, fine-grained clastic (shale) facies, and a brown sandstone facies, together interpreted as a turbidite fan complex. In the central block of the Macmillan Fold Belt (Figure 2), south of the area mapped during this project, the Niddery Lake member is absent and the Macmillan Pass member directly overlies the Sapper Formation.

On Barite Mountain (this project and Abbott 2013) and in the southeast corner of the map, above the thrust fault (Abbott 2013), the Niddery Lake member overlies the Sapper Formation and is overlain by a shale facies of the Macmillan Pass member. Below the thrust, however, the map generated during this project shows the Macmillan Pass member directly overlying the Sapper Formation without the Niddery Lake member in-between (Figure 4), a situation which also pertains in the central block of the Macmillan Fold Belt. The area below the thrust in the southeast corner of the map was not traversed and contacts were estimated from a georeferenced map with sparse base data, thus the locations of contacts are in doubt and alternative interpretations exist. One alternative interpretation is that the area mapped as the Macmillan Pass member below the thrust should be assigned to the Niddery Lake member. Another interpretation would re-locate the lenses of bioclastic limestone (Martel *et*

*al*. 2018, unit SDs-bl) southward and assign the area mapped as the Macmillan Pass member below the thrust to the Sapper Formation. On-the- ground investigation of this area is required before it can be interpreted with any confidence.

## Intrusive Rocks

Neither of the two granitic stocks in the map area, the Cirque Lake and the Rockslide Mountain stock, was examined as part of this project. Felsic dykes are fairly numerous and a number of them were crossed on mapping traverses.

### *Observations*

Felsic dykes (Figures 13D and 20B) are pink to pale tan weathering, cream coloured, and very fine grained to aphanitic. Some of the felsic dykes are very fine grained with medium grained quartz crystals. Some dykes contain sparse biotite phenocrysts up to 3 mm wide, whereas others contain muscovite and 2 mm to 3 mm quartz phenocrysts, or feldspar phenocrysts 5 mm across (Figure 22). The felsic dykes are from <1 to >10 m wide and tend to occur in swarms.

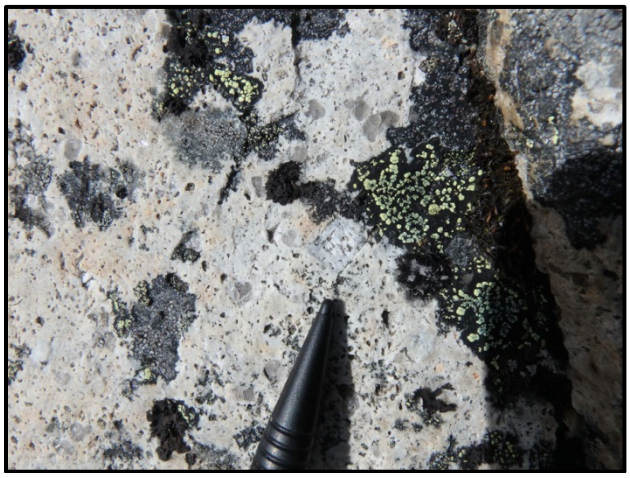

Figure 22. Granitic dyke with a 5-mm, euhedral feldspar phenocryst just above pencil tip, and numerous 2 mm to 3 mm anhedral quartz phenocrysts. From Barite Mountain.

## Structure

Cleavage is best developed in the phyllite of the Narchilla Formation (Figures 8B and 8C) and the siliciclastic rocks of the Portrait Lake Formation (Figure 23A). Cleavage is rarely observed in the hornfels or skarn (Figure 23B). The cleavage measured in the Narchilla Formation southeast of Mount Allan and at the east end of the north face of Mount Allan strikes north-northest (dips east-southeast), whereas on Tag Mountain, cleavage in the Narchilla, Duo Lake and Steel formations strikes west (dips north). Crenulations on bedding planes trend west-northwest and plunge very shallowly (Figure 23C).


Figure 23[A]. Cleavage and bedding in mudstone and siltstone of the Portrait Lake Formation. From the ranges east of Fold Mountain.


Figure 23[B]. A vertical face showing cleavage, bedding, and a subvertical quartz vein in member G of the Rabbitkettle Formation. Note that cleavage only develops in the more micaceous beds. Looking west. Head of hammer is about 12 cm long.


Figure 23[C]. Looking down at crenulations that trend 290 degrees and plunge 5 degrees. Metal part of hammer handle is 2 cm wide.


Figure 23[D]. Open fold in the Hess River Formation. Fold axis trends east and plunges very shallowly. Marker pen for scale. Looking northwest.

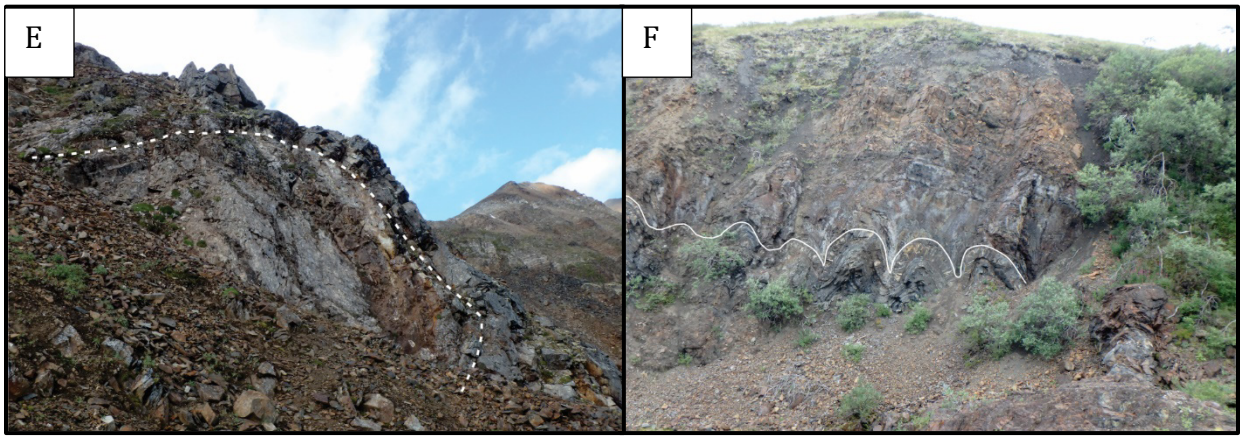


Figure 23[E] and [F]. [E] The Z-fold in the skarned Sekwi Formation (Banded facies) and the Hess River Formation. Fold plunges shallowly towards the east-northeast. This is the same open Z-fold as in Figure 9Q, taken from farther away at a different angle. Field of view is about 15 m. Looking west on the north face of Mount Allan. [F] M-folds in a limestone interval within the Lower member of the Duo Lake Formation in Dale Creek valley. Note the lack of folds near the top of the exposure. Field of view is about 40 m. Looking northwest.

Folds at the east end of the north face of Mount Allan plunge shallowly to the east (Figure 23D) whereas folds in the western half of the map area (western end of north face of Mount Allan, south slope of Mount Allan, Barite Mountain, and Tag Mountain) plunge shallowly to the west. The most prominent fold exposed on the property is at the east end of the north face of Mount Allan (Figure 23E). This fold is a concentric, partly recumbent Z-fold (looking west) that opens up towards the west. Thegeometry of the Z-fold is consistent with that of the fold interpreted from the drill core and drawn on cross-sections by mine geologists (Figure 6A). Gebru (2017) suggested that the doubly plunging nature of the fold axis is due to later, post-skarn development of north-south folds that are restricted to near the pluton margins.

A series of concentric M-folds in Dale Creek valley (Figure3) plunge shallowly towards the west-northwest (Figure 23F). The largest scale fold observed in the map area is on Fold Mountain (Figures 24A, and 24B). Although the fold axis cannot be measured directly, it appears to plunge shallowly towards the northeast. The fold on Fold Mountain appears to be tighter than others on the property, and likely has fault slip along the southernmost limb, perhaps related to the emplacement of the Rockslide Mountain stock.

Observations made during this project, taken into consideration with the regional structural geology described by Abbott (1982, 2013) and Cecile (2000), suggest that the folding is primarily the result of compression during Cordilleran orogenesis and was not caused by doming during post-compression plutonism. All of the folds observed, with one exception, are parallel folds (class 1b of Ramsay 1967) without hinge thickening.

The trace of a north-verging thrust fault on Tag Mountain (Abbott 2013) has been refined during this project, and it is now assumed to continue east of the Cirque Lake pluton, which post-dates it (Figure 4; Martel *et al.* 2018). A series of north-trending normal faults were interpreted on previous maps of the north face. During this project, vertical faults were observed only at the westernmost end of the north face of Mount Allan (Figure 24C), where they show displacement on a metre scale. The presence of the Narchilla(?) Formation in the central part of the map (Figure 4) requires the presence of north-south oriented normal faults. Abbott's (2013) map shows one of these faults apparently truncated by the Cirque Lake stock but displacing the Rockslide Mountain stock, which implies that the fault pre-dates one pluton and post-dates the other.

The structural measurements from this project, including selected measurements digitized from existing maps (Harris and Godfrey 1974; Lodder and Harris 1974; Abbott 2013), are available in shapefile format (Martel *et al.* 2018).

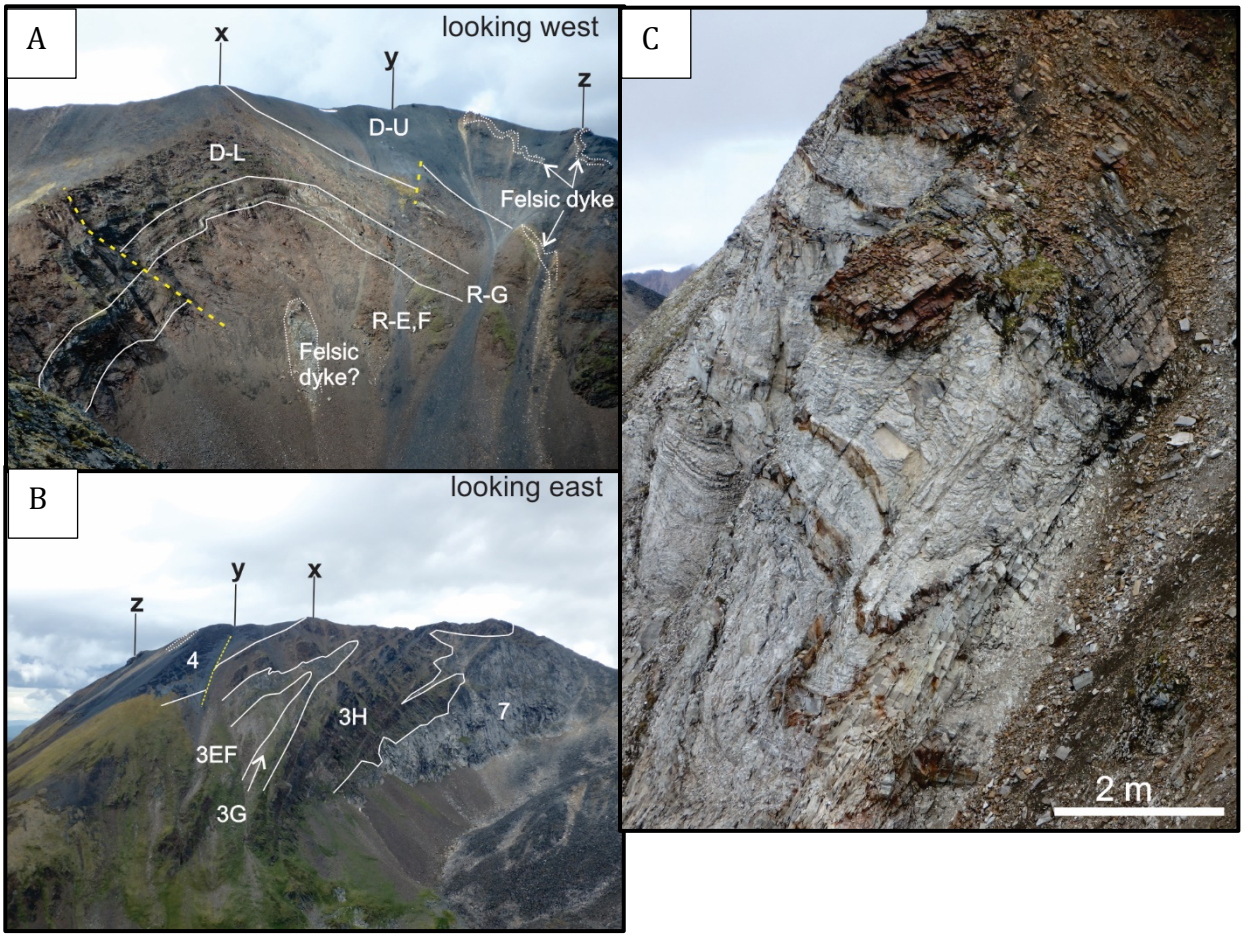


Figure 24. [A] and [B] The fold on Fold Mountain, viewed from different angles. [A] shows the east face of Fold Mountain, and [B] shows the west face. Solid white lines are stratigraphic contacts, dashed white lines are intrusive contacts, dashed yellow lines are faults. Units are: member EF of the Rabbitkettle Formation (R-E,F); light colored, banded member G of the Rabbitkettle Formation (R-G); the brown Lower member of the Duo Lake Formation (D-L); and the black, graptolitic Upper member of the Duo Lake Formation (D-U). Locations x, y, z along the ridge-line are the same for [A] and [B]. [C] Subvertical faults offset the contact between the uppermost Rabbitkettle Formation (member G; light grey) and the Lower member of the Duo Lake Formation (brown) on the west face of Mount Allan. Looking west.

## Chemistry

The geochemical analyses from the 2016 project are provided in Appendix B. Two samples were sent for assay, one sample of pyritic mudstone from the Hess River Formation and one of siliceous rusty mudstone from member E of the Rabbitkettle Formation. The assays returned low values of all metals, including 15 ppb Au in the sample of Hess River Formation (Figure 4; Appendix B). Six samples of phosphatic rock were analyzed for major- element oxides and trace elements, one sample from the basal Hess River Formation on Tag Mountain and the others from member D of the Rabbitkettle Formation on Tag Mountain, Fold Mountain, Mount Allan, and south of Cirque Lake (Figure 4; Appendix B). The analyses show that all the samples contained 10% to 19% $P_2O_5$, supporting the field identification of

phosphatic material. The analyses also show that oxides of calcium ranged from 35% to 46% and those of silicon from 14% to 31%, with the lowest calcium contents corresponding with the highest silicon and *vice versa*. This reflects the variable amounts of quartz sand in the phosphatic conglomerates. Other major-element oxide abundances were low. Total combined rare earth elements and yttrium was <230 ppm in each sample, with negative europium anomalies and mild negative cerium anomalies.

## Questions and Recommendations

1. Mineralized skarns at Mactung are best developed in the sediment gravity flows of the Sekwi Formation and the basal Rabbitkettle Formation (member D).
    - Do the extremely variable thicknesses of gravity-flow deposits in the Sekwi Formation near Mactung reflect a seismically active margin with a steep drop-off nearby? Does the absence of such deposits on Isolation Mountain reflect a significant facies change?
    - Did syn-depositional faulting contribute to sediment gravity flows in early Rabbitkettle time, or was a stormy or over-steepened shelf on which phosphogenesis took place sufficient cause for conglomerate formation?
    - An understanding of the paleogeographic and tectonic setting of Mactung during Sekwi and Rabbitkettle time, and especially whatever aspects of it led to formation of the conglomeratic deposits, is clearly relevant and should be pursued by detailed mapping and stratigraphic studies at Mactung and in the surrounding region for 5 km to 10 km from the deposit.

2. Member D, in particular, is complex and poorly understood.
    - Under what conditions did the phosphate minerals form?
    - There is evidence that the environment of transportation was energetic, and that the transportation processes included either debris flows or dense turbidity flows, but details are lacking. What processes generated the phosphatic clasts, which are largely structureless, and mixed them with plastically deformed clasts of lime mudstone? What processes re-brecciated the phosphatic breccia and transported the clasts to their final site of deposition?
    - Is marine cementation of cracks in a hardground a satisfactory explanation of the veined phosphatic clasts in the breccia? Or has fault brecciation contributed to the complexity?
    - Does member D contain an economically viable phosphate resource?

3. There is a Z-fold in the Lower ore zone under the eastern end of Mount Allan, inferred from drill and underground data and supported by surface observations. The plunge of the fold changes from east to west, suggesting doming under Mount Allan. The Z-fold is said to have thickened hinges and a thinned central limb that must have resulted from plastic deformation (Atkinson and Baker 1986). Although a more open fold is shown in the overlying units in some reports, Atkinson and Baker (1986) infer a complete absence of folding in the overlying strata. They make an unconvincing attempt to explain this absence, as well as the anomalous fold style, by invoking a component of syn-sedimentary deformation in formation of the Z-Fold.

- What is the true geometry of the Z-fold? How does it change farther west, under the central and western parts of Mount Allan? The available drill information should be re-examined to understand the constraints on the geometry of the Z- fold, and modelled in three dimensions with these constraints in mind.
- If strata under Mount Allan do form a dome, what caused the doming? Did a deeper intrusive body influence its formation?
- Have post-mineralization faults significantly affected the distribution of the ore?
- A structural study should be conducted concurrently with the stratigraphic study to further constrain the three-dimensional model. The shape of the Z-fold and how it changes laterally are crucial to delineating the ore and estimating resources.

4. Whereas earlier workers inferred that an unidentified buried pluton was the source of mineralizing fluids at Mactung (Atkinson and Baker 1986; Selby *et al.* 2003), recent work shows that both the Cirque Lake and Rockslide Mountain stocks were co-genetic with ore formation (Gebru 2017; Selby *et al.* 2003) and are therefore candidates to have sourced the mineralizing fluids.
    - What pluton was the source? Is there a buried pluton yet to be discovered? Do the two known plutons join at depth, as suggested by Gebru (2017)? If so, what are the implications for identifying new ore zones?
    - Can the plutons be imaged geophysically, despite the lack of magnetic contrast between Tungsten-suite plutons and the Mactung succession of sedimentary rocks? The geometry of buried intrusive bodies will be important in predicting the location of new mineral resources.
    - Is the age of the source pluton relevant to locating additional tungsten-skarn resources?

5. The entire Tungsten plutonic belt is thought to have been localized by structures involved in the Neoproterozoic rifting of Rodinia (Hart *et al.* 2004). What structures controlled the emplacement of the source pluton at Mactung? Were Devonian faults or Neoproterozoic faults re-activated during its emplacement? Are re-activated faults an important exploration criterion?

6. What conduits were used by the mineralizing fluids? Were there other highly permeable limestone units, besides the Sekwi and Rabbitkettle breccias, along the fluid path? These would have been susceptible to skarn mineralization.
    - The Rockslide Mountain stock was emplaced during fault activity. The Cirque Lake stock appears to post-date that activity (although much of the southern margin of the stock is covered and its northern margin has not been mapped in detail). Was syn-intrusion fault activity an important factor in ore formation, perhaps by providing conduits for fluid movement?

7. Scheelite grain size is important for recovery. There have been conflicting descriptions of scheelite grain sizes in the various skarn types at Mactung. Does scheelite grain size vary with skarn type, or is it controlled by other factors? What is the actual distribution of scheelite grain sizes?

8. What is the gold potential at Mactung? It has been suggested that the Tungsten plutonic suite might be prospective for gold (Mortensennd Lang 2001), good gold values have been obtained from scheelite ore at Mactung (Gebru 2017), and anomalous levels of gold were detected by government surveys in stream silts east of Mactung. Drill core should be re-analyzed for gold and the exposed intrusions should be explored for gold-bearing sheeted quartz veins.

# Appendix A: Mactung Deposit Resource Report

# Appendix B: Geochemistry

# Appendix C: Geochronology Summary*

*Geochronological ages from granitoids, veins, and skarn at Mactung. Location coordinates are for Universal Transverse Mercator (UTM) zone 9N based on North American Datum 1983 (NAD83).

## Disclaimer

This document has been prepared by the Northwest Territories Geological Survey (NTGS), Government of Northwest Territories (GNWT). It is provided for informational purposes only. It does not contain any warranties, representations or quality commitments, whether express or implicit, nor does it contain any guarantees regarding the correctness, integrity, and quality of the information. The NTGS has exercised all reasonable care in the compilation, interpretation, and production of this document and the information has been obtained from sources the NTGS believes to be reliable. However, it is not possible to ensure complete accuracy, and all persons who rely on the information do so at their own risk. Information is provided as is, where is and without warranty whatsoever, neither express nor implied. The GNWT does not accept liability for any errors, omissions, or inaccuracies that may be included in, or derived from, this document. In no event will the NTGS, the GNWT, nor any of their respective successors, assigns, agents or employees be held liable in any way for damages suffered, direct or indirect, as a result of any action or inaction taken in reliance on information provided herein.

## Terms of Use

# References

Abbott, J.G., 1983. Structure and stratigraphy of the Macmillan fold belt: Evidence for Devonian faulting. Department of Indian Affairs and Northern Development, Geology Section, Open File 1983-1, 16 pages and 3 maps at 1:50 000 scale.

Abbott, J.G., 2013. Bedrock geology of the Macmillan Pass area, Yukon and adjacent Northwest Territories (NTS 105O/1, 2 and parts of 105O/7, 8 and 105P/4, 5). Yukon Geological Survey, Geoscience Map 2013-1, 1 map at 1:50 000 scale and legend sheet.

Aitken, J.D., Macqueen, R.W., and Usher, J.L., 1973. Reconnaissance studies of Proterozoic and Cambrian stratigraphy, lower Mackenzie River area, (Operation Norman), District of Mackenzie; Geological Survey of Canada, Paper 73-9, 178 pages.

Anderson, R.G., 1982. Geology of the Mactung pluton in Niddery Lake map area and some of the plutons in Nahanni map area, Yukon Territory and District of Mackenzie. Geological Survey of Canada, Current Research, Part A, Paper 82-1A, p. 299-304.

Anderson, R.G., 1983. Selwyn plutonic suite and its relationship to tungsten skarn mineralization, southeastern Yukon Territory and District of Mackenzie; Geological Survey of Canada, Current Research, Part A, Paper 83-1B, p. 151-163.

Anderson, R.G., 1993. Granitic rocks. *In* Gordey, S.P. and Anderson, R.G., Evolution of the northern Cordilleran miogeocline, Nahanni map area (105I), Yukon and Northwest Territories; Geological Survey of Canada, GSC Memoir 428, p. 73-91.

Atkinson, D., 1982. Mactung - Mineralogy of Unit 2B within the proposed area of underground mining; Northwest Territories Geological Survey, Mactung collection, Memo number MT 19820625, 8 pages.

Atkinson, D. and Baker, D.J., 1986. Recent developments in the geologic understanding of Mactung. *In* Morin, J.A. (editor), Mineral Deposits of Northern Cordillera; Canadian Institute of Mining and Metallurgy, Special Volume 37, p. 234-244.

Baker, T. and Lang, J.R., 2001. Fluid inclusion characteristics of intrusion-related gold mineralization, Tombstone–Tungsten magmatic belt, Yukon Territory, Canada. Mineralium Deposita, Volume 36, p. 563–582.

Blusson, S.L., 1968. Geology and tungsten deposits near the headwaters of the Flat River, Yukon Territory and southwestern District of Mackenzie; Geological Survey of Canada, Paper 67-22, 77 pages.

Blusson, S.L., 1971. Sekwi Mountain map area, Yukon Territory and District of Mackenzie; Geological Survey of Canada, Paper 71-22, 17 pages.

Blusson, S.L., 1974. Five geological maps of northern Selwyn Basin (Operation Stewart), Yukon Territory and District of Mackenzie, NWT ; Geological Survey of Canada, Open File 205, 5 maps at 1:250 000 scale.

Cecile, M.P., 1982. The Lower Paleozoic Misty Creek Embayment, Selwyn Basin, Yukon and Northwest Territories; Geological Survey of Canada, Bulletin 335, 78 pages and 1 map at 1:500 000 scale.

Cecile, M.P., 1996. Geology and structure cross-section, Keele Peak (and NTS 105-O/9), Yukon Territory-Northwest Territories; Geological Survey of Canada, Map 1902A, 1:50 000 scale.

Cecile M.P., 2000. Geology of the northeastern Niddery Lake map area, east-central Yukon and adjacent Northwest Territories; Geological Survey of Canada, Bulletin 553, 119 pages.

Chevrier, T.S. and Turner, E.C., 2013. Lithostratigraphy of deep-water lower Paleozoic strata in the central Misty Creek Embayment, Mackenzie Mountains, Northwest Territories; Geological Survey of Canada, Current Research 2013-14, 21 pages.

Christie, R.L. and Sheldon, R.P., 1986. Chapter 8 - Proterozoic and Cambrian phosphorites - regional review: North America. In Cook, P.J. and Shergold, J.H., Phosphate Deposits of the World, Volume 1. Cambridge University Press, Cambridge, p. 101-107.

Colpron, M. and Nelson, J.L., 2011. A digital atlas of terranes for the northern Cordillera. Accessed online in August, 2017 at www.geology.gov.yk.ca.

Dick, L.A. and Hodgson, C.J., 1982. The Mactung W Cu (Zn) contact metasomatic and related deposits of the northeastern Canadian Cordillera; Economic Geology, Volume 77, p. 845- 867.

Dilliard, K., Pope, M.C., Coniglio, M., Hasiotis, S.M., and Lieberman, B., 2010, Active synsedimentary tectonism on a mixed carbonate-siliciclastic continental margin: third- order sequence stratigraphy of a ramp to basin transition, lower Sekwi Formation, Selwyn Basin, Northwest Territories, Canada: Sedimentology, Volume 57, p. 513-542.

Findlay, A., 1968. Drill logs MT-68-1, 1A, 2, 2A, 3, 4 and 5, with general unit descriptions; Northwest Territories Geological Survey, Mactung collection, Report number MT 1968-01, 57 pages.

Findlay, A., 1969a. Macmillan Pass Tungsten Property, geological map, Figure 3, to accompany report "Macmillan Pass Tungsten Property - 1968 program"; Northwest Territories Geological Survey, Mactung collection, 1 map at 1:6000 scale.

Findlay, A., 1969b. Macmillan Pass Tungsten Property, geological map, Figure 4, to accompany report "Macmillan Pass Tungsten Property - 1968 program"; Northwest Territories Geological Survey, Mactung collection, 1 map at 1:2400 scale.

Findlay, A., 1969c. Rockslide Mountain stock, geological map, Figure 5, to accompany report "Macmillan Pass Tungsten Property - 1968 program"; Northwest Territories Geological Survey, Mactung collection, 1 map at 1:15 840 scale.

Fischer, B.J., 2016. Bedrock geology of parts of the Misty Creek paleo-embayment, Mackenzie Mountains (NTS 106B); Northwest Territories Geological Survey, NWT Open File 2016-01, 1 map at 1:100 000 scale and legend.

Fritz W.H., 1982. Vampire Formation, a new upper Precambrian(?)/Lower Cambrian Formation, Mackenzie Mountains, Yukon and Northwest Territories; Geological Survey of Canada, Paper 82-1B, p.83-92.

Follmi, K.B., 1996. The phosphorus cycle, phosphogenesis and marine phosphate-rich deposits. Earth Science Reviews, Volume 40, p. 55-124.

Follmi, K.B., Badertscher, C., de Kaenel, E., Stille, P., John, C.M., Adatte, T. and Steinman, P., 2005. Phosphogenesis and organic-carbon preservation in the Miocene Monterey Formation at Naple Beach, California - The Monterey hypothesis revisited. Geological Society of America Bulletin, Volume 117, p. 589-619.

Gabrielse, H., Blusson, S.L., and Roddick, J.A., 1973. Geology of Flat River, Glacier Lake, and Wrigley Lake map-areas, District of Mackenzie and Yukon Territory; Geological Survey of Canada, Memoir 366, 153 pages and 3 maps.

Gabrielse, H., Murphy, D.C., and Mortensen, J.K., 2006. Cretaceous and Cenozoic dextral orogen-parallel displacements, magmatism and paleogeography, north-central Canadian Cordillera. *In*: Haggart, J.W., Enkin, R.J., and Monger, J.W.H (editors), Paleogeography of the North American Cordillera: Evidence for and against large-scale displacements; Geological Association of Canada, Special Paper 46, p. 255-276.

Gebru, A., 2017. Petrogenesis of granitoids in the vicinity of the Mactung tungsten skarn deposit, Northeast Yukon-Northwest Territories: Characterization of skarn mineralization and causative plutons through geological, petrochemical, mineralogical, and geochronological analysis; University of New Brunswick, Unpublished Ph.D. thesis, 752 pages.

Gerstner, M.R., Bowman, J.R., and Pasteris, J.D., 1989. Skarn formation at the Macmillan Pass tungsten deposit (Mactung), Yukon and Northwest Territories; I, P-T-X-V characterization of the methane-bearing, skarn-forming fluids. Canadian Mineralogist, Volume. 27, p. 545- 563.

Gordey, S.P., 1992. Geology, South Nahanni River area, Northwest Territories-Yukon Territory; Geological Survey of Canada, Preliminary Series Map 1-1992, ,14 maps at 1:50 000 scale.

Gordey, S.P., 2013. Evolution of the Selwyn Basin region, Sheldon Lake and Tay River map areas, central Yukon; Geological Survey of Canada, Bulletin 599, 176 pages.

Gordey, S.P. and Anderson, R.G, 1993. Evolution of the northern Cordilleran miogeocline, Nahanni map area (105I), Yukon and Northwest Territories; Geological Survey of Canada, Memoir 428, 214 pages.

Gordey, S.P., MacDonald, J.D., Turner, E.C., and Long, D.G.F., 2011. Chapter 5, Structural geology of the central Mackenzie Mountains; *in* Martel, E., Turner, E.C., and Fischer, B.J. (editors), Geology of the central Mackenzie Mountains of the northern Cordillera; Sekwi Mountain (105P), Mount Eduni (106A), and northwestern Wrigley Lake (95M) map areas, Northwest Territories; Northwest Territories Geological Survey, NWT Special Volume 1, p. 215-250.

Gordey, S.P., Pierce, K.L., Fallas, K., Martel, E., and Roots, C.F., 2012. GIS compilation for the geology of Sekwi Mountain, Mount Eduni and northwest Wrigley Lake areas, Mackenzie Mountains, Northwest Territories; Northwest Territories Geological Survey, NWT Open Report 2012-002, digital data.

Handfield, R.C., 1968, Sekwi Formation, a new Lower Cambrian formation in the southern Mackenzie Mountains, District of Mackenzie (95L, 105I, 105P); Geological Survey of Canada, Paper 68-47, 23 pages.

Harris, F.R., 1977. Geology of the Macmillan tungsten deposit. *In*: Morin, J.A., Sinclair, W.D., Craig, D.B., and Marchand, M. (editors), Mineral Industry Report 1976 - Yukon Territory; 1977-1, p. 20-32.

Harris, F.R., 1980. Geology of the Macmillan tungsten deposit, AMAX of Canada Limited, April, 1980; Northwest Territories Geological Survey, Mactung collection, Report number MT 1980-28, 15 pages.

Harris, F.R. and Godfrey, T.J.R., 1974. Geological map, west half, 1" = 200', Macmillan Tungsten Property, Amax Potash Limited, Figure 5 to accompany report "Geology and Ore Reserves - Macmillan Tungsten Property"; Northwest Territories Geological Survey; Mactung collection, Drawing number 01E-GE-073, 1:2400 scale.

Harris, F.R. and Godfrey, T.J.R., 1975. Geology and ore reserves - Macmillan Tungsten Property - 1973 Property report, AMAX Northwest Mining Company Limited; Northwest Territories Geological Survey, Mactung collection, Report number MT 1975-06, 59 pages.

Hart, C.J.R., Mair, J.L., Goldfard, R.J., and Groves, D.I., 2004. Source and redox controls on metallogenic variations in intrusion-related ore systems, Tombstone-Tungsten Belt, Yukon Territoy, Canada. Transactions of the Royal Society of Edinburgh; Earth Sciences, Volume 95, p. 339-356.

Hunt, P.A. and Roddick, J.C., 1987. A compilation of K-Ar ages. Radiogenic Age and Isotopic Studies; Geological Survey of Canada, Report 1 p. 143-204.

Lodder, W. and Harris, F.R., 1974. Geological map, east half, 1" = 200', Macmillan Tungsten Property, Amax Potash Limited, Figure 3b to accompany report "1972 Property Report - Macmillan Tungsten Property"; Northwest Territories Geological Survey, Mactung collection, Drawing number 01E-GE-072, 1:2400 scale.

Lowe, D.R., 1982. Sediment gravity flows II: Depositional models with special reference to the deposits of high-density turbidity currents; Journal of Sedimentary Petrology, Volume 52, p. 279-297.

Martel, E., Turner, E.C., and Fischer, B.J. (editors), 2011. Geology of the central Mackenzie Mountains of the northern Cordillera; Sekwi Mountain (105P), Mount Eduni (106A), and northwestern Wrigley Lake (95M) map areas, Northwest Territories; Northwest Territories Geological Survey, NWT Special Volume 1,423 pages.

Martel, E., Fischer, B.J., Pierce, K.L, and Falck, H., 2018. Geology of the Mactung tungsten skarn deposit; Northwest Territories Geological Survey, NWT Open File 2018-01, 1 map at 1:10 000 scale and digital files.

Mortensen, J.K., Lang, J.R., and Baker, T., 1997. Age and gold potential of the Tungsten plutonic suite in the Macmillan Pass area, western NWT. *In*: Program and abstracts of talks and posters, Northwest Territories Geoscience Forum 25th Anniversary Yellowknife; Northwest Territories Geological Survey, Yellowknife Geosicence Forum Abstracts Volume, 1997, p. 79-80.

Narisco, N., 2009. Technical report on the Mactung property. Prepared by Wardrop for North American Tungsten Corporation Ltd., April 3, 2009; Northwest Territories Geological Survey, Mactung collection, Report number MT 2009-04, 333 pages.

Nelson, J.L., Colpron, M., and Israel, S., 2013. The Cordillera of British Columbia, Yukon, and Alaska: Tectonic and metallogeny. *In* Colpron, M., Bissig, T., Rusk, B.G., and Thompson, J.F.H. (editors), Tectonics, Metallogeny, and Discovery: The North American Cordillera and Similar Accretionary Settings; Society of Economic Geologists, Special Publication 17, p.53- 109.

NORMIN, 2016. NORMIN Showings [online]; Northwest Territories Geological Survey, Yellowknife. Accessed at http://www.ntgomap.nwtgeoscience.ca, 2016.

Odekirk, J.R., 1979a. Preliminary investigation of rock types from the upper ore units (3D, 3E, 3F) at the Macmillan Pass tungsten deposit (1218), Amax, May 16, 1979; Northwest Territories Geological Survey, Interoffice memorandum to R.C. Steininger, Mactung collection, Report number MT 1979-08, 23 pages.

Odekirk, J.R., 1979b. Comparison of the Upper ore zone (3D, 3E, 3F) and Lower ore zone (2B) rock types at the Mac Pass tungsten deposit (1218), Amax, July 25, 1979; Northwest Territories Geological Survey, Interoffice memorandum to R.C. Steininger, Mactung collection, Report number MT 1979-09, 14 pages.

Okulitch, A.V. and Irwin, D., 2014. Geological compilation of the Western Mainland and Southern Arctic Islands regions, Northwest Territories; Northwest Territories Geological Survey, NWT Open File 2014-01, digital data.

Ramsay, J.G., 1967. Folding and fracturing of rocks. McGraw-Hill, New York, 568 pages.

Rasmussen, K.L., 2013. The timing, composition, and petrogenesis of syn- to post-accretionary magmatism in the northern Cordilleran miogeocline, eastern Yukon and southwestern Northwest Territories. Unpublished Ph.D. dissertation, University of British Columbia, Vancouver, 788 pages.

Roddick, J.A., 1967. Tintina Trench. Journal of Geology, Volume 75, p. 23-33.

Selby, D., Creaser, R.A., Heaman, L.M., and Hart, C.J.R., 2003. Re-Os and U-Pb geochronology of the Clear Creek, Dublin Gulch, and Mactung deposits, Tombstone Gold Belt, Yukon, Canada: absolute timing relationships between plutonism and mineralization. Canadian Journal of Earth Sciences, Volume 40, p. 1839-1852.

Staples, R.D., Murphy, D.C., Gibson, H.D., Colpron, M., Berman, R.G., and Ryan, J.J., 2014. Middle Jurassic to earliest Cretaceous mid-crustal tectono-metamorphism in the northern Cordillera: Recording foreland-directed migration of an orogenic front; The Geological Society of America, GSA Bulletin, Volume 126, Number 11/12, p. 1511-1530.

Turner, E.C., Roots, C.F., MacNaughton, R.B., Long, D.G.F., Fischer, B.J., Gordey, S.P., Martel, E., and Pope, M.C., 2011. Chapter 3, Stratigraphy; *In* Martel, E., Turner, E.C., and Fischer, B.J.( editors), Geology of the central Mackenzie Mountains of the northern Cordillera; Sekwi Mountain (105P), Mount Eduni (106A), and northwestern Wrigley Lake (95M) map areas, Northwest Territories; Northwest Territories Geological Survey, NWT Special Volume 1, p. 31-192.

Wheeler, A., 2012. Report NI 43-101: Technical report on the mineral resources and reserves of the Los Santos Mine project, Spain; Prepared for Daytal Resources Spain S.L. Accessed in 2017 at: www.sedar.com under Almonty Industries Inc., 2012.

Wolf Minerals, 2015. Wolf Minerals announces 34% increase in ore reserves at Hemerdon tungsten and tin project. ASX Announcement, 25 March 2015. Accessed at: http://www.wolfminerals.com.au/IRM/Company/ShowPage.aspx/PDFs/1572-10000000/34PercentIncreaseinOreReservesatHemerdonPr, 2017.

Yukon Geological Survey. Yukon Digital Bedrock Geology [online]; Yukon Geological Survey. Accessed on 2017/03/22 at http://www.geology.gov.yk.ca/update_yukon_bedrock_geology_map.html.

Yukon MINFILE, mineral occurrences in the Yukon; Yukon Geological Survey. Accessed on 2017 at http://data.geology.gov.yk.ca.

# Appendix A - Mactung deposit resource report

**Garth Kirkham, P.Geo., FGC**

**Date: January 9, 2018**

*Recommended Citation:*
*Kirkham, G., 2018. Appendix A: Mactung deposit resource report. In: Fischer, B.J., Martel, E., and Falck, H., Geology of the Mactung tungsten skarn and area – Review and 2016 field observations; Northwest Territories Geological Survey, NWT Open File 2018-02, 84 pages and appendices.*

# 1. Mineral Resource Estimate

## 1.1. Mactung Estimation

### 1.1.1. Introduction

A three-dimensional digital model of the Mactung deposit, including solids for the ore zones in Sekwi Formation (mine unit 2B) and Rabbitkettle Formation members D, E, and F (mine units 3D, 3E, 3F), was created by G. Kirkham using data from 249 drill holes, which had been logged and compiled by North American Tungsten Corp. Ltd. personnel. The exercise was conducted to ensure the completeness of the digital database and no examination of the core was done. The modeling exercise was also used to examine the potential for alternative mining approaches to optimize the extraction of tungsten, including a combination open pit/underground mining scenario. This contrast the most recent published resource calculations by Narisco (2009), which only considered an underground mine utilizing a combination of long-hole blast and mechanized cut-and-fill mining methods.

The reader is cautioned that these values should not be misconstrued as a "Mineral Resource" or "Mineral Reserve" for National Instrument 43-101 purposes. The reported quantities and grades are only presented to demonstrate the sensitivity of the resource model to the selection of cut-off grade and to examine the resource without the influence of political and economic constraints.

The magnitude of the mineral resources is sensitive to the selection of cut-off grade, which is shown by the presentation of resource estimates for cut-off grades ranging in increments of 0.1 % from 0 % to 1.0 %$WO_3$. For a cut-off grade of 0.5 %, an indicated resource has been estimated of 14.0 Mt at 1.008 %$WO_3$ and 0.082 %Cu, and an additional inferred resource of 3.4 Mt grading 0.81 %$WO_3$ and 0.06 %Cu.

The Mactung deposit was modelled using LeapFrog®. Tthe block models were then created using **MineSight™ and** analysed in order to reduce variability and better reflect the Selective Mining Unit.

### 1.1.2. Data

The drillhole database with 249 drillholes was supplied in electronic format. This included collars, down hole surveys, lithology descriptions and assay data (including $WO_3$% and Cu%). Validation and verification checks were performed during import to insure no overlapping intervals, typographic errors and anomalous entries. No errors were found.

**Table 1-1: Example of Electronic Drillhole Log**

| REF# | FROM | -TO- | -AI- | %WO3 | %CU | ZONE | CCODE | UNIT | GE01 | GEO2 | XTRA1 | XTRA2 |
|---|---|---|---|---|---|---|---|---|---|---|---|---|
| 9 | 231.50 | 233.00 | 1.50 | 0.13 | 0.01 | 13 | 7 | 3D | 7^dg | X | 15 | 13 |
| 9 | 233.00 | 234.90 | 1.90 | 2.33 | 0.04 | 13 | 2 | 3D | 2^qd | RQ | 15 | 13 |
| 9 | 234.90 | 235.75 | 0.85 | - | - | 13 | 2 | 3D | 2^qd | RQ | 15 | 13 |
| 9 | 235.75 | 237.60 | 1.85 | 0.20 | 0.02 | 13 | 2 | 3D | 2^qd | RQ | 15 | 13 |
| 9 | 237.60 | 239.20 | 1.60 | 0.34 | 0.01 | 13 | 2 | 3D | 2^qd | RQ | 15 | 13 |
| 9 | 239.20 | 241.00 | 1.80 | 1.71 | 0.02 | 13 | 2 | 3D | 2^qd | RQ | 15 | 13 |
| 9 | 241.00 | 243.20 | 2.20 | 1.01 | 0.03 | 13 | 2 | 3D | 2^qd | RQ | 15 | 13 |
| 9 | 243.20 | 244.30 | 1.10 | 0.06 | 0.02 | 13 | 2 | 3D | 2^qd | RQ | 15 | 13 |
| 9 | 244.30 | 246.00 | 1.70 | 1.20 | 0.04 | 13 | 2 | 3D | 2^qd | RQ | 15 | 13 |
| 9 | 246.00 | 247.50 | 1.50 | 0.08 | 0.03 | 13 | 6 | 3C | 6<qd | RQ1/ | 19 | 13 |
| 9 | 247.50 | 249.30 | 1.80 | 0.53 | 0.08 | 13 | 6 | 3C | 6<qd | RQ1/ | 19 | 13 |
| 9 | 249.30 | 250.45 | 1.15 | 0.38 | 0.03 | 0 | 6 | 3C | 6<qd | RQ1/ | 19 | 13 |
| 9 | 250.45 | 252.10 | 1.65 | - | - | 0 | 6 | 3C | 6<qd | RQ1/ | 19 | 0 |

The QA/QC data was reviewed and no issues or concerns were identified.

### 1.1.3. Geology Model

A solid model of mine units 2B, 3D, 3E, and 3F within the Mactung deposit (respectively the Lower ore zone, lower horizon of Upper ore zone, middle horizon, and upper horizon of Upper ore zone) were created using LeapFrog®.

Every intersection was inspected and the solid was then manually adjusted to match the drill intercepts. Subdivisions of the lithological units were based on structural breaks or faults. These are shown in Figures 1-1 and 1-2. Once the solid model was created, it was used to code the drill hole assays and composites for subsequent geostatistical analysis. The solid zone was utilized to constrain the block model by matching assays to those within the zones. The orientation and ranges (distances) utilized for search ellipsoids used in the estimation process were derived from strike and dip of the mineralized zone and site knowledge and on-site observations.

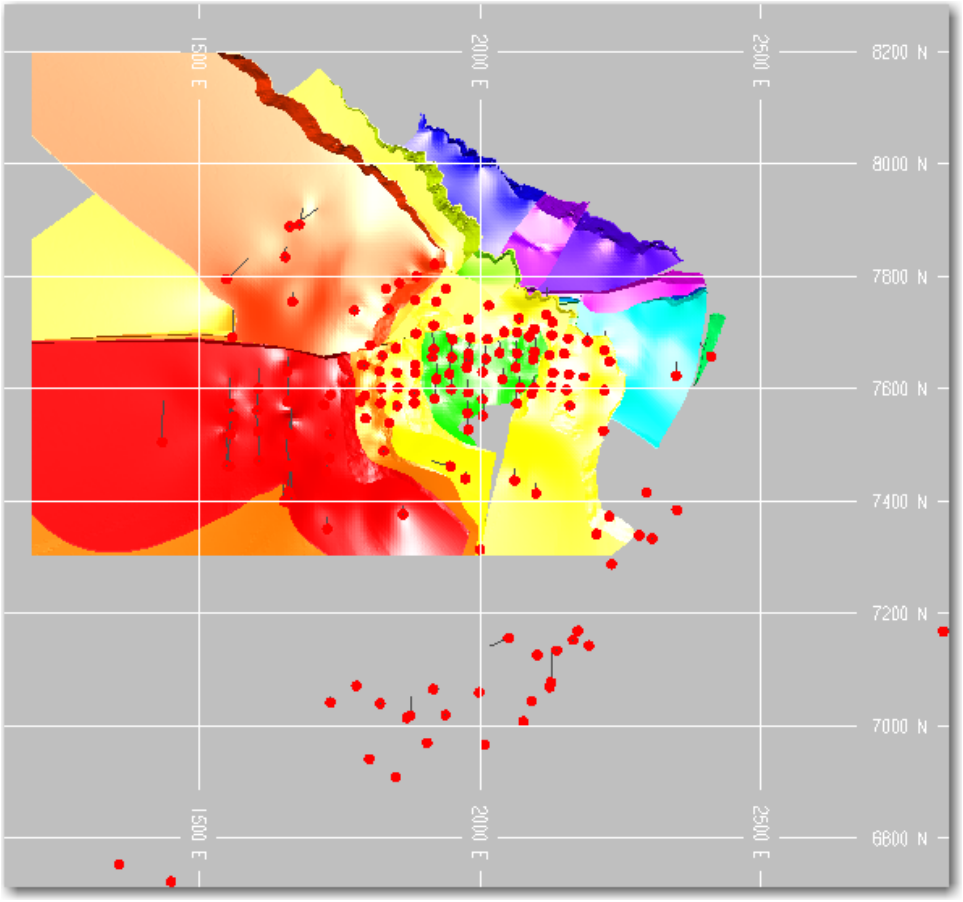


**Figure 1-1: Mactung solids with drillhole collars (red dots) in plan view.**

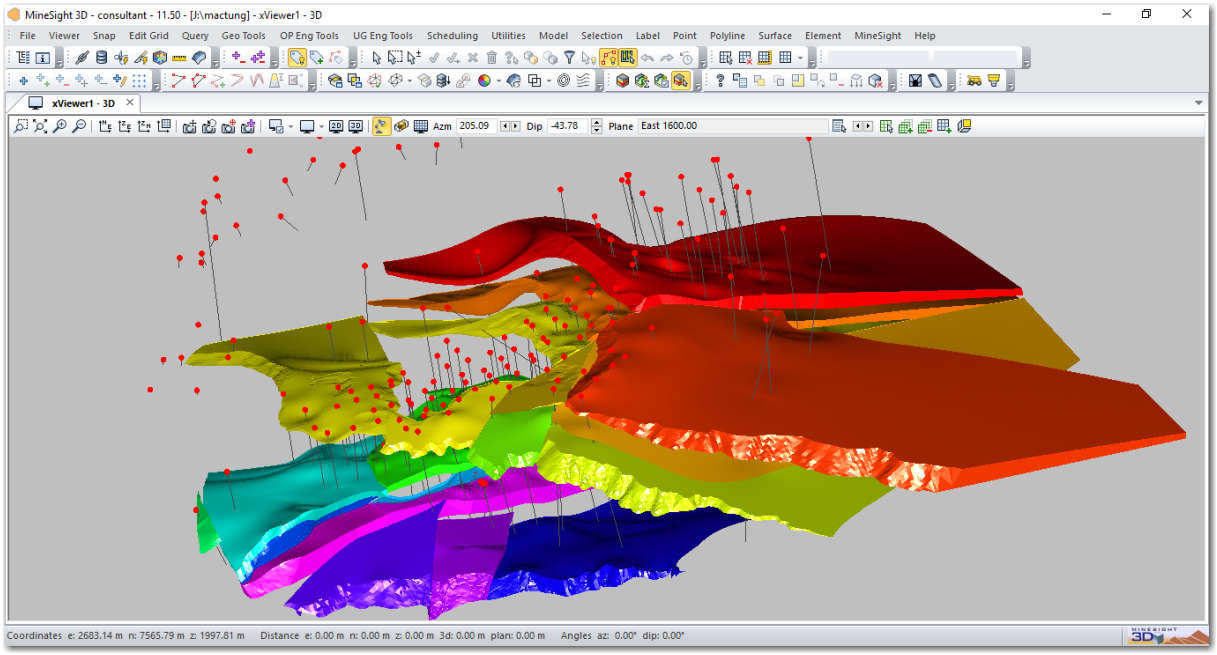


**Figure 1-2: Mactung solids based on structurally bounded ore zones as defined by the length-weighted composites in Table 1-3.**

### 1.1.4. Data Analysis

The database was numerically coded by mineralized zone solids for Mactung. The database was then manually adjusted drill hole by drill hole to ensure accuracy of zonal intercepts. Table 1-2 and Figure 1-3 show statistics of $WO_3$ and Cu assays.

**Table 1-2: Statistics for length-weighted assays $WO_3$% and copper by zone.**

| LITH CODE | LITHOLOGY | GRADE | # | Length | Max | Mean | COV |
|---|---|---|---|---|---|---|---|
| 0 | OB/-1 | WO3 | 46 | 60 | 3.84 | **0.91** | 1.2 |
| | | CU | 41 | 54 | 0.44 | 0.12 | 1.0 |
| 1 | 1 | WO3 | 394 | 488 | 2.61 | **0.15** | 2.1 |
| | | CU | 321 | 406 | 1 | 0.03 | 2.0 |
| 2 | 1A | WO3 | 14 | 17 | 3.2 | **0.21** | 2.0 |
| | | CU | 12 | 16 | 0.32 | 0.04 | 1.2 |
| 7 | 7 | WO3 | 49 | 73 | 4.58 | **0.17** | 4.8 |
| | | CU | 4 | 7 | 0.05 | 0.02 | 0.9 |
| 8 | 8 | WO3 | 2 | 1 | 0.07 | **0.07** | 0.1 |
| | | CU | 0 | | | | |
| 9 | 9 | WO3 | 16 | 14 | 2.96 | **0.83** | 1.1 |
| | | CU | 11 | 13 | 0.59 | 0.15 | 1.2 |
| 10 | 3G | WO3 | 51 | 66 | 1.68 | **0.24** | 1.9 |
| | | CU | 37 | 46 | 0.14 | 0.02 | 1.7 |
| 11 | 3H | WO3 | 57 | 78 | 1.12 | **0.15** | 1.7 |
| | | CU | 25 | 42 | 0.04 | 0.02 | 0.5 |
| 12 | 2B | WO3 | 2,490 | 2981 | 8.4 | **1.26** | 0.9 |
| | | CU | 2,266 | 2742 | 1 | 0.15 | 0.9 |
| 13 | 3F | WO3 | 768 | 998 | 7.53 | **0.64** | 1.2 |
| | | CU | 507 | 662 | 0.16 | 0.01 | 1.3 |
| 14 | 3E | WO3 | 1,399 | 1893 | 4.78 | **0.32** | 1.4 |
| | | CU | 648 | 921 | 0.2 | 0.01 | 1.1 |
| 15 | 3D | WO3 | 1,178 | 1470 | 4.97 | **0.62** | 1.0 |
| | | CU | 651 | 830 | 0.34 | 0.04 | 1.0 |
| 19 | 3C | WO3 | 1,844 | 2385 | 9.41 | **0.14** | 2.3 |
| | | CU | 763 | 996 | 0.56 | 0.03 | 1.2 |
| 21 | 21 | WO3 | 1 | 1 | 0.88 | **0.88** | |
| | | CU | 1 | 1 | 0.07 | 0.07 | 0.0 |
| 22 | 12 | WO3 | 7 | 9 | 0.77 | **0.18** | 1.5 |
| | | CU | 0 | 0 | 0 | 0 | 0 |
| Total | | WO3 | 8,316 | 10533 | 9.41 | 0.61 | 1.4 |
| | | CU | 5,287 | 6733 | 1 | 0.08 | 1.5 |

**Table 1-3: Statistics for length-weighted composites by ore zone.**

| ORE CODE | ORE ZONE | GRADE | # | Length | Max | Mean | COV |
|---|---|---|---|---|---|---|---|
| 0 | WASTE | WO3 | 3,205 | 4,264 | 4.58 | **0.107** | 1.9 |
| | | CU | 1,435 | 1,970 | 0.53 | 0.02 | 1.2 |
| 3 | 3F SOUTH | WO3 | 366 | 458 | 7.53 | **0.932** | 1.0 |
| | | CU | 263 | 343 | 0.16 | 0.012 | 1.7 |
| 4 | 3F NORTH | WO3 | 192 | 255 | 3.71 | **0.706** | 0.9 |
| | | CU | 106 | 132 | 0.04 | 0.012 | 0.7 |
| 8 | 3E SOUTH | WO3 | 408 | 559 | 4.78 | **0.588** | 1.0 |
| | | CU | 260 | 373 | 0.09 | 0.012 | 0.9 |
| 9 | 3E NORTH | WO3 | 194 | 263 | 3.28 | **0.512** | 1.0 |
| | | CU | 85 | 123 | 0.03 | 0.011 | 0.4 |
| 10 | 3E NE | WO3 | 36 | 43 | 1.84 | **0.385** | 1.1 |
| | | CU | 0 | | | | |
| 11 | 3D SE | WO3 | 133 | 153 | 2.35 | **0.302** | 1.2 |
| | | CU | 42 | 31 | 0.02 | 0.009 | 0.8 |
| 12 | 3D SW WEDGE | WO3 | 42 | 46 | 2 | **0.601** | 1.0 |
| | | CU | 24 | 22 | 0.03 | 0.012 | 0.8 |
| 13 | 3D SOUTH | WO3 | 714 | 904 | 9.41 | **0.73** | 0.9 |
| | | CU | 451 | 608 | 0.56 | 0.043 | 1.0 |
| 14 | 3D NORTH | WO3 | 189 | 239 | 4.3 | **0.649** | 1.0 |
| | | CU | 101 | 125 | 0.18 | 0.023 | 1.0 |
| 15 | 3D NE | WO3 | 64 | 78 | 3.76 | **0.837** | 0.9 |
| | | CU | 17 | 18 | 0.02 | 0.015 | 0.3 |
| 16 | 2B UPPER1 W16 | WO3 | 1,956 | 2,307 | 8.2 | **1.269** | 0.9 |
| | | CU | 1,814 | 2,162 | 1 | 0.159 | 0.9 |
| 17 | 2B MIDDLE | WO3 | 80 | 83 | 4.1 | **0.904** | 1.0 |
| | | CU | 76 | 78 | 0.8 | 0.165 | 1.1 |
| 18 | 2B LOWER1 | WO3 | 466 | 567 | 8.4 | **1.229** | 1.0 |
| | | CU | 440 | 537 | 0.74 | 0.094 | 1.1 |
| 19 | 2B LOWER2 W_Z19 | WO3 | 103 | 119 | 6.15 | **0.532** | 1.5 |
| | | CU | 54 | 64 | 0.25 | 0.021 | 1.8 |
| 21 | 2B UPPER1 C_Z21 | WO3 | 118 | 136 | 2.96 | **0.672** | 0.9 |
| | | CU | 74 | 92 | 0.41 | 0.093 | 1.0 |
| 24 | 2B LOWER2 C_Z24 | WO3 | 46 | 57 | 5.38 | **1.28** | 0.8 |
| | | CU | 45 | 56 | 0.44 | 0.154 | 0.9 |
| 26 | 2B UPPER1 E_Z26 | WO3 | 4 | 4 | 0.36 | **0.283** | 0.3 |
| | | CU | 0 | 0 | 0 | 0 | 0 |
| Total | | WO3 | 8,316 | 10,533 | 9.41 | **0.61** | 1.4 |
| | | CU | 5,287 | 6,733 | 1 | 0.075 | 1.5 |

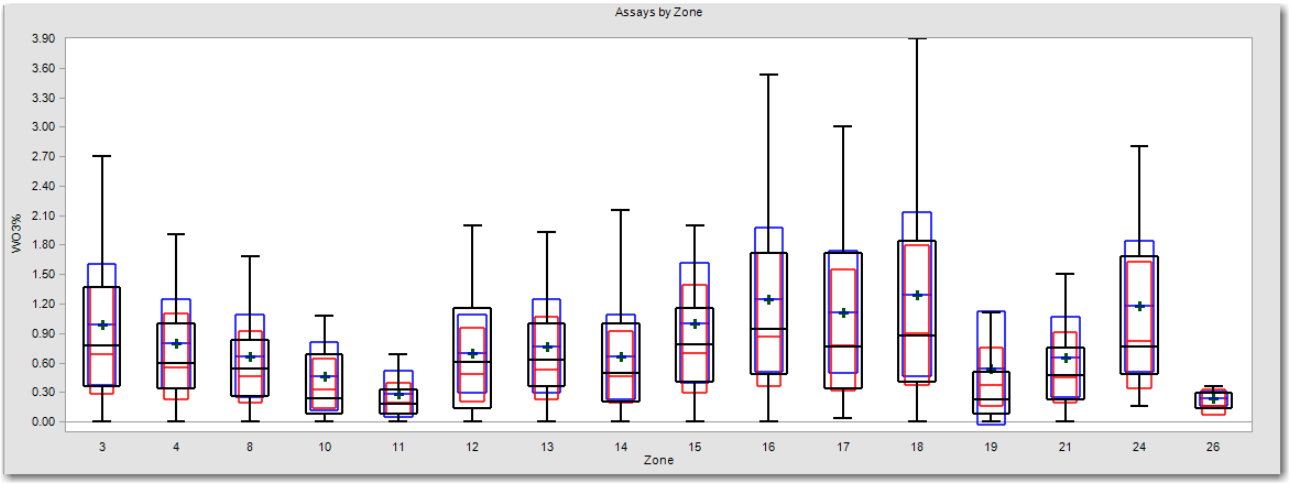


**Figure 1-3: Box and whisker diagram of tagged composite from each zone as per ore code in Table 1-3.**

### 1.1.5. Composites

In previous estimates, the 2.5-metre composite length offered a balance between supplying common support for samples and minimizing the smoothing of the grades. This was taking into consideration that the vertical block dimension was five metres, which is the predominant direction of drilling. In addition, the sample length was consistent with the distribution of sample lengths within the mineralized domains. Figures 1-4 and 1-5 show the combined zone histograms for $WO_3$ and Cu, respectively.

It should be noted that although 2.5 metres is the composite length, any residual composites of length greater than one metre and less than 2.5 metres were retained to represent a composite while any composite residuals less than one metre were combined with the composite above.

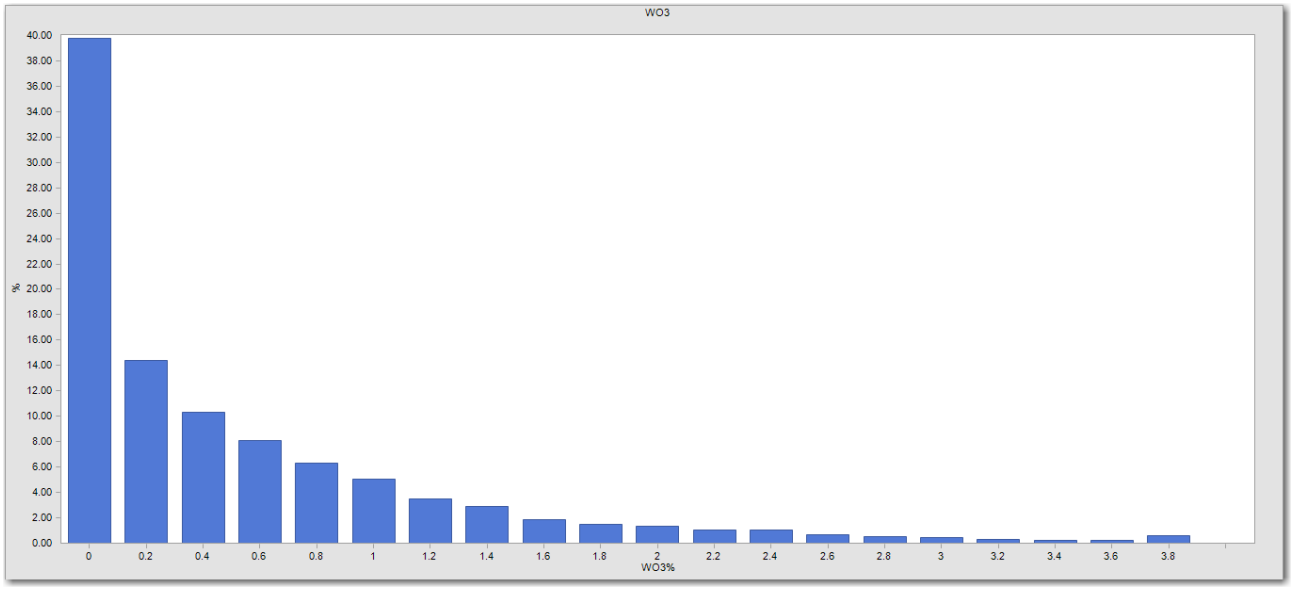


**Figure 1-4: Histogram of $WO_3$ composites.**

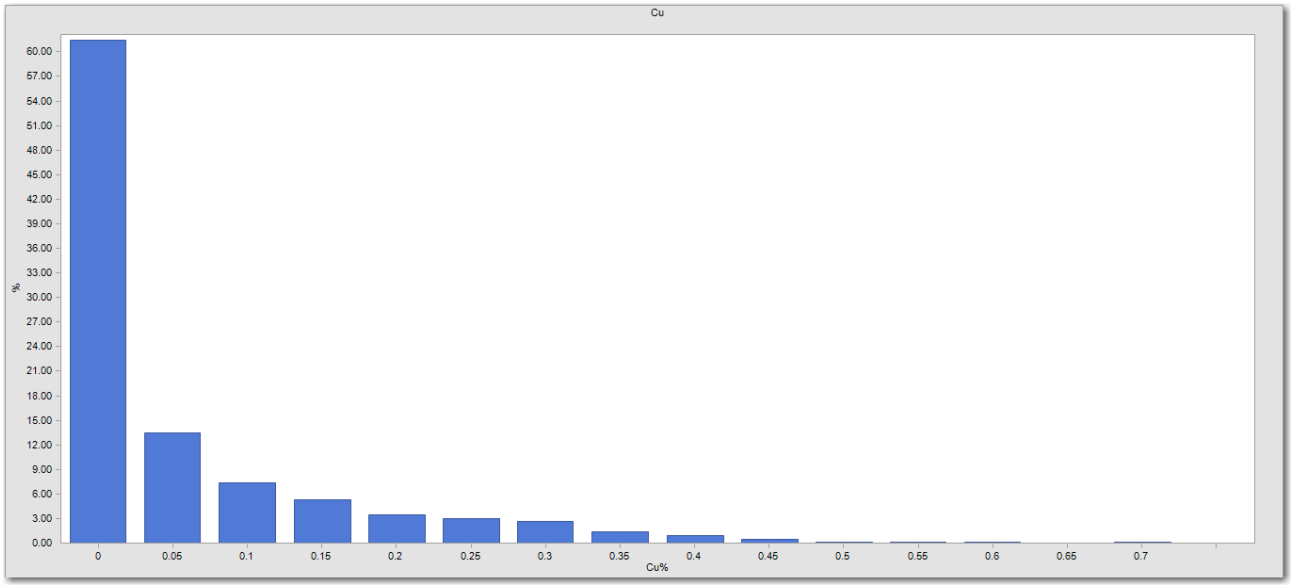


**Figure 1-5: Histogram of Cu composites.**

Box plots for all zones for Mactung deposit for $WO_3$ are shown in Figures 1-6. Note that the numeric coding for the box plots are based on the lithological unit.

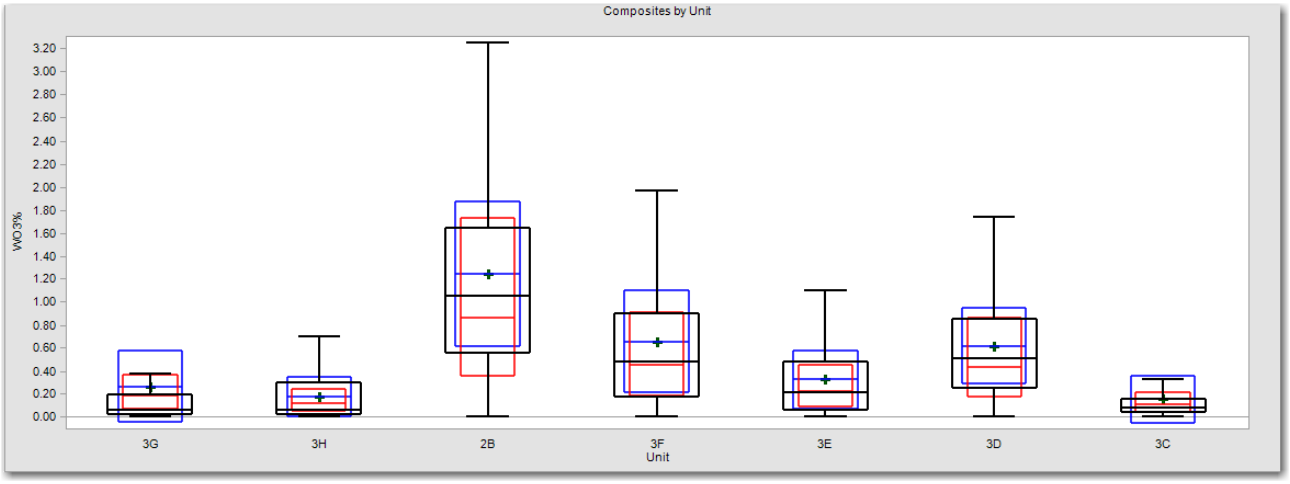


**Figure 1-6: Box and whisker plot of $WO_3$ composites.**

### 1.1.6. Evaluation of Outlier Assay Values

A common method for determining outlier populations is to identify changes in slope or "breaks" in the cumulative frequency plot. During the estimation process, the influence of composites greater than 4% $WO_3$ have been cut, based on the breaks in the cumulative frequency plots shown in Figure 1-7.

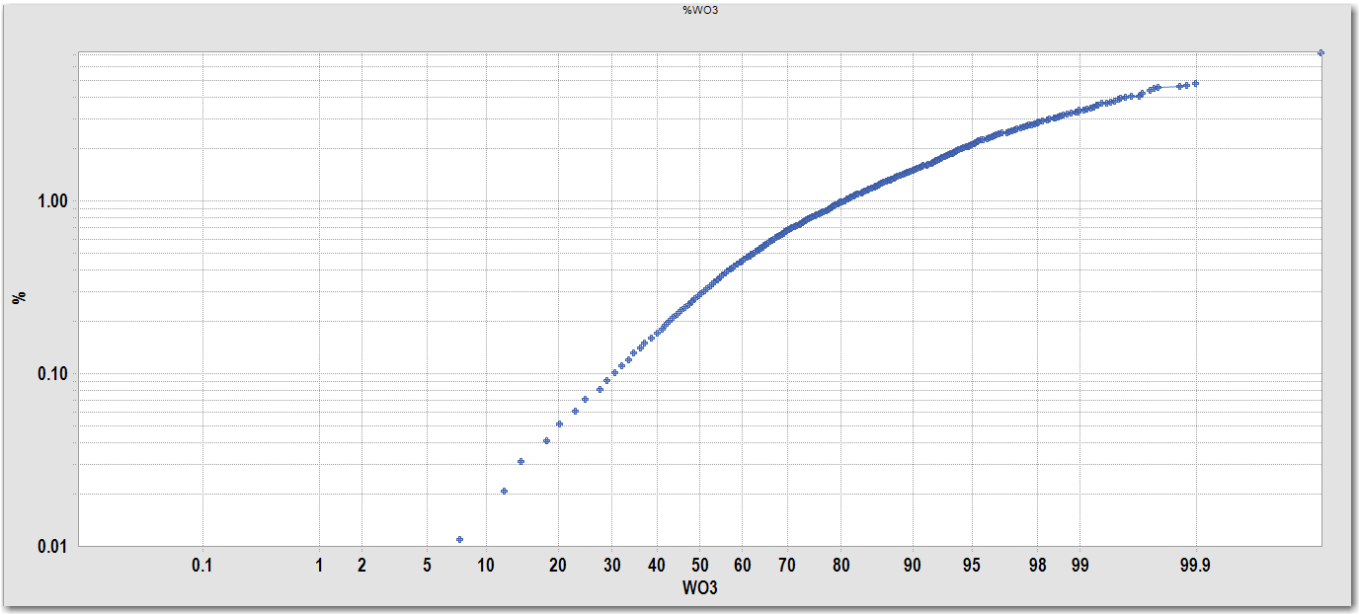


**Figure 1-7: Mactung cumulative frequency plot.**

### 1.1.7. Specific Gravity Estimation

A Specific Gravity (SG) value of 2.99 was used for mine unit 2B and of 3.14 for mine units 3D, 3E and 3F. The SG value of 2.7 was used for calculating the tonnage of waste material.

### 1.1.8. Variography

Experimental variograms and variogram models in the form of correlograms were generated for $WO_3$ grades. Previously, the individual zones did not have sufficient data to generate meaningful variogram results however when combined, which is valid in the opinion of the author, the results are meaningful and there is justification for utilizing ordinary kriging for the estimation process. The definition of the nugget effect for each of the metals was taken from the downhole variograms. The correlogram models for $WO_3$ within the mine unit 2B along with 3D, 3E and 3F are shown in Tables 1-3 and 1-4, respectively.

**Table 1-3: $WO_3$ 2B correlogram model.**

# Calculate Sample Variograms

Medsystem and Vulcan Rotation Conventions

Nugget ==> 0.31379
C1 ==> 0.55979
C2 ==> 0.12642

First Structure -- Spherical

LH Rotation about the Z axis ==> -66
RH Rotation about the X' axis ==> -42
LH Rotation about the Y' axis ==> 49
Range along the Z' axis ==> 21.5 Azimuth ==> 234 Dip ==> 29
Range along the Y' axis ==> 14.9 Azimuth ==> 294 Dip ==> -42
Range along the X' axis ==> 6.7 Azimuth ==> 346 Dip ==> 34

Second Structure -- Spherical

LH Rotation about the Z axis ==> -75
RH Rotation about the X' axis ==> 30
LH Rotation about the Y' axis ==> -27
Range along the Z axis ==> 401.9 Azimuth ==> 58 Dip ==> 51
Range along the X' axis ==> 71.8 Azimuth ==> 0 Dip ==> -23
Range along the Y' axis ==> 209.0 Azimuth ==> 285 Dip ==> 30

Modeling Criteria

Minimum number pairs req'd ==> 50
Sample variogram points weighted by # pairs

**Table 1-4: $WO_3$ 3D, 3E and 3F correlogram model.**

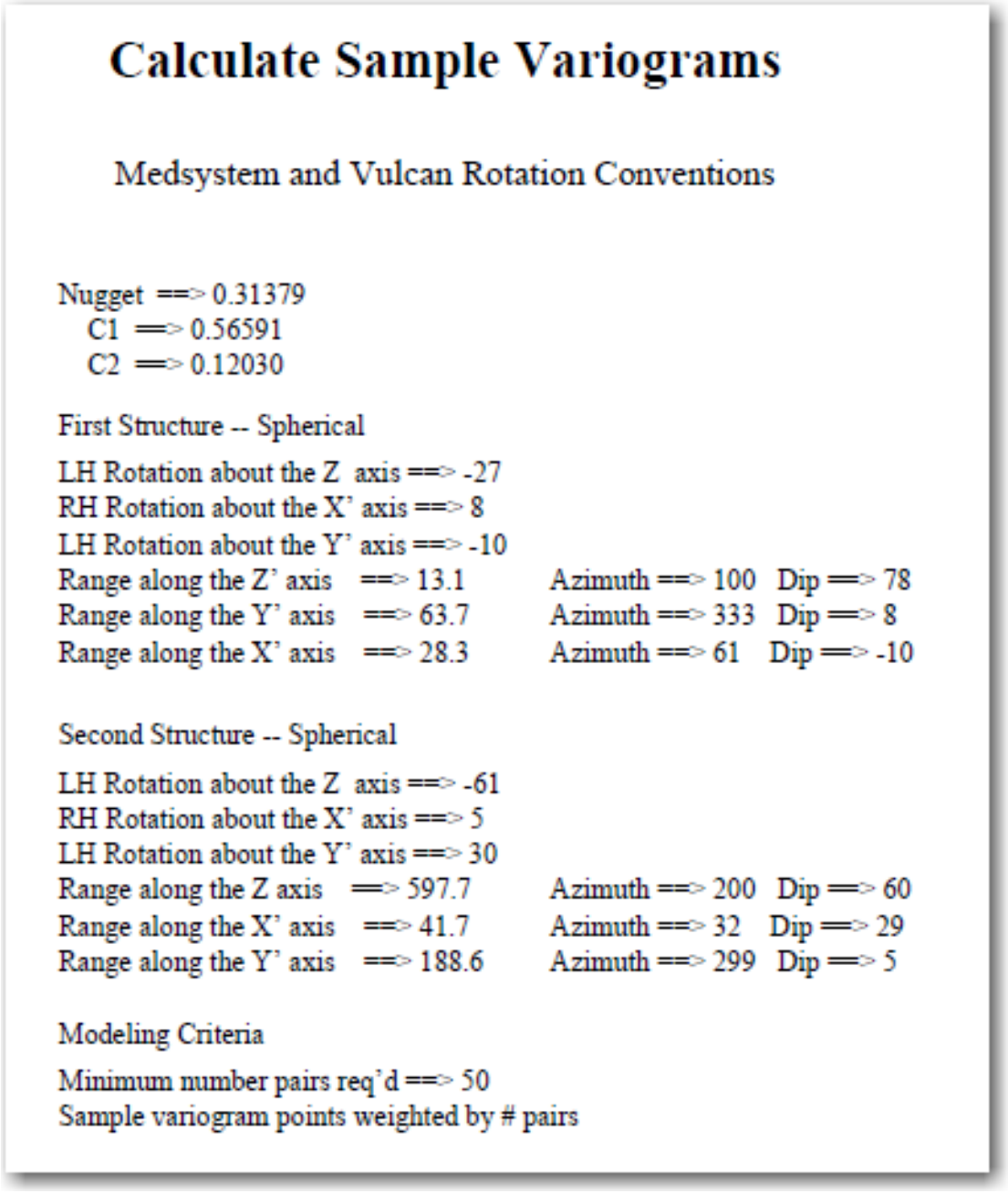

Calculate Sample Variograms

Medsystem and Vulcan Rotation Conventions

Nugget ==> 0.31379
C1 ==> 0.56591
C2 ==> 0.12030

First Structure -- Spherical

LH Rotation about the Z axis ==> -27
RH Rotation about the X' axis ==> 8
LH Rotation about the Y' axis ==> -10
Range along the Z' axis ==> 13.1 Azimuth ==> 100 Dip ==> 78
Range along the Y' axis ==> 63.7 Azimuth ==> 333 Dip ==> 8
Range along the X' axis ==> 28.3 Azimuth ==> 61 Dip ==> -10

Second Structure -- Spherical

LH Rotation about the Z axis ==> -61
RH Rotation about the X' axis ==> 5
LH Rotation about the Y' axis ==> 30
Range along the Z axis ==> 597.7 Azimuth ==> 200 Dip ==> 60
Range along the X' axis ==> 41.7 Azimuth ==> 32 Dip ==> 29
Range along the Y' axis ==> 188.6 Azimuth ==> 299 Dip ==> 5

Modeling Criteria

Minimum number pairs req'd ==> 50
Sample variogram points weighted by # pairs

### 1.1.9. Block Model Definition

The block model used for estimating the resources was defined according to the limits specified in Figure 1-8. The block model is orthogonal and non-rotated reflecting the orientation of the deposit. The block size chosen was 5 metres by 5 metres by 5 metres, to align with the Selective Mining Unit as previously discussed. Note that MineSight™ uses the centroid of the blocks as the origin.

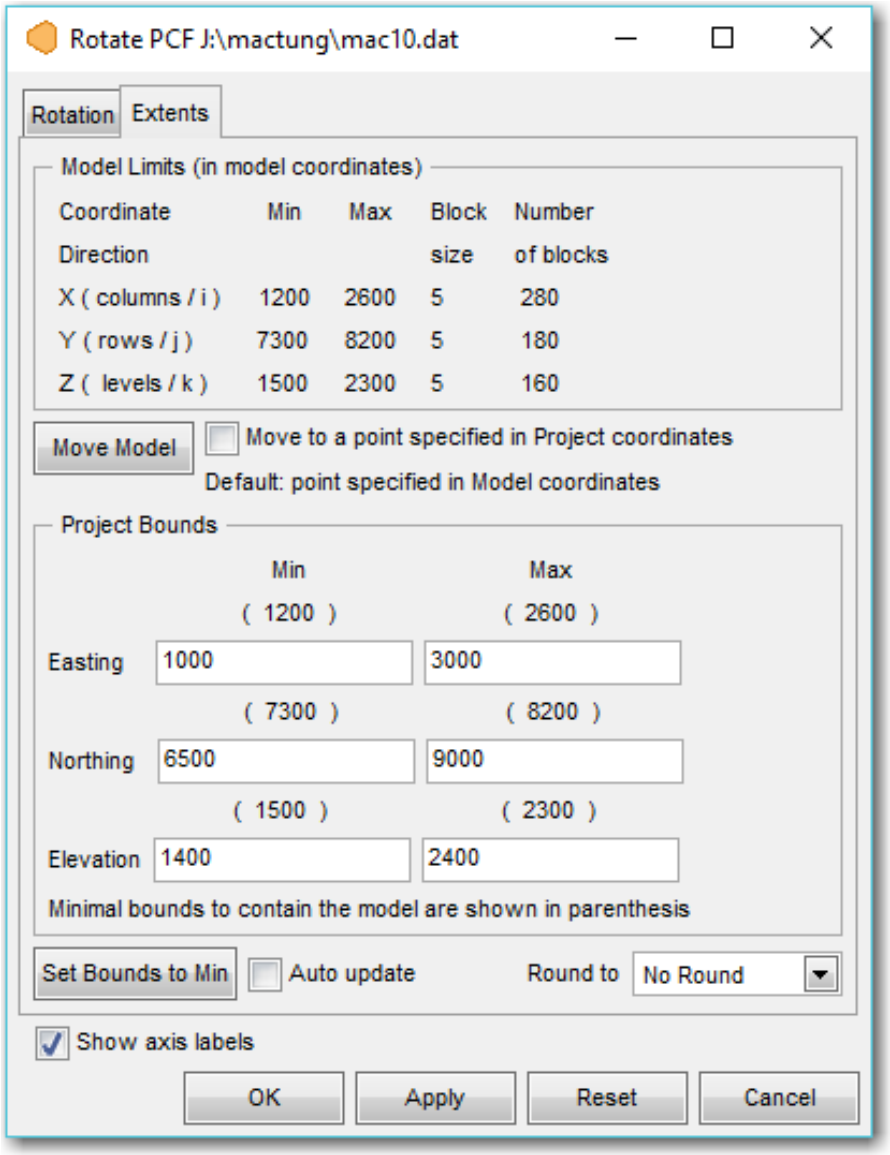


**Figure 1-8: Specifications for the Mactung block model.**

### 1.1.10. Resource Estimation Methodology

The estimation plan includes the following items:

- Mineralized zone code and percentage of modeled mineralization in each block;
- Estimated bulk specific gravity based on an inverse distance squared method;
- Estimated block $WO_3$ and Cu grades by ordinary kriging, using a single estimation pass.

The search ellipsoids were oriented along the direction of continuity as shown in Table 1-5. The rotation convention used is a rotation about the Z axis with clockwise being positive, rotation about the semi-major axis which is the X axis with clockwise being positive and rotation about the minor axis which is the Y axis with clockwise being positive.

**Table 1-5: Search ellipse parameters.**

| Major Axis | Semi-Major Axis | Minor Axis | 1st Rotation Angle Azimuth | 2nd Rotation Angle Dip | 3rd Rotation Angle | Min. No. Of Comps | Max. No. Of Comps | Max. Samples per Drill hole |
|---|---|---|---|---|---|---|---|---|
| 150 | 150 | 100 | 0 | 0 | 0 | 5 | 15 | 4 |

### 1.1.11. Resource Validation

A graphical validation was done on the block model. This graphical validation serves several purposes:

- Checks the reasonableness of the estimated grades, based on the estimation plan and the nearby composites;
- Checks that the general drift and the local grade trends compared to the drift and local grade trends of the composites;
- Ensures that all blocks in the core of the deposit have been estimated;
- Checks that topography has been properly accounted for;
- Checks against manual approximate estimates of tonnage to determine reasonableness; and
- Inspection and explanation for potentially high grade block estimates in the neighborhood of the extremely high assays.

A full set of cross-sections, long-sections and plans were used to check the block model on the computer screen, showing the block grades and the composites. No evidence of any block being wrongly estimated was found; it appears that every block grade could be explained as a function of the surrounding composites and the estimation plan applied. These validation techniques included the following:

- Visual inspections on a section-by-section and plan-by-plan basis;
- The use of Grade Tonnage Curves;
- Swath Plots comparing Kriging estimated block grades with Inverse Distance and Nearest Neighbour estimates; and
- An inspection of histograms of distance of first composite to nearest block, average distance to blocks for all composites used which gives a quantitative measure of confidence that blocks are adequately informed in addition to assisting in the classification of resources.

### 1.1.12. Mineral Resource Classification

The details for the grid spacing of each resource category used to classify resources are:

- Indicated: Resources in this category would be delineated by multiple drill holes located on a nominal 500-m grid pattern.
- Inferred: Any material not falling in the categories above and within a maximum 100 m of one hole.

The spacing distances are intended to define contiguous volumes, and they should allow for some irregularities due to actual drillhole placement. The final classification volume results typically must be smoothed manually to come to a coherent classification scheme.
To ensure additional confidence and continuity, the blocks were displayed at the chosen threshold of 40 metres to the nearest composite, and a boundary was digitized to create a smooth surface and to reduce the "spotted dog" effect. A solid was then created and coded back into the model by majority code, and using >50% partials to be classified as measured or indicated. The remainder, that is greater than 50 metres but not more than 150 metres from nearest composite, was classified as inferred.

### 1.1.13. Sensitivity of the Block Model to Selection Cut-off Grade

The mineral resources are sensitive to the selection of cut-off grade. Table 1-6 shows global quantities and grade in the Mactung deposit, at different $WO_3$ cut-off grades. The reader is cautioned that these values should not be misconstrued as a mineral reserve. The reported quantities and grades are only presented as a sensitivity of the resource model to the selection of cut-off grade.

**Table 1-6: Mactung deposit – sensitivity analyses of global tonnage and grades at various cut-off grades.**

| CLASS | CUTOFF | TONNES | WO3% | CU% |
|---|---|---|---|---|
| Indicated | 0 | 16,960,359 | 0.894 | 0.07 |
| | 0.1 | 16,955,329 | 0.894 | 0.07 |
| | 0.2 | 16,737,221 | 0.904 | 0.071 |
| | 0.3 | 16,151,248 | 0.927 | 0.073 |
| | 0.4 | 15,245,606 | 0.962 | 0.077 |
| | 0.5 | 14,000,794 | 1.008 | 0.082 |
| | 0.6 | 12,181,803 | 1.077 | 0.091 |
| | 0.7 | 10,400,491 | 1.151 | 0.102 |
| | 0.8 | 8,593,735 | 1.236 | 0.116 |
| | 0.9 | 7,130,584 | 1.317 | 0.131 |
| | 1 | 5,962,940 | 1.39 | 0.145 |
| | | | | |
| Inferred | 0 | 4,887,084 | 0.674 | 0.048 |
| | 0.1 | 4,882,687 | 0.674 | 0.048 |
| | 0.2 | 4,759,718 | 0.687 | 0.049 |
| | 0.3 | 4,519,182 | 0.71 | 0.051 |
| | 0.4 | 4,079,903 | 0.749 | 0.055 |
| | 0.5 | 3,401,541 | 0.809 | 0.064 |
| | 0.6 | 2,453,453 | 0.912 | 0.083 |
| | 0.7 | 1,867,731 | 0.998 | 0.104 |
| | 0.8 | 1,521,460 | 1.057 | 0.121 |
| | 0.9 | 1,164,071 | 1.12 | 0.135 |
| | 1 | 975,246 | 1.154 | 0.147 |

### 1.1.14. Mineral Resource Statement

CIM Definition Standards for Mineral Resources and Mineral Reserves (2014) defines a mineral resource as:

> *"[A] concentration or occurrence of diamonds, natural solid inorganic material, or natural solid fossilized minerals in or on the Earth's crust in such form and quantity and of such a grade or quality that it has reasonable prospects for eventual economic extraction. The location, quantity, grade, geological characteristics and continuity of a Mineral Resource are known, estimated or interpreted from specific geological evidence and knowledge."*

The "reasonable prospects for eventual economic extraction" requirement generally implies that the quantity and grade estimates meet certain economic thresholds and that the mineral resources are reported at an appropriate cut-off grade taking into account the likely extraction scenarios and process metal recoveries. It is the opinion of the Qualified Person, the resources as classified, have a reasonable expectation of eventual economic extraction.

Table 1-7 and Table 1-8 present the mineral resource statement with a global statement shown in Table 1-9.

**Table 1-7 Mineral Resource Statement at 0.5% $WO_3$ cut-off.**

| CLASS | CUTOFF | TONNES | WO3% | CU% |
|---|---|---|---|---|
| INDICATED | 0.5 | 14,000,794 | 1.008 | 0.082 |
| | | | | |
| INFERRED | 0.5 | 3,401,541 | 0.809 | 0.064 |
| | | | | |
| TOTAL | 0.5 | 17,402,336 | 0.969 | 0.078 |
| | | | | |
| WASTE | | 66,706,479 | S/R | 3.83 |

**Table 1-8 Mineral Resource Statement at various $WO_3$ cut-offs.**

| CLASS | CUTOFF | TONNES | WO3% | CU% |
|---|---|---|---|---|
| INDICATED | 0.5 | 14,000,794 | 1.008 | 0.082 |
| | 0.6 | 12,181,803 | 1.077 | 0.091 |
| | 0.7 | 10,400,491 | 1.151 | 0.102 |
| | 0.8 | 8,593,735 | 1.236 | 0.116 |
| | 0.9 | 7,130,584 | 1.317 | 0.131 |
| | 1 | 5,962,940 | 1.39 | 0.145 |
| | | | | |
| INFERRED | 0.5 | 3,401,541 | 0.809 | 0.064 |
| | 0.6 | 2,453,453 | 0.912 | 0.083 |
| | 0.7 | 1,867,731 | 0.998 | 0.104 |
| | 0.8 | 1,521,460 | 1.057 | 0.121 |
| | 0.9 | 1,164,071 | 1.12 | 0.135 |
| | 1 | 975,246 | 1.154 | 0.147 |
| | | | | |
| TOTAL | 0.5 | 17,402,336 | 0.969 | 0.078 |
| | 0.6 | 14,635,256 | 1.049 | 0.09 |
| | 0.7 | 12,268,222 | 1.127 | 0.102 |
| | 0.8 | 10,115,195 | 1.21 | 0.117 |
| | 0.9 | 8,294,655 | 1.29 | 0.132 |
| | 1 | 6,938,186 | 1.357 | 0.145 |
| | | | | |
| WASTE | | 66,706,479 | S/R | 3.83 |

**Table 1-9 Global Mineral Resource at various $WO_3$ cut-offs.**

| CLASS | CUTOFF | TONNES | WO3% | CU% |
|---|---|---|---|---|
| Indicated | 0 | 31,309,944 | 0.86 | 0.06 |
| | 0.1 | 31,304,588 | 0.86 | 0.06 |
| | 0.2 | 31,039,430 | 0.87 | 0.06 |
| | 0.3 | 30,269,420 | 0.88 | 0.06 |
| | 0.4 | 28,767,558 | 0.91 | 0.06 |
| | 0.5 | 26,345,465 | 0.95 | 0.07 |
| | 0.6 | 22,734,957 | 1.02 | 0.07 |
| | 0.7 | 19,114,854 | 1.09 | 0.08 |
| | 0.8 | 15,509,891 | 1.17 | 0.09 |
| | 0.9 | 12,102,903 | 1.26 | 0.10 |
| | 1 | 9,442,082 | 1.35 | 0.12 |
| Inferred | 0 | 33,931,555 | 0.53 | 0.02 |
| | 0.1 | 33,239,474 | 0.54 | 0.02 |
| | 0.2 | 31,052,418 | 0.56 | 0.03 |
| | 0.3 | 26,692,823 | 0.61 | 0.03 |
| | 0.4 | 21,889,660 | 0.67 | 0.03 |
| | 0.5 | 15,753,683 | 0.76 | 0.03 |
| | 0.6 | 11,461,061 | 0.84 | 0.04 |
| | 0.7 | 7,684,221 | 0.94 | 0.04 |
| | 0.8 | 5,031,494 | 1.04 | 0.06 |
| | 0.9 | 3,523,296 | 1.12 | 0.06 |
| | 1 | 2,592,258 | 1.19 | 0.07 |
| Total | 0 | 65,241,500 | 0.69 | 0.04 |
| | 0.1 | 64,544,063 | 0.69 | 0.04 |
| | 0.2 | 62,091,847 | 0.71 | 0.04 |
| | 0.3 | 56,962,243 | 0.76 | 0.05 |
| | 0.4 | 50,657,218 | 0.81 | 0.05 |
| | 0.5 | 42,099,149 | 0.88 | 0.05 |
| | 0.6 | 34,196,018 | 0.96 | 0.06 |
| | 0.7 | 26,799,075 | 1.05 | 0.07 |
| | 0.8 | 20,541,384 | 1.14 | 0.08 |
| | 0.9 | 15,626,199 | 1.23 | 0.09 |
| | 1 | 12,034,341 | 1.32 | 0.11 |

## Publication Disclaimer

This document has been created through the joint contribution of the Northwest Territories Geological Survey (NTGS), Government of Northwest Territories (GNWT) and a third party contributor. It is provided for informational purposes only. It does not contain any warranties, representations or quality commitments, whether express or implicit, nor does it contain any guarantees regarding the correctness, integrity, and quality of the information. The NTGS has exercised all reasonable care in the compilation, interpretation, and production of this document and the information has been obtained from sources that the NTGS believes to be reliable. However, it is not possible to ensure complete accuracy, and all persons who rely on the information contained herein do so at their own risk. The NTGS, the GNWT nor the third party contributor accept liability for any errors, omissions, or inaccuracies that may be included in, or derived from, this document. In no event will the NTGS, the GNWT, the third party contributor nor any of their respective successors, assigns, agents or employees be held liable in any way for damages suffered, direct or indirect, as a result of any action or inaction taken in reliance on information provided herein.

## Publication Terms of Use

# NWT Open File 2018-02
# Geology of the Mactung tungsten skarn and area – Review and 2016 field observations

## Appendix B - Geochemistry

**B.J. Fischer, E. Martel, and H. Falck**

*Recommended Citation:*
*Fischer, B.J., Martel, E., and Falck, H., Geology of the Mactung tungsten skarn and area – Review and 2016 field observations; Northwest Territories Geological Survey, NWT Open File 2018-02, 84 pages and appendices.*

## Appendix B
## Geochemistry

| Analyte Symbol | | | | | Au | Mass | SiO2 | Al2O3 | Fe2O3(T) | MnO | MgO | CaO | Na2O | K2O | TiO2 | P2O5 | LOI |
|---|---|---|---|---|---|---|---|---|---|---|---|---|---|---|---|---|---|
| Unit Symbol | | | | | ppb | g | % | % | % | % | % | % | % | % | % | % | % |
| Detection Limit | | | | | 1 | | 0.01 | 0.01 | 0.01 | 0.001 | 0.01 | 0.01 | 0.01 | 0.01 | 0.001 | 0.01 | |
| Analysis Method | | | | | FA-INAA | FA-INAA | FUS-ICP | FUS-ICP | FUS-ICP | FUS-ICP | FUS-ICP | FUS-ICP | FUS-ICP | FUS-ICP | FUS-ICP | FUS-ICP | FUS-ICP |
| Identifier* | Sample | Unit | Lithology | Description | | | | | | | | | | | | | |
| 39 | 16EM39B | Hess River Fm. | Mudstone | Pyritic mudstone | 15 | 10 | | | | | | | | | | | |
| 41 | 16EM41A | Member E | Mudstone | Rusty siliceous laminated mudstone | 6 | 10 | | | | | | | | | | | |
| 40 | 16EM40A | Member D | Phosphatic-clast limestone conglomerate | Black oval clasts of lime mudstone and of phosphatic material in calcareous cement | | | 15.5 | 0.98 | 1.54 | 0.045 | 0.43 | 45.15 | 0.04 | 0.27 | 0.062 | 19.04 | 15.97 |
| 73 | 16EM73C | Member D | Phosphatic-clast limestone conglomerate; Quartz sandstone | Phosphatic granule to cobble clasts in lime cement; laminated & cross-laminated quartz-sandy limestone to fine quartz sandstone | | | 31.55 | 1.52 | 1.88 | 0.057 | 1.45 | 34.96 | 0.04 | 0.71 | 0.109 | 14.08 | 12.45 |
| 75 | 16EM75 | Hess River Fn | Phosphatic-granule sandstone | Bluish grey weathering, phosphatic-granule sandstone to conglomerate with calcite cement. | | | 14.22 | 1.73 | 1.36 | 0.085 | 0.92 | 45.08 | 0.04 | 0.66 | 0.134 | 10.68 | 23.6 |
| 95 | 16EM95B | Member D | Phosphatic-clast limestone conglomerate | Thin bedded, clast supported, granule (to pebble) phosphatic clasts, 10% replacive pyrite | | | 28.06 | 1.97 | 2.73 | 0.048 | 1.58 | 36.5 | 0.04 | 0.67 | 0.138 | 16 | 9.67 |
| 104 | 16EM104C | Member D | Quartz-sandy phosphatic-clast limestone conglomerate | Sandstone with very fine sand to silt-sized grains of grey carbonate in calcite cement, grades into conglomerate with dark grey granule to pebble sized phosphatic clasts | | | 14 | 1.02 | 1.21 | 0.055 | 0.85 | 46.72 | 0.03 | 0.37 | 0.129 | 11.24 | 22.97 |
| 107 | 16EM107B | Member D | s | Granule to pebble sized, black, phosphatic(?), calcareous clasts packed in white calcite cement; calc-silicate minerals? | | | 20.88 | 0.86 | 0.96 | 0.054 | 0.52 | 43.3 | 0.04 | 0.29 | 0.059 | 18.84 | 12.04 |

* Identifier is the label used in Figure 5

## Appendix B
## Geochemistry

| Analyte Symbol | Total | Sc | Be | V | Cr | Co | Ni | Cu | Zn | Ga | Ge | As | Rb | Sr | Y | Zr | Nb | Mo | Ag | In | Sn | Sb | Cs | Ba | La | Ce | Pr | Nd | Sm | Eu | Gd |
|---|---|---|---|---|---|---|---|---|---|---|---|---|---|---|---|---|---|---|---|---|---|---|---|---|---|---|---|---|---|---|---|
| Unit Symbol | % | ppm | ppm | ppm | ppm | ppm | ppm | ppm | ppm | ppm | ppm | ppm | ppm | ppm | ppm | ppm | ppm | ppm | ppm | ppm | ppm | ppm | ppm | ppm | ppm | ppm | ppm | ppm | ppm | ppm | ppm |
| Detection Limit | 0.01 | 1 | 1 | 5 | 20 | 1 | 20 | 10 | 30 | 1 | 1 | 5 | 2 | 2 | 1 | 2 | 1 | 2 | 0.5 | 0.2 | 1 | 0.5 | 0.5 | 2 | 0.1 | 0.1 | 0.05 | 0.1 | 0.1 | 0.05 | 0.1 |
| Analysis Method | FUS-ICP | FUS-ICP | FUS-ICP | FUS-ICP | FUS-MS | FUS-MS | FUS-MS | FUS-MS | FUS-MS | FUS-MS | FUS-MS | FUS-MS | FUS-MS | FUS-ICP | FUS-ICP | FUS-ICP | FUS-MS | FUS-MS | FUS-MS | FUS-MS | FUS-MS | FUS-MS | FUS-MS | FUS-ICP | FUS-MS | FUS-MS | FUS-MS | FUS-MS | FUS-MS | FUS-MS | FUS-MS |
| Identifier* | | | | | | | | | | | | | | | | | | | | | | | | | | | | | | | |
| 39 | | | | | | | | | | | | | | | | | | | | | | | | | | | | | | | |
| 41 | | | | | | | | | | | | | | | | | | | | | | | | | | | | | | | |
| 40 | 99.03 | 2 | < 1 | 48 | < 20 | < 1 | < 20 | 20 | < 30 | 2 | < 1 | 11 | 7 | 636 | 16 | 21 | 2 | < 2 | < 0.5 | < 0.2 | < 1 | 0.9 | 1.1 | 3819 | 11.7 | 14.7 | 1.63 | 6.1 | 1.3 | 0.29 | 1.5 |
| 73 | 98.81 | 2 | < 1 | 85 | < 20 | < 1 | < 20 | 20 | < 30 | 3 | < 1 | 9 | 16 | 679 | 32 | 81 | 3 | 4 | < 0.5 | < 0.2 | < 1 | 0.6 | 1.7 | 3829 | 22.7 | 34.2 | 3.98 | 15.6 | 3.4 | 0.76 | 3.6 |
| 75 | 98.52 | 4 | < 1 | 52 | < 20 | < 1 | < 20 | 20 | < 30 | 2 | < 1 | 8 | 12 | 660 | 41 | 57 | 3 | 3 | < 0.5 | < 0.2 | < 1 | 0.6 | < 0.5 | 9709 | 39.5 | 73.3 | 8.84 | 34 | 6.6 | 1.72 | 6.7 |
| 95 | 97.4 | 3 | < 1 | 97 | < 20 | < 1 | < 20 | 20 | 40 | 3 | < 1 | 11 | 14 | 752 | 33 | 111 | 3 | 5 | < 0.5 | < 0.2 | < 1 | < 0.5 | 0.5 | 5847 | 32.5 | 48.6 | 4.77 | 17.9 | 4 | 1.05 | 4.3 |
| 104 | 98.59 | 3 | < 1 | 56 | < 20 | < 1 | < 20 | 10 | < 30 | 2 | < 1 | 10 | 10 | 415 | 24 | 31 | 2 | 4 | < 0.5 | < 0.2 | < 1 | 0.5 | 0.7 | 480 | 14.9 | 25.7 | 2.98 | 11.8 | 2.5 | 0.65 | 2.8 |
| 107 | 97.84 | 2 | < 1 | 42 | < 20 | < 1 | < 20 | 20 | 120 | 2 | < 1 | < 5 | 13 | 693 | 30 | 23 | 2 | 3 | < 0.5 | < 0.2 | 1 | < 0.5 | 0.8 | 1412 | 24.5 | 32.3 | 3.64 | 13 | 2.5 | 0.63 | 2.9 |

* Identifier is the label used in Figure 5

## Appendix B
## Geochemistry

| Analyte Symbol | Tb | Dy | Ho | Er | Tm | Yb | Lu | Hf | Ta | W | Tl | Pb | Bi | Th | U | Al | As | Be | Bi | Ca | Co | Cr | Cs | Cu | Fe | K | Ga | Ge |
|---|---|---|---|---|---|---|---|---|---|---|---|---|---|---|---|---|---|---|---|---|---|---|---|---|---|---|---|---|
| Unit Symbol | ppm | ppm | ppm | ppm | ppm | ppm | ppm | ppm | ppm | ppm | ppm | ppm | ppm | ppm | ppm | % | % | % | % | % | % | % | % | % | % | % | % | % |
| Detection Limit | 0.1 | 0.1 | 0.1 | 0.1 | 0.05 | 0.1 | 0.01 | 0.2 | 0.1 | 1 | 0.1 | 5 | 0.4 | 0.1 | 0.1 | 0.01 | 0.001 | 0.001 | 0.001 | 0.01 | 0.001 | 0.01 | 0.001 | 0.001 | 0.05 | 0.1 | 0.001 | 0.001 |
| Analysis Method | FUS-MS | FUS-MS | FUS-MS | FUS-MS | FUS-MS | FUS-MS | FUS-MS | FUS-MS | FUS-MS | FUS-MS | FUS-MS | FUS-MS | FUS-MS | FUS-MS | FUS-MS | FUS-Na2O2 | FUS-MS-Na2O2 | FUS-MS-Na2O2 | FUS-MS-Na2O2 | FUS-Na2O2 | FUS-MS-Na2O2 | FUS-MS-Na2O2 | FUS-MS-Na2O2 | FUS-MS-Na2O2 | FUS-Na2O2 | FUS-Na2O2 | FUS-MS-Na2O2 | FUS-MS-Na2O2 |
| Identifier* | | | | | | | | | | | | | | | | | | | | | | | | | | | | |
| 39 | | | | | | | | | | | | | | | | 3.66 | 0.001 | < 0.001 | < 0.001 | 4.58 | < 0.001 | < 0.01 | < 0.001 | 0.008 | 1.48 | 2 | 0.001 | < 0.001 |
| 41 | | | | | | | | | | | | | | | | 4.36 | < 0.001 | < 0.001 | < 0.001 | 3 | 0.003 | < 0.01 | 0.001 | 0.007 | 3.37 | 1 | 0.001 | < 0.001 |
| 40 | 0.2 | 1.5 | 0.3 | 1.1 | 0.16 | 1.2 | 0.2 | 0.4 | 0.2 | 4 | 0.1 | < 5 | < 0.4 | 0.8 | 9.5 | | | | | | | | | | | | | |
| 73 | 0.6 | 3.9 | 0.8 | 2.5 | 0.36 | 2.1 | 0.35 | 1.7 | 0.2 | < 1 | 0.1 | < 5 | < 0.4 | 2 | 19.8 | | | | | | | | | | | | | |
| 75 | 1 | 6 | 1.2 | 3.1 | 0.39 | 2.4 | 0.33 | 1.2 | 0.2 | < 1 | < 0.1 | 5 | < 0.4 | 2 | 10.6 | | | | | | | | | | | | | |
| 95 | 0.7 | 4.4 | 1 | 2.9 | 0.39 | 2.5 | 0.4 | 2.3 | 0.3 | < 1 | < 0.1 | < 5 | < 0.4 | 2.6 | 23.8 | | | | | | | | | | | | | |
| 104 | 0.5 | 2.9 | 0.6 | 1.8 | 0.25 | 1.5 | 0.26 | 0.7 | < 0.1 | < 1 | < 0.1 | 5 | < 0.4 | 1 | 16.3 | | | | | | | | | | | | | |
| 107 | 0.5 | 3.4 | 0.8 | 2.5 | 0.34 | 2.3 | 0.36 | 0.4 | 0.2 | 1 | < 0.1 | < 5 | < 0.4 | 0.7 | 16.4 | | | | | | | | | | | | | |

* Identifier is the label used in Figure 5

## Appendix B
## Geochemistry

| Analyte Symbol | In | Li | Mg | Mn | Mo | Nb | Ni | Pb | Re | S | Se | Si | Sn | Ta | Te | Th | Ti | Tl | U | W | Zn |
|---|---|---|---|---|---|---|---|---|---|---|---|---|---|---|---|---|---|---|---|---|---|
| Unit Symbol | % | % | % | % | % | % | % | % | % | % | % | % | % | % | % | % | % | % | % | % | % |
| Detection Limit | 0.001 | 0.001 | 0.01 | 0.001 | 0.001 | 0.001 | 0.001 | 0.001 | 0.001 | 0.01 | 0.001 | 0.01 | 0.001 | 0.001 | 0.001 | 0.001 | 0.01 | 0.001 | 0.001 | 0.001 | 0.001 |
| Analysis Method | FUS-MS-Na2O2 | FUS-MS-Na2O2 | FUS-Na2O2 | FUS-MS-Na2O2 | FUS-MS-Na2O2 | FUS-MS-Na2O2 | FUS-MS-Na2O2 | FUS-MS-Na2O2 | FUS-MS-Na2O2 | FUS-Na2O2 | FUS-MS-Na2O2 | FUS-Na2O2 | FUS-MS-Na2O2 | FUS-MS-Na2O2 | FUS-MS-Na2O2 | FUS-MS-Na2O2 | FUS-Na2O2 | FUS-MS-Na2O2 | FUS-MS-Na2O2 | FUS-MS-Na2O2 | FUS-MS-Na2O2 |
| Identifier* | | | | | | | | | | | | | | | | | | | | | |
| 39 | < 0.001 | 0.004 | 1.07 | 0.011 | < 0.001 | < 0.001 | 0.003 | < 0.001 | < 0.001 | 0.81 | < 0.001 | 32.3 | < 0.001 | < 0.001 | < 0.001 | < 0.001 | 0.26 | < 0.001 | < 0.001 | < 0.001 | 0.002 |
| 41 | < 0.001 | 0.008 | 1.43 | 0.022 | < 0.001 | 0.002 | 0.005 | 0.001 | < 0.001 | 2.44 | < 0.001 | 33.8 | < 0.001 | < 0.001 | < 0.001 | < 0.001 | 0.48 | < 0.001 | < 0.001 | < 0.001 | 0.005 |
| 40 | | | | | | | | | | | | | | | | | | | | | |
| 73 | | | | | | | | | | | | | | | | | | | | | |
| 75 | | | | | | | | | | | | | | | | | | | | | |
| 95 | | | | | | | | | | | | | | | | | | | | | |
| 104 | | | | | | | | | | | | | | | | | | | | | |
| 107 | | | | | | | | | | | | | | | | | | | | | |

* Identifier is the label used in Figure 5

# NWT Open File 2018-02
# Geology of the Mactung tungsten skarn and area – Review and 2016 field observations

## Appendix C -Geochronology Summary

**B.J. Fischer, E. Martel, and H. Falck**

Recommended Citation:
Fischer, B.J., Martel, E., and Falck, H., Geology of the Mactung tungsten skarn and area – Review and 2016 field observations; Northwest Territories Geological Survey, NWT Open File 2018-02, 84 pages and appendices.

# Appendix C-Geochronology Summary

| Sample: Field # / GSC # | Body / Unit /Zone | Lithology | Location | Easting[1] | Northing[1] | Mineral Dated | Dating Method | Age(s) (Ma) | Reference | Interpretation[2] |
|---|---|---|---|---|---|---|---|---|---|---|
| FJ68-320-2 / 73-74 | Cirque Lake stock | Granodiorite | 240 m southwest of Cirque Lake, 610 m northeast of the main mineralized zone | 442902 | 7017664 | Biotite | K-Ar | 89 ± 4 | Anderson (1993)[3] | Thermal event post-dating granitoid crystallization (Gebru 2017) |
| ANMT-81-8-1 / 87-130 | Cirque Lake stock | Granodiorite; mafic equigranular phase | West end of Cirque Lake, 1 km northeast of Mount Allan | 443253 | 7018587 | Biotite | K-Ar | 89 ± 2 | Anderson (p. 171-180) in Hunt and Roddick (1987) | Thermal event post-dating granitoid crystallization (Gebru 2017) |
| ANMT-81-5-6 / 87-131 | Cirque Lake stock | Biotite monzogranite; peralmuninous marginal equigranular phase | 2 km northeast of Mount Allan | 443269 | 7019515 | Biotite | K-Ar | 90 ± 2 | Anderson (p. 171-180) in Hunt and Roddick (1987) | Thermal event post-dating granitoid crystallization (Gebru 2017) |
| ANMT-82-331-1 / 87-133 | Dyke | Monzogranite; aplitic apopysis of Cirque Lake stock's peraluminous marginal equigranular phase | 2 km northeast of Mount Allan | 442855 | 7019708 | Muscovite | K-Ar | 90 ± 1 | Anderson (p. 171-180) in Hunt and Roddick (1987) | Thermal event post-dating granitoid crystallization (Gebru 2017) |
| MT-02 | Vein | Quartz-pyrrhotite-pyrite-molybdenite veins, steeply dipping, associated with greisen-like alteration, cutting Cirque Lake pluton and sedimentary country rock | Mount Allan | 442640 | 7017910 | Molybdenite | Re-Os | 97.2 ± 0.5<br>96.9 .± 0.5 | Selby *et al* . (2003) | |
| DS8-01 | Vein | | Mount Allan | 442630 | 7018056 | Molybdenite | Re-Os | 97.1 ± 0.4<br>97.1 ± 0.4 | Selby *et al.* (2003) | |
| DS9-01 | Vein | | Mount Allan | 442651 | 7017804 | Molybdenite | Re-Os | 97.2 ± 0.4 | Selby *et al.* (2003) | |
| DS12-01 | Vein | Quartz-pyrite-pyrrhotite-molybdenite vein with pyroxene-garnet alteration assemblage, cutting siltstone of Rabbitkettle Formation. | shaft workings dump | | | Molybdenite | Re-Os | 97.6 ± 0.4 | Selby *et al.* (2003) | |
| Above samples (MT-02, DS8-01, DS9-01, DS12-01) | Veins | | Mount Allan | | | Molybdenite | Re-Os isochron | 97.5 ± 0.5 | Selby *et al* . (2003) | Age of mineralization |
| DS10-01 | Cirque Lake stock | Biotite quartz monzonite | 0.65 km southwest of the west end of Cirque Lake | 442619 | 7018063 | Zircon | U-Pb con-chordia | 92.1 ± 0.4 | Selby *et al* . (2003) | Age of youngest thermal pulse related to emplacement of Cirque Lake stock (Gebru 2017) |
| MAC-156 | Dyke | Aplite | Dale Creek valley | 441501 | 7015976 | Biotite | Ar-Ar | 94.0 ± 0.5 | Gebru (2017) | Thermal event post-dating dyke crystallization |
| | | | | | | Zircon | U-Pb | 97.2 ± 0.2 | | Age of dyke crystallization |

| Sample: Field # / GSC # | Body / Unit /Zone | Lithology | Location | Easting[1] | Northing[1] | Mineral Dated | Dating Method | Age(s) (Ma) | Reference | Interpretation[2] |
|---|---|---|---|---|---|---|---|---|---|---|
| MAC-165 | Dyke | Leucocratic granitoid | 1.2 km southwest of Cirque Lake, a few hundred metres south of southeast margin of Cirque Lake stock | 442733 | 7017826 | Muscovite | Ar-Ar | 92.9 ± 0.4<br>95.3 ± 0.4 | Gebru (2017) | Thermal event post-dating granitoid crystallization (this granitoid dyke is cut by a vein of same generation as MAC-176C, and therefore must be older than MAC-176C) |
| | | | | | | Zircon | U-Pb | 97.1 ± 0.2 | | Age of dyke crystallization |
| MAC-177A | Cirque Lake stock | Biotite granite | 0.9 km southwest of Cirque Lake | 442806 | 7018033 | Muscovite | Ar-Ar | 95.6 ± 0.3 | Gebru (2017) | Thermal event post-dating stock crystallization |
| | | | | | | Biotite | Ar-Ar | 94.0 ± 0.3<br>91.8 ± 0.4 | | |
| | | | | | | Zircon | U-Pb | 97.1 ± 0.1 | | Age of Cirque Lake stock crystallization |
| MAC-177B | Cirque Lake stock | Leucogranite cutting the biotite granite of MAC-177A | 0.9 km southwest of Cirque Lake | 442806 | 7018033 | Muscovite | Ar-Ar | 93.3 ± 1.2 | Gebru (2017) | Thermal event post-dating stock crystallization |
| MAC-224A | Cirque Lake stock | Biotite granite | South edge of stock, north face of Mount Allan | 441839 | 7018089 | Muscovite | Ar-Ar | 98.1 ± 2 | Gebru (2017) | Thermal event post-dating stock crystallization |
| | | | | | | Biotite | Ar-Ar | 95.1 ± 0.8 | | |
| | | | | | | Zircon | U-Pb | 97.6 ± 0.2 | | Age of Cirque Lake stockcrystallization |
| MAC-303 | Rockslide Mountain stock | Biotite granite | Rockslide Mountain | 440026 | 7015106 | Biotite | Ar-Ar | 95.57 ± 0.55<br>97.56 ± 1.02 | Gebru (2017) | Thermal event post-dating stock crystallization |
| | | | | | | Zircon | U-Pb | 97.2 ± 0.2 | | Age of Rockslide Mountain stock crystallization |
| MAC-223A | Hess River Formation between Lower and Upper ore zones | Biotite hornfels | North face of Mount Allan | 441889 | 7018110 | Biotite | | 97.1 ± 1.9<br>96.9 ± 0.6 | Gebru (2017) | Age of metamorphism (contact?) |
| MAC-226 | Described only as "ore zone" | Pyrrhotite-garnet-pyroxene skarn | North face of Mount Allan | 441910 | 7018082 | Pyroxene (or amphhibole with a pyroxene core) | Ar-Ar | 127 ± 20 maximum | Gebru (2017) | Maximum age of skarning |
| MAC72-27-778 | Narchilla/ Vampire formation | Cordierite-muscovite-biotite schist | Drill hole MT72-27 collared on Mount Allan about 0.5 km southeast of the summit | 441979 | 7017724 | Biotite | Ar-Ar | 95.7 ± 0.4 | Gebru (2017) | Age of metamorphism (possibly related to post-intrusion local shear deformation) |
| MAC79-117-501.5 | Described only as "northeast flank of the skarn orebody" | Biotite-bearing pyroxene-pyrrhotite skarn | Drill hole MT79-117 collared on Mount Allan about 0.7 km southeast of the summit | 442117 | 7017731 | Biotite | Ar-Ar | 89.9 ± 2.9 | Gebru (2017) | Age of young thermal event |

| Sample: Field # / GSC # | Body / Unit /Zone | Lithology | Location | Easting[1] | Northing[1] | Mineral Dated | Dating Method | Age(s) (Ma) | Reference | Interpretation[2] |
|---|---|---|---|---|---|---|---|---|---|---|
| MS72-59-278 | Not given | Pyroxene-pyrrhotite skarn | Drill hole MT72-59 collared on Mount Allan about 0.6 km southeast of the summit | 441976 | 7017638 | Titanite | U-Pb | 97.1 ± 4.1 | Gebru (2017) | Age of mineralization |
| MAC-176C | Vein | Quartz vein cutting leucogranite dyke (same generation of dyke as MAC-165) | 0.7 km southwest of west end of Cirque Lake | 442770 | 7017886 | Molybdenite | U-Pb | 100.7 ± 3.5 [4] | Gebru (2017) | Age of quartz veining |
| MAC-222B | Vein | Quartz vein cutting granitic rock of Cirque Lake stock | North face of Mount Allan | 441899 | 7018126 | Molybdenite | U-Pb | 106.3 ± 0.4 | Gebru (2017) | Age of quartz veining |
| MAC-223C | Vein | Molybdenite-tourmaline-quartz vein cutting biotite granite of Cirque Lake stock, hornfels, and skarned hornfels | North face of Mount Allan | 441889 | 7018110 | Molybdenite | U-Pb | 99.1 ± 0.5 | Gebru (2017) | Age of quartz veining |
| [1] | Coordinates are presented as published, except for the first four, which were published as latitudes and longitudes: #73-74: 130° 08.3' W, 63° 17' N; #87-130: 130° 07'54" W, 63° 17'30" N; #87-131: 130° 07'54" W, 63° 18'00" N; #87-133: 130° 08'24" W, 63° 18'06" N. | | | | | | | | | |
| [2] | Interpretation is by author(s) except where referenced differently. | | | | | | | | | |
| [3] | The original date reported by Wanless *et al* . (1974) is 87±4 Ma. Anderson (1993, and in Hunt and Roddick, 1987) reports an age of 89±4 for the same sample. Anderson (1982) explains that Harris (1977) misquoted the original date as 89 Ma, which "was then changed to 91 Ma consistent with the new decay constants". It is here presumed that Anderson (1993) provides the correct date using the newer decay constants. | | | | | | | | | |
| [4] | Age is for initial Os = 1. Age for this sample varies strongly with initial Os: Age is 97.3 for initial Os=2 (crust-like), 103.8 for initial Os=0.13 (mantle-like). | | | | | | | | | |